

# **Modeling Soot in Pulverized Coal Flames**

A Thesis

Presented to the

Department of Mechanical Engineering

Brigham Young University

In Partial Fulfillment

of the Requirements for the Degree

Master of Science

Alexander L Brown

August 1997

This thesis by Alexander L Brown is accepted in its present form by the Department of Mechanical Engineering of Brigham Young University as satisfying the thesis requirement for the degree of Master of Science.

---

Thomas H. Fletcher, Advisor

---

Dale R. Tree, Advisory Committee

---

Brent W. Webb, Advisory Committee

---

Craig C. Smith, Graduate Coordinator

---

Date

# TABLE OF CONTENTS

TABLE OF CONTENTS.....	ii
LIST OF TABLES.....	iii
LIST OF FIGURES.....	iv
ACKNOWLEDGMENTS.....	vii
NOMENCLATURE.....	viii
1. INTRODUCTION.....	1
2. BACKGROUND.....	6
2.1 Radiation Predictions.....	6
2.2 Soot Chemistry.....	8
2.3 Fluid Dynamics.....	13
2.4 Summary.....	15
3. PREVIOUS WORK.....	17
3.1 Soot Radiative Properties.....	17
3.2 Soot Formation.....	20
3.3 Summary.....	25
4. OBJECTIVES.....	26
5. METHOD.....	27
5.1 Approach.....	27
5.2 Validation.....	32
5.2.1 Flat Flame Burner.....	33
5.2.2 Controlled Profile Reactor.....	35
5.2.3 Fireside Performance Test Facility.....	36
6. RESULTS.....	39
6.1 Flat Flame Burner.....	39
6.1.1 Soot Formation Predictions.....	41
6.1.2 Soot Particle Size Predictions.....	45
6.1.3 Convergence Time.....	48
6.1.4 Predicted Contours.....	48
6.2 Controlled Profile Reactor.....	51
6.2.1 Temperature and Species Predictions.....	57
6.2.2 Soot Predictions.....	60
6.3 Fireside Performance Test Facility.....	62
6.3.1 Gas Temperature and Species Predictions.....	63
6.3.2 Contour Plots.....	68
7. DISCUSSION.....	76
7.1 Flat Flame Burner Predictions.....	76
7.2 Controlled Profile Reactor Predictions.....	78
7.3 Fireside Performance Test Facility Predictions.....	80
7.4 General Discussion.....	81
7.5 Recommendations.....	83
8. CONCLUSIONS.....	86
REFERENCES.....	89
APPENDIX.....	94

## LIST OF TABLES

Table 5.1	Boundary Conditions for the Soot Conservation Equations.....	27
Table 5.2	Transport Equation Source Terms.....	30
Table 6.1	Single Macro-iteration Run Times in the FFB.....	48
Table 6.2	A Description of the Case Nomenclature.....	52
Table 6.3	A Comparison Between Predicted Line of Sight Soot Volume Fractions and Measurements for the CPR at 30 cm Below the Inlet.....	62
Table 6.4	Maximum Difference Between Gas Temperature and NO <sub>x</sub> Concentration Predictions With and Without Soot at Various Heights.....	68
Table A.1	Changes to PCGC-3 Required for the Soot Model.....	88
Table C.1	Characteristics of the Various Coals Modeled (percent daf).....	109
Table C.2	<sup>13</sup> C NMR Data for the Coals Modeled.....	109
Table C.3	<sup>13</sup> C NMR Predictions from the Correlation of Genetti et al. (1997).....	110
Table D.1	Characteristic Parameters of the Facilities Modeled.....	111

## LIST OF FIGURES

Figure 2.1	Presumed pathway for coal product formation (Ma, 1996).....	11
Figure 3.1	A comparison of two soot emissivity models ( $L_e=1.0$ , $C =7.0$ ).....	20
Figure 5.1	A schematic of the flat flame burner (From Ma, 1996).....	34
Figure 5.2	A schematic of the controlled profile reactor.....	35
Figure 5.3	A schematic of the fireside performance test facility (from Flores, 1996)..	38
Figure 6.1	A comparison of centerline temperature measurements and predictions for the FFB.....	40
Figure 6.2	A comparison of predicted and measured soot yields in the FFB for a Pittsburgh #8 coal using measured NMR parameters.....	42
Figure 6.3	A comparison of predicted and measured soot yields in the FFB for a Pittsburgh #8 coal using the correlation of Genetti et al. (1997).....	43
Figure 6.4	A comparison of predicted and measured soot yields in the FFB for an Illinois #6 coal using measured NMR parameters.....	43
Figure 6.5	A comparison of predicted and measured soot yields in the FFB for an Illinois #6 coal using the correlation of Genetti et al. (1997).....	44
Figure 6.6	A comparison of predicted and measured soot yields in the FFB for a Utah Hiawatha coal using the correlation of Genetti et al. (1997).....	44
Figure 6.7	FFB centerline node $d$ , $f_{v,C}$ and $N_C$ predictions for a Pittsburgh #8 coal.....	46
Figure 6.8	FFB centerline node $d$ , $f_{v,C}$ and $N_C$ predictions for an Illinois #6 coal.....	46
Figure 6.9	FFB centerline node $d$ , $f_{v,C}$ and $N_C$ predictions for a Utah Hiawatha coal...	47
Figure 6.10	A FFB soot cloud cross section prediction for an Illinois #6 coal.....	49
Figure 6.11	FFB tar cloud cross section prediction for an Illinois #6 coal.....	50
Figure 6.12	$N_C$ contours at a cross section in the FFB for an Illinois #6 coal.....	50
Figure 6.13	An illustration of the technique used to represent the predictions for the CPR.....	54
Figure 6.14	An illustration of the typical CPR temperature predictions and curve fit versus measurements. Data are at 95 cm below the inlet.....	55
Figure 6.15	Predicted and measured gas temperatures in the CPR at 30 cm below the inlet.....	57
Figure 6.16	Predicted and measured $NO_x$ concentrations in the CPR at 30 cm below the inlet.....	58
Figure 6.17	Predicted and measured gas temperatures in the CPR at 95 cm below the inlet.....	58
Figure 6.18	Predicted and measured $NO_x$ concentrations in the CPR at 95 cm below the inlet.....	59
Figure 6.19	Horizontal Line of sight soot volume fractions in the CPR at 30 cm below the inlet.....	61
Figure 6.20	Predicted and measured $O_2$ concentrations in the FPTF at 68.6 cm above the inlet.....	64
Figure 6.21	Predicted and measured $O_2$ concentrations in the FPTF at 144.8 cm above the inlet.....	64

Figure 6.22	Predicted and measured gas temperatures in the FPTF at 68.6 cm above the inlet.....	65
Figure 6.23	Predicted and measured NO <sub>x</sub> concentrations in the FPTF at 68.6 cm above the inlet.....	66
Figure 6.24	Predicted and measured gas temperatures in the FPTF at 144.8 cm above the inlet.....	66
Figure 6.25	Predicted and measured NO <sub>x</sub> concentrations in the FPTF at 144.8 cm above the inlet.....	67
Figure 6.26	N <sub>C</sub> contour predictions in the FPTF using the transport equation.....	69
Figure 6.27	Y <sub>T</sub> contour predictions in the FPTF.....	71
Figure 6.28	f <sub>v,C</sub> contour predictions in the FPTF.....	73
Figure 6.29	f <sub>v,C</sub> contour predictions in the FPTF.....	74
Figure D.1	The Controlled Profile Reactor Inlet.....	113
Figure D.2	The Fireside Performance Test Facility Inlet.....	115
Figure D.3	The Fireside Performance Test Facility Radiative Section.....	116
Figure E.1	Predicted and measured gas temperatures in the CPR at 15 cm below the inlet.....	119
Figure E.2	Predicted and measured NO <sub>x</sub> concentrations in the CPR at 15 cm below the inlet.....	119
Figure E.3	Predicted and measured gas temperatures in the CPR at 55 cm below the inlet.....	120
Figure E.4	Predicted and measured NO <sub>x</sub> concentrations in the CPR at 55 cm below the inlet.....	120
Figure E.5	Predicted and measured gas temperatures in the CPR at 70 cm below the inlet.....	121
Figure E.6	Predicted and measured NO <sub>x</sub> concentrations in the CPR at 70 cm below the inlet.....	121
Figure E.7	Predicted and measured gas temperatures in the CPR at 110 cm below the inlet.....	122
Figure E.8	Predicted NO <sub>x</sub> concentrations in the CPR at 110 cm below the inlet.....	122
Figure E.9	Predicted and measured gas temperatures in the CPR at 150 cm below the inlet.....	123
Figure E.10	Predicted gas temperatures in the CPR at 190 cm below the inlet.....	123
Figure F.1	Predicted and measured gas temperatures in the FPTF at 30.5 cm above the inlet.....	124
Figure F.2	Predicted and measured NO <sub>x</sub> concentrations in the FPTF at 30.5 cm above the inlet.....	124
Figure F.3	Predicted and measured O <sub>2</sub> concentrations in the FPTF at 30.5 cm above the inlet.....	125
Figure F.4	Predicted and measured gas temperatures in the FPTF at 106.7 cm above the inlet.....	125
Figure F.5	Predicted and measured NO <sub>x</sub> concentrations in the FPTF at 106.7 cm above the inlet.....	126
Figure F.6	Predicted and measured O <sub>2</sub> concentrations in the FPTF at 106.7 cm above the inlet.....	126
Figure F.7	Predicted and measured gas temperatures in the FPTF at 182.9 cm above	

	the inlet.....	127
Figure F.8	Predicted and measured NO <sub>x</sub> concentrations in the FPTF at 182.9 cm above the inlet.....	127
Figure F.9	Predicted and measured O <sub>2</sub> concentrations in the FPTF at 182.9 cm above the inlet.....	128
Figure F.10	Predicted and measured gas temperatures in the FPTF at 259.1 cm above the inlet.....	128
Figure F.11	Predicted and measured NO <sub>x</sub> concentrations in the FPTF at 259.1 cm above the inlet.....	129
Figure E.12	Predicted and measured O <sub>2</sub> concentrations in the FPTF at 259.1 cm above the inlet.....	129

## **ACKNOWLEDGMENTS**

I would like to thank those who have contributed to the success of this project. Particularly my faculty advisors who have given superb input on such a complex problem. I also need to recognize the National Science Foundation, whose financial contribution has facilitated and motivated this work. I would also like to thank my family for moral support.

## NOMENCLATURE

Symbol	Definition
A	Arrhenius pre-exponential factor
a	area
C	optical constant
$C_1$	empirical soot formation constant
$C_2$	empirical soot oxidation constant
Ca	collision constant
CF	collision frequency
$C_{min}$	number of carbon atoms per incipient soot particle
c	concentration (moles/m <sup>3</sup> )
D	diffusivity
d	diameter
E	Arrhenius activation energy
$E_b$	Plank's blackbody emission function
Eq	equivalence ratio
f	fraction
I	intensity
k	Boltzman's constant or turbulent kinetic energy
$L_e$	mean beam path length
p	partial pressure
M	molecular weight
m	mass
N	number of particles
$N_c$	soot particles per unit mass
$N_a$	Avagadro's number
R	universal gas constant
S	path length (radiation) or source term (transport)
SA	total surface area
SP	particle source term
T	temperature
u	velocity
V	volume
X	size parameter
x	a direction
Y	mass fraction

## Greek

$\mu$

## Definition

empirical soot correction factor  
local atomic mass content  
emissivity or turbulent energy dissipation  
coal gas mixture fraction  
angle  
absorption coefficient  
wavelength  
viscosity  
density  
Schmidt number, Stephan-Boltzman's constant or  
scattering coefficient  
scattering phase function  
equivalence ratio  
solid angle

## Subscripts

C  
FC  
G  
g  
i  
j  
k  
m  
M  
N  
OC  
OT  
p  
s  
T  
v

## Definition

carbon or soot  
formation of soot  
gasification of tar  
gas  
the i component (i.e. 1, 2, 3...)  
the j component (i.e. 1, 2, 3...)  
the k component (i.e. 1, 2, 3...)  
mass  
mixture  
number of particles  
oxidation of soot  
oxidation of tar  
primary stream  
secondary stream  
tar  
volumetric basis  
wavelength  
perpendicular to

## 1. INTRODUCTION

Computational fluid dynamics (CFD) codes, with the advent of powerful computers, are gaining considerable attention as design tools. Properly written codes and models have the capability of predicting important details of fluid flow problems.

An ongoing project at BYU is the modeling of coal reactors, and considerable effort has been spent to develop a comprehensive computer model for coal combustion called Pulverized Coal Gasification and Combustion in 3 dimensions (PCGC-3). This model is capable of predicting temperature, pressure, particle path, energy transport, and chemical reactions in a pulverized coal reactor. The ability to accurately predict such parameters can aid in reactor design by allowing computer testing and optimization of new designs or modifications at a much lower cost than full-scale testing.

While many of the calculations performed by CFD codes are grounded in proven theoretical models, some empiricism and lack of detail still exists. The complexities of many of the molecular interactions, even if completely understood, simply can not be modeled at a fundamental level with existing chemical reaction data and computer technology. This is particularly true for many large industrial scale applications. Assumptions are generally made which simplify the computational load on the computer but still maintain sufficient accuracy to describe the reactor of interest. An example of such a process where empiricism is generally used is fluid turbulence. Detailed theoretical models are beyond the capacity of current computer technology to generate practical

solutions for large and complex cases. Due to this fact, empirical simplifications of the theoretical equations are often used which are compatible with current computing technology. These simplified equations can give quite accurate predictions for some practical cases. Many of the current turbulence models, however, may lack the accuracy required to make useful predictions for every case.

An important aspect of combustion CFD codes is the thermal heat transfer due to radiation. Radiative heat transfer occurs predominantly for wavelengths between approximately 0.2  $\mu\text{m}$  and 1000  $\mu\text{m}$  (Siegel and Howell, 1992). Hot gases radiate in two distinct forms. Atoms and small molecules radiate in distinct bands due to the quantum nature of these species. Larger molecules with more degrees of freedom tend to radiate across a broader range of wavelengths, and more closely approximate ideal gray or black bodies. Flames are typically significantly hotter than their surroundings, so most of the radiative heat transferred from the gases is lost to the surroundings. Predicted gas temperatures are therefore presumed to be lower in the flame zone than they would be in the absence of radiative predictions for most cases. A simple example of the importance of the radiation in these flames can be shown by considering a thermocouple measurement. A thermocouple inserted into a hot gaseous flame will not accurately measure the temperature of the surrounding gas. This is because the equilibrium temperature for a hot thermocouple radiating in such a flame can be several hundred degrees lower than the actual gas temperature. The radiative heat loss from the thermocouple bead balances the convective and radiative heat transfer from the surrounding hot gases. Thermocouple measurements, when corrected properly for radiative effects, can be quite accurate.

Accurately determining the thermal radiation effects of the combustion products is essential to assure reasonable predictions of gas temperatures and heat fluxes. A submodel to treat the radiative heat transfer of H<sub>2</sub>O, CO<sub>2</sub>, coal, char, and ash is generally included in CFD codes for coal flame predictions (Brewster et al., 1993). While these gases and particulates certainly contribute to radiative heat transfer, combustion-generated soot may also be important but is often neglected. Accurate soot radiation models for coal flames have yet to be established. Soot is thought to contribute significantly in many combustion cases, particularly in large furnaces where soot loading may be high in some regions. It is expected that by adding a soot radiation model, the predicted temperature in the flame zone of the combustion chamber should drop. This is because the energy should be more readily transported from the combustion region to the chamber walls. Due to this effect on flame temperature, the addition of a soot formation model should also improve the near-burner pollutant predictions, which can be highly temperature dependent. Thus the description of soot radiation in coal flames may also have a significant impact on NO<sub>x</sub> formation.

Another common approximation in CFD codes is the description of local chemistry in turbulent systems. One assumption used to solve combustion problems frequently used in CFD codes is to assume that the chemical reactions are mixing-limited. This means that the important chemical reactions occur at a much faster rate than the mixing rate between reactants and products. Such a case may then be solved by determining the fraction of the mass at a given location coming from each stream and calculating the chemical equilibrium based on such a mixture. PCGC-3 utilizes a form of this method. This assumption reduces the need for time intensive kinetics calculations,

allowing predictions to be made in practical systems which would otherwise be computationally impossible. It also limits the accuracy of the modeling. One drawback of this approach is that detailed chemistry, such as that of soot production, is not calculated. Because current turbulent chemistry models currently require empirical assumptions, describing chemical reactions in turbulent systems is an important research topic.

Developing a soot radiation model is not an easy task. Soot is understood to be a particulate formed from gas phase reactions. Additionally, soot formation mechanisms vary with different types of fuels. This would require the soot formation model to vary depending on the type of fuel used in the combustion flame. Accurate modeling of soot may require extensive work in various fields and significant computational time.

Measuring the location and concentration of the soot in the flame is difficult. This is difficult because in a flame the soot may undergo simultaneous nucleation, agglomeration, surface growth, and oxidation. This is one of the reasons very little data are available regarding soot in coal flames. Most practical flames occur in turbulent environments, which further complicates the matter. Another difficulty is determining the radiative properties of the soot. Information regarding the radiative properties of coal soot is scarce and has yet to be proven reliable; some information is known, however. The local absorption coefficient is known to be a strong function of the local volume fraction and complex index of refraction of soot. Further, large agglomerates of soot are capable of scattering radiation. The scattering and absorption properties are strong functions of the agglomeration morphology. Because soot is a transient product of

combustion, reliable data are unavailable, and the accuracy of the data that are available is difficult to ascertain.

The goal of this project was to develop and evaluate a model for the formation, agglomeration, transport and oxidation of soot in pulverized coal flames, including the radiation to and from the soot particles. This model was then to be incorporated as a submodel into PCGC-3 and interfaced with the existing models for gas, particle, and wall radiation. The resulting model provides a means through which evaluations and comparisons can be made between the model predictions and measured data.

## 2. BACKGROUND

Because of the complexity of the reactions and transport phenomena occurring within a coal flame, the ability to describe soot radiation requires a broad range of understanding of several pertinent topics. This section will examine briefly the major issues relating to the individual fields of study that pertain to this research.

### 2.1 Radiation Predictions

The Radiative Transfer Equation (RTE) is generally used to solve radiation problems in a semi-transparent medium. It may be considered as the transport equation for radiation. The RTE is an integro-differential equation, and numerical methods are generally used to estimate a solution to this equation. Additionally, solutions to the RTE require a description of the radiative medium properties as input. These are parameters such as the absorption coefficient, scattering coefficient, wall emissivity, and scattering phase function. A generic form of the RTE is as follows (Siegel and Howell, 1992):

$$\frac{dI}{dS} = -\kappa I(S) + \kappa_b I_b(S) - \kappa_s I(S) + \frac{\kappa_s}{4} \int_{\Omega} I(S, \Omega') \Phi(\Omega, \Omega') d\Omega' \quad (2.1)$$

The RTE can be solved using several different published approaches. One of the many methods is known as the Discrete Ordinates Method (Fiveland, 1984). PCGC-3 is

capable of predicting radiative heat transfer using this method. The Discrete Ordinates Method simplifies the RTE by assuming a non-continuous shape for the scattering phase function ( ). The simplified equation may then be solved using numerical methods. More information is available on solution methods for the RTE in other sources (e.g., Siegel and Howell, 1992).

Radiative properties of particles are strong functions of the particle morphology. The absorption coefficient is a strong function of the particle surface area available to radiate. In most practical applications, absorption/emission is the dominant mode of radiative heat transfer. Scattering, though, may contribute significantly to the net radiative effect. The scattering coefficient varies significantly depending on the size parameter:

$$X = \frac{d}{\lambda} \quad (2.2)$$

or the ratio of the particle circumference to the wavelength of incident radiation. Most soot particles are on the order of 0.005-0.7  $\mu\text{m}$  (Siegel and Howell, 1992). Scattering is described theoretically based on several regimes. Size parameters of less than approximately 0.3 indicate that the scattering falls in the Rayleigh regime, while Mie scattering occurs for  $0.3 < X < 5.0$  (Siegel and Howell, 1992). Large particle theory describes absorption and scattering effects for higher values of X. By considering the typical wavelengths for thermal radiation and typical unagglomerated soot particle diameters, it can be seen that most of the thermal radiation would fall within the Rayleigh and Mie regimes for scattering. Because (a) scattering effects are generally less important, (b) details required to make scattering predictions are costly to calculate, and (c) radiative properties are scarce, scattering is frequently neglected when dealing with soot. This

assumption is suspect, though, because flames with large agglomerates are likely to scatter significantly. More sophisticated models might require scattering predictions to assure accuracy. Scattering effects by soot in coal flames are more likely to be insignificant because scattering due to other particles present in the flame may dominate.

Radiation between walls, gases and particles is generally included in combustion CFD codes. Estimates of either the wall temperatures (boundary conditions) or wall heat flux are required as input boundary conditions for predictive purposes. Various methods exist for determining radiative properties for the gases and particulates in the flames. The radiation subroutine is normally called in between macro-iterations of the gas phase calculations. Results are incorporated into the gas phase enthalpy equation as a source term that treats radiative effects.

## **2.2 Soot Chemistry**

Soot is considered to be a solid particle produced in hydrocarbon flames. More specifically, the general chemical composition of soot consists of groups of Polycyclic Aromatic Hydrocarbons (PAHs) which tend to aggregate through a complex series of chemical reactions in the hot combustion gases. Most soot particles contain high carbon contents, with typical C/H ratios ranging from 72 to 168 by mass (Rigby, 1996).

Quantitative measurements of the yields and properties of soot are difficult to perform. A common technique for determining gas-phase chemistry is to simply sample the fluid from the flow field using a probe; chemical composition is then measured with a gas chromatograph or a spectrometer. The presence of intrusive probes in flames often introduces unwanted errors. Another method is to use optical measuring techniques such

as a Fourier Transform Infrared (FTIR) spectroscopy, or Rayleigh and Raman scattering techniques. Optical measurement techniques rely on the absorbing, emitting, and scattering characteristics of the soot to determine soot chemistry. These techniques suffer from interference, not only from the radiating walls and gases, but also from coal/char/ash particle radiation. Because of the inevitable char and ash particles in pulverized coal flames, soot data through optical techniques are particularly difficult to obtain.

As was mentioned previously, soot is typically 0.005-0.7  $\mu\text{m}$  in diameter. Of course this is based on the assumption that soot is a spherical particle. This assumption is not necessarily accurate. Soot, much like a snowflake, may form agglomerates with innumerable asymmetric shapes. The larger soot particles are typically understood to be agglomerates. Transmission Electron Microscopy (TEM) pictures of soot indicate that unagglomerated particles are relatively spherical, while agglomerates may appear as groups of combined spheres (Ma, 1996). Because of this and the reduced computational complexity, unagglomerated soot particles are generally treated as spheres. Because agglomeration is difficult to describe, frequently agglomerates are treated as spheres as well. Often agglomeration is completely ignored. Most engineering particle radiation models are incapable of describing the effects of the non-uniformity and non-sphericity of soot particles.

Several pathways which contribute to large quantities of soot in a flame have been proposed. Fuel rich flames lack the oxygen necessary to completely oxidize the soot. Insufficient mixing will create local fuel-rich zones within which there is insufficient oxygen to eliminate the soot. Also, rapid cooling can eliminate the activation energy

potential necessary for the complete oxidation of soot to occur. Many industrial gaseous flames are designed to minimize soot as a combustion product. For instance, modern gas turbines operate under fuel lean conditions to minimize CO and NO<sub>x</sub>, which is also favorable to minimize soot formation.

The first step that occurs in the formation/destruction of a soot particle is inception. When small hydrocarbon radicals in gaseous form combine to form larger hydrocarbon molecules, this is called nucleation. Nucleation is considered to be the first step in the formation of soot in most light gas flames, and acetylene is understood to be the major species involved. In heavier gas flames, benzene and other PAHs may contribute to soot formation as well (Bartok and Sarofim, 1991). Soot is formed as these PAHs combine with radicals and other hydrocarbon nuclei to form heavier soot particles. As these larger gas molecules condense, they form soot particles. Soot formation in coal is thought to occur as the tars, or the higher molecular weight hydrocarbons given off during devolatilization, combine and condense to form soot particles. This is a different mechanism than for soot formation from gaseous fuels, since acetylene is not heavily involved. Evidence of this comes from coal pyrolysis experiments where the sum of the mass of the soot and tar remains relatively constant (Nenninger et al., 1983; Wornat et al., 1987; Chen, 1991; and Ma, 1996). This is further supported by the fact that benzene and acetylene, the primary precursors to gas-derived soot formation, are not found to be significant products of coal devolatilization (Smith et al., 1994). Figure 2.1 illustrates what is thought to be the principal pathway for the formation of coal derived soot. The formation pathway from tar to soot involves the agglomeration of gas phase tar molecules combined with a phase change which results in the solid phase primary soot particles.

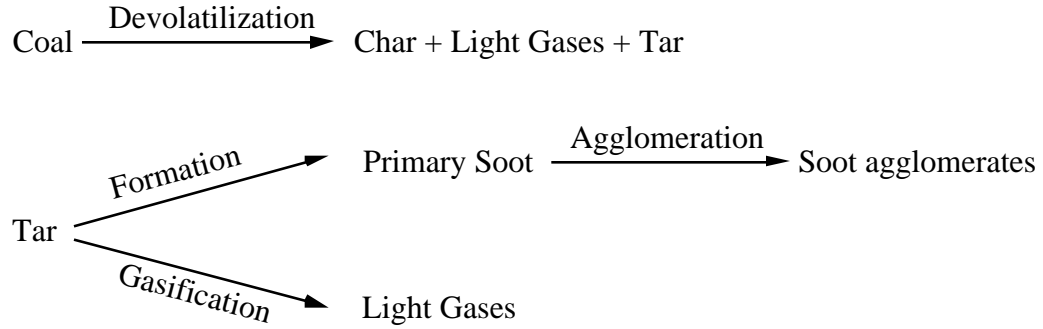


**Figure 2.1 Presumed pathway for coal product formation (Ma, 1996).**

Following inception, a soot particle continues to undergo transformations. Surface growth, or the condensation of hydrocarbon gases on the surface of a soot particle, is expected to contribute to the size of the particle, particularly in fuel rich flames. Hot soot particle surfaces are highly reactive. Acetylene, benzene and aromatic compounds contribute significantly to soot particle growth (Bartok and Sarofim, 1991).

Agglomeration, or the combining of multiple soot particles to form a cluster of connecting particles, is also known to occur. Data collected from single particle coal combustion tests indicates the formation of long agglomerate chains of soot (McLean et al., 1981). Measurements of soot collected from fuel rich flames also indicate the existence of soot agglomerates but not the long agglomerate chains (Ma, 1996). Available data in coal systems are preliminary in nature, and do not provide an adequate understanding of soot agglomeration tendencies within a flame.

Finally, oxidation frequently is a dominant factor in determining the amounts and sizes of soot within a flame. In most flames, oxidation will occur during the particle inception as well as during surface growth and agglomeration. Several soot oxidation rates

of various types exist (Magnussen and Hjertager, 1977; Lee et al., 1962; and Nagle and Strickland-Constable, 1961). The presence of oxygen obviously contributes to oxidation rates, although some research indicates that reactions with OH may be significant as well. OH may even be the dominant oxidizer in fuel rich flames (Puri et al., 1994, and Villasenor and Kennedy, 1992).

Typically, the amount of soot is represented numerically by the soot volume fraction ( $f_{v,C}$ ). This is because most radiation models use this parameter to predict radiative properties. Typical soot volume fractions for sooting flames may be as high as  $10^{-6}$  (Bartok and Sarofim, 1991). Axelbaum et al. (1988) measured various gas derived soot parameters under varying conditions. Their results indicate that while the volume fraction increases as a function of time, the number density of soot particles decreases. If surface growth is assumed to be small, this suggests that the effects of agglomeration are significant. Ma (1996) similarly reported an increase in average soot agglomerate diameter as a function of time.

In practical flames, particle inception, oxidation, surface growth and agglomeration are concurrent processes. Most of these processes occur quite rapidly as well. Factoring in the complex chemistry of a flame with the inability to accurately measure soot characteristics within a flame makes the task of modeling soot quite formidable. An additional complexity to the problem of modeling coal soot is that most of the published soot research and data have been performed using fuels other than coal.

As shown in Figure 2.1, soot in coal flames is assumed to be derived principally from the coal tar. This fact, to a certain extent, facilitates the ability to predict the soot. Coal devolatilization models have been developed which are capable of accurately

predicting yields of tar and volatile matter released from a given coal particle. Examples of these models are the functional group-depolymerization, vaporization, and cross-linking (FG-DVC) model (Solomon et al., 1988), the linear chain pyrolysis (FLASHCHAIN) model (Niksa and Kerstein, 1991), and the Chemical Percolation Devolatilization (CPD) model (Fletcher et al., 1992). These models base predictions on proximate and ultimate analysis as well as  $^{13}\text{C}$  NMR data regarding chemical structure.  $^{13}\text{C}$  NMR data may be either measured for a given coal or estimated from empirical correlations (Genetti and Fletcher, 1997). Simpler models are incapable of predicting tar. PCGC-3 allows the option of using either the CPD or a two-step method for determining coal devolatilization. By using the CPD model and modifying the PCGC-3 code, tar formed from the particle phase may be calculated as the precursor to soot.

### 2.3 Fluid Dynamics

CFD codes solve the complex fluid mechanics and reactions that occur in systems such as pulverized coal boilers. Differential equations (sometimes referred to as transport equations) describe the changes occurring in conserved flow variables:

$$\nabla \cdot (\bar{u} Y_i) = \nabla \cdot (D_i \nabla Y_i) + S_{Y_i} \quad (2.3)$$

This equation describes the steady-state conservation of mass of species  $Y_i$  in any coordinate system. The computer algorithms that solve these equations generally require some form of finite differencing or finite element formulation, and this leads to the discretization of the geometric space into elements of finite volume. Though computations can be performed with unstructured and curvilinear grids, generally with

codes such as PCGC-3 the grids conform to the natural rectangular elements in Cartesian coordinates or the curved rectangular elements in cylindrical systems. Reasonable accuracy can be obtained using finite volume methods (a form of finite differencing), and with the inclusion of boundary conditions, numerous methods exist to obtain a solution to these equations. More information regarding solution techniques to these equations is available (e.g., Patankar, 1980)

Critical to the accurate calculation of the solutions to the transport equations is the inclusion of proper source terms. The source terms indicate the addition of the variable into the volume element from sources other than the neighboring grids. For example, if an equation were derived for the conservation of H<sub>2</sub>O in a CH<sub>4</sub> flame, the source term would need to describe the formation rate of H<sub>2</sub>O from O<sub>2</sub> and CH<sub>4</sub>. Formulation of proper boundary conditions are also essential.

Various forms of the transport equations may be used for combustion purposes to model flow variables such as the velocities, enthalpy, and turbulence variables. An important parameter in PCGC-3 is the mixture fraction. The mixture fraction expresses the ratio of mass coming from the primary stream to that of the primary and the secondary streams:

$$f_M = \frac{m_p}{m_s + m_p} \quad (2.4)$$

The mixture fraction may be used to calculate the local atomic mass content (the mass of carbon, nitrogen, etc.) within a given cell:

$$= {}_p f_M + {}_s (1 - f_M) \quad (2.5)$$

Where  $w_p$  and  $w_s$  represent the atomic mass content of the primary and secondary streams, respectively.  $w$  may be any conserved scalar. Knowing  $w$  for all atomic species and having calculated the enthalpy, an equilibrium code may be used to predict the molecular species present for each value of  $w$ . Based on predictions of the mean and variance of the mixture fraction, and assuming a probability density function distribution, a mean value of  $Y_i$  may be calculated. The fact that an equilibrium code is used to estimate the chemistry restricts the prediction accuracy to mixing-limited cases. This method is explained in more detail by Smoot and Smith (1985).

An additional mixture fraction must be used to account for the gas phase mass originating from the particle phase in coal flame predictions (Smoot and Smith, 1985). An extension of this method that used multiple mixture fractions has recently been developed (Flores, 1995); PCGC-3 contains a second mixture fraction variable option that predicts the mass fraction of char reaction products as well as the mass fraction of coal devolatilization products.

Gas velocities and turbulence parameters are calculated from conservation equations. Accurately predicting these values are essential to flame predictions. Variations of the  $k$ -turbulence model exist which provide a simplified method for predicting turbulence effects, and are widely used in CFD codes.

## **2.4 Summary**

The depth of knowledge required from different fields to develop a comprehensive model of coal combustion is extensive. Because of the complexity, a comprehensive soot

model invariably requires an understanding of many of the working aspects of a coal model.

This research involved the use of a comprehensive coal combustion code (PCGC-3), which is based on much of the theory described in this section. Many researchers over several years have worked to implement the various subroutines. Some PCGC-3 features described in this section are key components of the predictions made in this research. Examples of these are the k- turbulence model, the mixing-limited assumption, the use of two mixture fractions, the discrete ordinates method, and the CPD devolatilization model. Additional details on the code may be found in the users manual for the code (PCGC-3, 1993).

### 3. PREVIOUS WORK

#### 3.1 Soot Radiative Properties

The primary mode of thermal radiation attenuation due to soot is absorption, especially since unagglomerated soot is within the low-scattering regimes. The spectral absorption coefficient is used to describe absorption in a radiatively participating medium. For most gases, this value may be measured by simply passing a length of monochromatic light through gas with a known density. This cannot be done accurately for soot because the soot in the flame is not a gas, and generally undergoes rapid chemical changes. A frequently referenced, simplified method for estimating the spectral absorption coefficient of soot has been developed from theoretical models (Siegel and Howell, 1992):

$$= \frac{C f_{v,C}}{\quad} \quad (3.1)$$

In this equation,  $C$  is a constant developed from Mie theory. This theory describes scattering due to spheres interacting with electromagnetic radiation.  $C$  is dependent on the complex index of refraction, or the simple refractive index and the extinction coefficient. Various methods have been used to measure the radiative properties of soot, with  $C$  values for soot ranging from 3.5-7.0 (Siegel and Howell, 1992; Mengüç and Webb, 1993). Other research gives data that indicate that this model does not completely describe the observations (Siegel and Howell, 1992). Correlations of data suggest that the

absorption coefficient can be better derived by modifying the theoretical equation to include a power-law dependence on  $\lambda$ , as follows:

$$k_{\lambda} = \frac{C}{\lambda^n} f_{v,C} \quad (3.2)$$

Values for  $n$  vary significantly depending on the origin of the soot, the wavelength of the radiation and the measurement technique used.

While Equations 3.1 and 3.2 are a good method of determining the spectral absorption coefficient, often the gray absorption coefficient or the average absorption coefficient over the entire spectrum of radiation is required. Several methods exist for determining the absorption coefficient for wide bands of radiation. Sarofim and Hottel (1978) developed a simplified model for the determination of the emissivity of soot, disregarding the spectral effects. Their gray gas assumption is:

$$k_c = 1 - (1 + 350 f_{v,C} T L_e)^{-4} \quad (3.3)$$

The emissivity may be related to the absorption coefficient through Bouguer's Law:

$$\epsilon_c = -\frac{1}{L_e} \ln(1 - k_c) \quad (3.4)$$

to give:

$$k_c = \frac{4}{L_e} \ln(1 + 350 f_{v,C} T L_e) \quad (3.5)$$

These modeling equations require the specification of a mean beam length. This parameter is used for optically thin gases radiating to an entire boundary, and is based on the assumption of an isothermal cloud and constant soot volume fraction over the entire path length. The value can be reasonably estimated from the furnace geometry:

$$L_e = \frac{4V}{SA} \quad (3.6)$$

This assumption may limit the accuracy in cases with complex geometry, and particularly in combustion cases that are not isothermal with a uniform soot cloud. Kent et al. (1992) illustrates another method for determining the absorption coefficient. It involves Equations 3.1 and 3.4. These equations are combined with Plank's blackbody emission function, integrated over a range of wavelengths, and divided by the total blackbody emission to give an expression for the emissivity over that range of wavelengths:

$$\epsilon_c = \frac{1}{T^4} \int_0^{\infty} E_b(\lambda) (1 - \exp(-L_e)) d\lambda \quad (3.7)$$

Kent et al. likewise suggested a simplified solution for his case:

$$\epsilon_c = 266(C)f_{v,c}T \quad (3.8)$$

A recent comparison of optical properties of soot measurements taken from several different researchers shows significant variability (Mengüç and Webb, 1993). Recent measurements by Majidi et al. (1994), using gas-derived soot, and Rigby (1996), using coal and gas-derived soot, have indicated that the optical properties for soot vary significantly depending on the chemistry of the fuel of origin. This implies that an accurate estimation of the soot radiative properties may require detailed information regarding the chemistry of the soot, which is currently unavailable and beyond the scope of most practical modeling efforts. In the absence of extensive soot radiative property information, generally either a constant value for C must be chosen or one of the simplified absorption coefficient equations must be used.

### 3.2 Soot Formation

In order to determine the optical properties of soot, it is necessary to know its volume fraction, which is often difficult to determine. Radiation models are highly sensitive to the soot volume fraction. Assuming a mean beam length and radiative constants and using Equations 3.3 and 3.7, the cloud emissivity may be calculated. Figure 3.1 shows the emissivities plotted as a function of the soot volume fraction assuming a mean beam length of 1 m and an optical constant  $C$  of 7.0. The Kent et al. (1992) method required numerical integration of Equation 3.7. As seen in Figure 3.1, a few orders of magnitude in soot volume fraction changes the cloud emissivity from non-radiating to nearly a blackbody radiator.

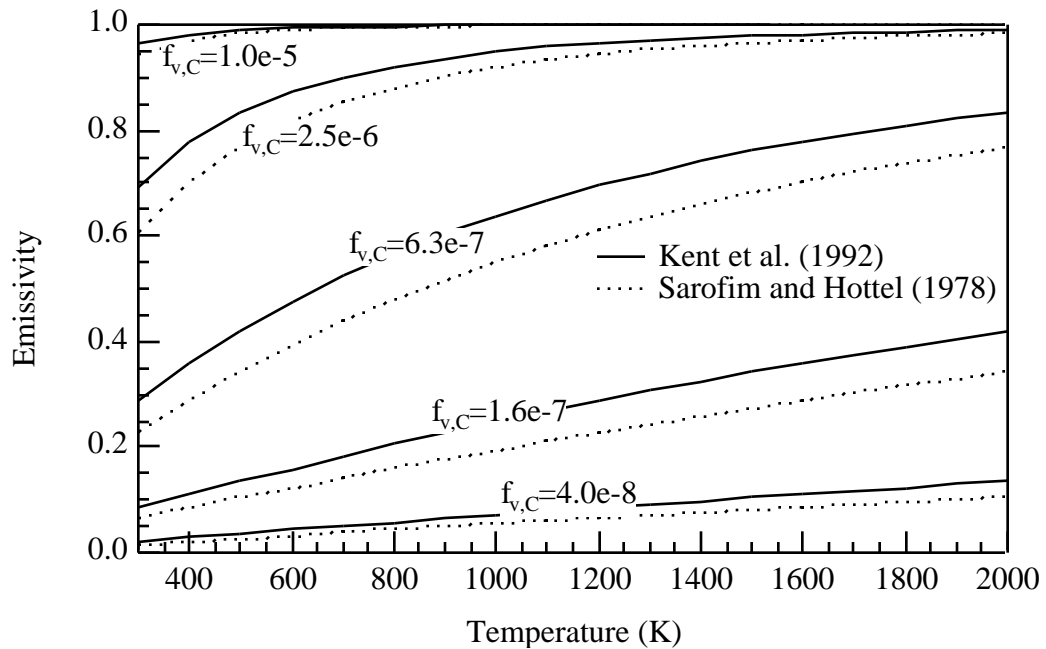


**Figure 3.1** A comparison of two soot emissivity models ( $L_e=1.0$ ,  $C=7.0$ )

A broad range of models have been formulated using a variety of techniques to describe the formation of soot. Perhaps the simplest of the several methods is an

empirical correlation used by Adams (1993). This model for turbulent soot formation relates the soot volume fraction to the local equivalence ratio ( $\phi$ ). Adams assumed that due to oxidation, soot exists where the local equivalence ratio is 1.0 and above, and increases linearly to a maximum value at an equivalence ratio of 2.0 and above:

$$C_2 = \text{Max}(0.0, \text{Min}(Eq - 1.0, 1.0)) \quad (3.9)$$

The maximum soot volume fraction is calculated as a direct function of the amount of volatile carbon found to exist at that point. It was assumed that 10 percent of the volatile carbon forms soot ( $C_1 = 0.1$ ). The soot volume fraction may then be calculated:

$$f_{v,c} = \frac{C_1 C_2}{c} M_C \quad (3.10)$$

The soot volume fraction is then related to the radiative properties using Equation 3.5.

Adams and Smith (1995) concluded that the inclusion of a soot radiation model increases predicted radiative transfer, however the maximum local temperature difference between predictions with and without the soot model was lower than expected (about 50 K). They attributed this to the soot absorbing nearly as much radiant energy as it emits. Also, they suggested the need for a more advanced soot model.

Ahluwalia and Im (1994) took a similar approach, assuming that 10 percent of the volatile carbon given off becomes soot. They restricted the soot to the burner zone. Their results indicate that soot is responsible for between 14 and 15 percent of the total heat transfer in the furnaces modeled. Methods such as these rely heavily on empirical assumptions, and hence, the accuracy of these models is questionable, especially in the absence of any soot data in practical furnaces.

Another technique for modeling soot is to derive complex kinetic expressions for the chemistry of soot. While large kinetic mechanisms can be quite accurate, these

methods are computationally intensive and beyond the capabilities of most current comprehensive modeling codes. Despite the inability of using large mechanisms in comprehensive codes, they still prove useful in comparing to measured data and to benchmarking other reduced mechanisms. Frenklach (1991) developed a model for hydrocarbon flames using detailed kinetics to describe soot formation. He reports a kinetic mechanism with 337 reactions and 70 species. Leung et al. (1991) similarly developed a more simplified kinetic model with 111 reactions. Leung and coworkers also further reduced his model, deriving individual expressions for soot inception, oxidation, and surface growth. The kinetic expressions in these mechanisms assume that soot forms principally from light gases, and would not apply correctly to coal soot which is formed principally from tar. Additionally, the fact that coal devolatilizes from a solid state would complicate the implementation of such a scheme in a comprehensive code.

Moss et al. (1988) developed a more complex relationship for axi-symmetric laminar gaseous diffusion flames using transport equations for the mass fraction, including nucleation, surface growth, and oxidation source terms. Other researchers have recently used variations of this relationship by solving transport equations for soot number density, soot volume fraction and mass fraction of soot (Kennedy et al., 1990; Honnery and Kent, 1992; and Sivathanu and Gore, 1994). The mass fraction of soot is related to the soot volume fraction by the ratio of the average gas density to the average soot density:

$$f_{v,c} = \frac{\rho}{\rho_c} Y_c \quad (3.11)$$

Most of these studies involve the derivation of new estimates for the nucleation, surface growth, and oxidation terms. In a study by Coelho and Carvalho (1994), two different

soot formation models were coupled with three different oxidation models taken from different researchers in an effort to determine which models correspond the best to measured data. These reaction models were coupled with the conservation equations for the number densities and concentrations of soot. Comparisons were made regarding the predictions of soot in a turbulent propane diffusion flame between the various combinations of models and measured data. Recently, more evaluations of this general approach have been performed, including modeling of a turbulent 3-dimensional gas flame (Fairweather et al., 1992; Moss et al., 1995; and Kennedy et al., 1996). In all of these studies, reasonable agreement existed between measured soot volume fractions and predicted ones.

The transport equation method for estimating soot requires several assumptions. Soot is assumed to behave like a continuum (i.e. a gas), and an estimate for the turbulent diffusivity is required. For the formulation of the soot and number density equations, it is necessary to assume that soot is an agglomerate of many linked carbon atoms (i.e. no hydrogen). This is a major assumption behind the simplification of some of the source terms. Since soot is not a gas, oxidation rates for soot are dependent not only on the concentrations of soot and oxidizer, but also on the surface area exposed to the oxidant. This requires knowledge of the particle size, which may be expressed through the average particle diameter. Kennedy et al. (1990) and Bartok and Sarofim (1991) describe a method whereby the need to predict the particle diameter is eliminated. Using a particle number density and assuming a spherical shape, expressions may be written for the particle surface area per unit reactor volume and the volume fraction of soot:

$$SA_v = N_c \left( d^2 \right) \quad (3.12)$$

$$f_{C,v} = \rho_g N_C \frac{d^3}{6} \quad (3.13)$$

By solving Equation 3.13 for the average particle diameter and substituting that into Equation 3.12, the reliance on particle diameter is eliminated in favor of the number of soot particles per unit mass of gas plus soot ( $N_C$ ):

$$SA_{C,v} = 6^{2/3} \rho_g^{1/3} (N_C)^{1/3} f_{v,C}^{2/3} \quad (3.14)$$

The soot volume fraction, average diameter, and number density are dependent variables; if two are known, then the other is automatically specified. Kennedy et al. (1990) assumed an average particle number density ( $N_C$ ) based on the measurements of Axelbaum et al. (1988). Fairweather et al. (1992) extended and improved this technique by including a transport equation expression for the soot number density. The source terms used the same kinetic expression for soot formation, normalizing it by the assumed mass per incipient particle ( $C_{\min} M_C / 2N_a$ ). The constant “2” accounts for the two carbon atoms in each acetylene molecule. They also included a soot agglomeration term. The derivation of this term is described by Ulrich (1971). It is based on the collision frequency for uncharged spherical aerosols of varying sizes (j and k):

$$CF_{jk} = 8 kT \frac{(m_j + m_k)^{1/2}}{m_j m_k} \frac{d_j + d_k}{2} \left( \rho_g N \right)_j \left( \rho_g N \right)_k \quad (3.15)$$

An expression for the relationship between the collision frequency and the rate of change in number of particles is available from the Smoluchowski particle rate equation Ulrich (1971):

$$\frac{d(\rho_g N)}{dt} = Ca \sum_{j=1}^{j-1} \sum_{k=1}^{k=1} (1/2) CF_{k,j-k} + (1/2) \sum_{j=1} CF_{jj} - \sum_{j=1} \sum_{k=1} CF_{jk} \quad (3.16)$$

This equation is reduced assuming only one particle size ( $j = k = 1$ ). Writing an expression for the number of particles per unit mass:

$$N_c = \frac{(6Y_c)}{(d^3)} \quad (3.17)$$

and the mass of a particle:

$$m = \frac{d^3}{6} \quad (3.18)$$

and combining these with Equations 3.15 and 3.16 along with some simple transformations, the following equation used by Fairweather et al. (1992) may be derived:

$$\frac{dN}{dt} = -2Ca \frac{6M_c}{c} \frac{6kT}{c} \frac{Y_c}{M_c} (N_c)^{11/6} \quad (3.19)$$

Kennedy et al. (1996) includes an additional multiplying factor of 2 in this equation. They added an OH oxidation term in their soot model and upon recalibrating the equations they discovered that this empirical factor improved model agreement with measurements.

### 3.3 Summary

Coal derived soot modeling has been attempted in the past, but the models are empirical and thus unacceptable, particularly in light of the recent improvements in gas derived soot models which appear to reasonably predict soot formation. Within a typical furnace, volume fractions vary by several orders of magnitude. Optical constants are similarly uncertain, but probable upper and lower limits of  $C$  typically differ by a factor of 2 to 3 (Rigby, 1996). Since absorption coefficients depend equally on the soot volume fraction and the optical constants (see Equation 3.1), it is apparent that the accurate

prediction of the soot volume fraction is of primary importance to soot radiative predictions, particularly coal-derived soot.

#### **4. OBJECTIVES**

The primary objective of this research is to develop an improved model to describe the formation and destruction of coal-derived soot. The focus of the improvements is on the accurate determination of the soot volume fraction. Improved capabilities for modeling the soot volume fraction should provide greater model accuracy.

Performance of the model is primarily based on the ability to accurately predict the local amount of soot. The accuracy of the new model predictions are validated by comparing predictions to existing soot, gas temperature and  $\text{NO}_x$  concentration measurements. Comparing model predictions with and without the presence of soot indicates the resulting impact on predictive capabilities. Also, comparisons between existing soot models give insights into the relative performance of the various models. Additional performance criteria include estimations of the increased computational load, the numerical stability, and the ability to converge based on the addition of the soot model.

## 5. METHOD

### 5.1 Approach

This research extends the approach of Moss et al. (1988) and Fairweather et al. (1992) to coal-derived soot by generating the proper conservation equations, source terms, and boundary conditions for the 3-dimensional calculation of coal-derived soot mass fraction, soot particles per unit (total) mass, and tar mass fraction ( $Y_C$ ,  $N_C$ , and  $Y_T$  respectively). The boundary conditions for the conservation equations of soot mass fraction, tar mass fraction, and the soot particles per unit mass are similar to the boundary conditions for other flowfield variables such as the coal gas mixture fraction ( $\phi$ ) and the mixture fraction variance ( $g$ ). Table 5.1 lists these boundary conditions:

**Table 5.1**

**Boundary Conditions for the Soot Conservation Equations.**

<i>Location</i>	<i>Soot Mass Fraction</i>	<i>Tar Mass Fraction</i>	<i>Soot Particles per Unit Mass</i>
Primary Jet	0.0	0.0	0.0
Secondary Jet	0.0	0.0	0.0
Walls	$d/dx = 0.0$	$d/dx = 0.0$	$d/dx = 0.0$
Outlet	Quadratic Extrapolation	Quadratic Extrapolation	Quadratic Extrapolation
Symmetry Plane	$d/dx = 0.0$	$d/dx = 0.0$	$d/dx = 0.0$

Detailed descriptions of the treatment of boundary conditions are contained elsewhere (PCGC-3 Users Manual, 1993; Smoot and Smith, 1985). In all of these variables, the ‘per mass,’ or fractional mass, represents the total mass of solids and gas in a given cell.

Initially, an average soot number density was assumed following Kennedy et al. (1990), but preliminary examinations indicated that detailed calculations of the local number density might be important to assure the accuracy of the model. Some axi-symmetric models in the literature have included a thermophoretic velocity in the diffusion term. No instance of this term being used is found in the literature on three-dimensional soot equations, and this is suspected to be an intentional omission due to the increased numerical difficulty. The equations for conservation of the mass of soot and tar are as follows:

$$\bar{\rho} \cdot \left( \bar{u} Y_C \right) = \bar{\rho} \cdot \frac{\mu}{Sc_C} Y_C + S_{Y_C} \quad (5.1)$$

$$\bar{\rho} \cdot \left( \bar{u} Y_T \right) = \bar{\rho} \cdot \frac{\mu}{Sc_T} Y_T + S_{Y_T} \quad (5.2)$$

The equation for conservation of number of soot particles is:

$$\bar{\rho} \cdot \left( \bar{u} N_C \right) = \bar{\rho} \cdot \frac{\mu}{Sc_N} N_C + S_{N_C} \quad (5.3)$$

Where  $\mu$  is the turbulent viscosity,  $Sc$  is the turbulent Schmidt number,  $\bar{\rho}$  is the time-averaged density, and  $\bar{u}$  represents a directional component of the Favre-averaged velocity. Values for the Schmidt number are 700 for the soot mass fraction ( $Y_C$ ) and particles per unit mass equation ( $N_C$ ). These values are the standard values used for soot transport equations in hydrocarbon flames (Fairweather et al., 1992; Sivathanu and Gore, 1994). For the tar mass fraction equation ( $Y_T$ ), 0.7 was assumed for the Schmidt number, which is the value commonly assumed for the gas phase Schmidt number (Sivathanu and Gore, 1994).  $S$  represents the source terms for each transport equation. Soot and tar source terms were derived based on the assumed pathways illustrated in Figure 2.1. The

source terms for the particles per unit mass were derived following Fairweather et al. (1992). The contribution of light gases to the formation of soot has been neglected in the development of this model, as well as oxidation by OH. Also, surface growth by tar molecules and other light gases has been neglected. The following are the source term equations used in this research:

$$S_{Y_C} = \text{Formation}_C - \text{Oxidation}_C \quad (5.4)$$

$$S_{Y_T} = \text{Formation}_T - \text{Formation}_C - \text{Gasification}_T - \text{Oxidation}_T \quad (5.5)$$

$$S_{N_C} = \frac{N_a}{M_C C_{\min}} \text{Formation}_C - \text{Agglomeration}_N \quad (5.6)$$

where:

$$\text{Formation}_T = SP_{tar} \quad (5.7)$$

$$\text{Oxidation}_T = [c_T][c_{O_2}]A_{OT}e^{-E_{OT}/RT} \quad (5.8)$$

$$\text{Gasification}_T = [c_T]A_{GT}e^{-E_{GT}/RT} \quad (5.9)$$

$$\text{Formation}_C = [c_T]Ae_{FC}e^{-E_{FC}/RT} \quad (5.10)$$

$$\text{Oxidation}_C = SA_{v,C} \frac{P_{O_2}}{T^{1/2}} A_{OC}e^{-E_{OC}/RT} \quad (5.11)$$

$$SA_{v,C} = \frac{6^{2/3} \cdot 1/3 \left( \frac{N_C}{g} \right)^{1/3} Y_C^{2/3} \cdot 2/3}{\frac{2/3}{C}} \quad (5.12)$$

$$\text{Agglomeration}_N = 2Ca \frac{6M_C}{C}^{1/6} \frac{6kT}{C}^{1/2} \frac{Y_C}{M_C}^{1/6} \left( \frac{N_C}{g} \right)^{11/6} \quad (5.13)$$

In these equations and throughout this research, the average carbon soot density is assumed to be 1950 kg/m<sup>3</sup>. Following Fairweather et al. (1992), 3.0 is assumed to be the value of the collision constant (Ca). Table 5.2 gives a description of the Arrhenius constants used.

**Table 5.2****Transport Equation Source Terms.**

<i>Term</i>	<i>A</i>	<i>E (kJ/g-mol)</i>	<i>Source</i>
Formation <sub>T</sub>	N/A	N/A	Particle Phase Calculations
Oxidation <sub>T</sub>	6.77x10 <sup>5</sup> (1/s)	52.3	Shaw et al. (1990)
Gasification <sub>T</sub>	9.77x10 <sup>10</sup> (1/s)	286.9	Ma (1996)
Formation <sub>C</sub>	5.02x10 <sup>8</sup> (1/s)	198.9	Ma (1996)
Oxidation <sub>C</sub>	1.09x10 <sup>4</sup> (K <sup>1/2</sup> /s)	164.5	Lee et al. (1962)
A <sub>o</sub>	N/A	N/A	Kennedy et al. (1990)
Agglomeration <sub>N</sub>	N/A	N/A	Fairweather et al. (1992)

Once the value of  $Y_C$  has been calculated from Equation 5.1, the soot volume fraction may be calculated using Equation 3.11. The absorption coefficient may then be determined using Equation 3.5 or 3.1. This absorption coefficient is then summed with the calculated absorption coefficient for the radiating gases (i.e., CO<sub>2</sub> and H<sub>2</sub>O) to form a total absorption coefficient:

$$\alpha_{cell} = \alpha_{gases} + \alpha_{soot} \quad (5.14)$$

This research uses Equation 3.5 to determine the absorption coefficient.

Tar yields are calculated from the particle phase, which uses the CPD model (Fletcher et al., 1992) to determine devolatilization rates. When <sup>13</sup>C NMR data were not available as input parameters to the CPD model, a correlation was used to determine these parameters based on elemental composition (Genetti and Fletcher, 1997). The reaction rates of coal volatiles with oxygen for different coals were measured by Shaw et al. (1990) and fit with a global one-step model. Since one aim of this research is to develop a comprehensive model, and their data do not cover all of the coals, the rate constants were

averaged to obtain the rate reported in Table 5.2. The error induced as a result of this assumption is difficult to ascertain. However, it is possible that much of the tar for many flames is released in a fuel rich region and that the majority is converted to soot before it is oxidized. Currently, the tar release from the CPD model is only used for determining the soot. The combustion of tar is treated using the mixture fraction approach, which does not calculate detailed chemistry for every gas species.

It should be noted that the number of soot particles per unit mass ( $N_C$ ) only impacts the oxidation rate for soot. Soot yield predictions in a non-oxidizing environment are not significantly affected by  $N_C$ .

In order to maintain robustness of the model, several additional constraints were added to the model. The soot mass fraction variable ( $Y_C$ ) would occasionally be predicted slightly above 1.0 or slightly below 0.0 during the early stages of convergence. Also, the tar mass fraction variable would occasionally drop below 0.0 under similar circumstances. These conditions cause numeric problems in the source terms, so precautions are taken against these occurring. Similar constraints were placed on the  $N_C$  equation. The upper limit was selected to be  $1.0 \times 10^{20}$  and the lower limit was 0.0. The upper limit was selected based on a rough calculation because it represented approximately the number of incipient sized particles that would fill half of the volumetric space. Prior to the calculation of the soot mass fraction ( $Y_C$ ), negative values of tar and soot mass fractions ( $Y_C$  and  $Y_T$ ) are changed to 0.0 and soot mass fractions ( $Y_C$ ) greater than 1.0 are reduced to 0.5. Prior to the calculation of  $N_C$ , the variable is constrained similarly. Also, within the tar mass fraction and soot particles per unit mass source terms ( $Y_T$  and  $N_C$ ), the tar and soot mass fractions ( $Y_C$  and  $Y_T$ ) are specified as an absolute value. Occurrences of

these violations of constraints are monitored by a progress variable, and indication of these violations are printed to the log file, which tracks convergence and intermediate output. The lower limit on the  $N_C$  equation was never violated in the process of convergence of any cases.

The soot model developed here was included in the PCGC-3 code. This involved the addition and modification of numerous subroutines. Table A.1 in the Appendix gives a list of the modified and new subroutine names. FORTRAN code for the new subroutines developed for this model are included in Appendix B.

## 5.2 Validation

In order to validate the model, predictions are compared with measured values of soot yield, gas temperature, and  $NO_x$  concentration. It was expected that the model would give reasonable soot yields, and that  $NO_x$  and temperature predictions near the burner would agree with measured values. Since  $NO_x$  is generally in non-equilibrium as a combustion intermediate,  $NO_x$  can not be estimated properly using the mixing limited assumption and equilibrium code. To circumvent this problem, PCGC-3 uses a  $NO_x$  post-processor which is capable of more accurately predicting  $NO_x$  based on a chemical kinetics scheme and the converged predictions from the equilibrium based code (Boardman et al., 1993; Hill et al., 1984).

The model of Adams and Smith (1995) was also coded for comparison purposes. Preliminary comparisons of the two models showed the Adams and Smith (1995) model predicted high soot yields in regions of high tar yield. It was postulated that the method

of the Adams and Smith (1995) soot model could be modified to predict a mass fraction of tar rather than a soot volume fraction:

$$Y_T = C_1 C_2 M_{C \text{ } c \text{ } g} \quad (5.15)$$

A simple test indicated that tar yields using this equation were on the order of tar yields from Equation 5.2. This option was coded and is presented as an alternative. Another alternative considered was to assume an average number density, in a manner similar to Kennedy et al. (1990). The average value used for the number density ( $N_C$ ) by Kennedy et al. (1990) and in this research was  $1 \times 10^{16}$  particles/m<sup>3</sup>.

To validate the model, measurements from three coal combustion test cases of different scale were obtained. More detailed descriptions of these three experiments are given below.

### 5.2.1 Flat Flame Burner

The Flat Flame Burner (FFB) is a laminar flow reactor at BYU. Premixed fuel-rich methane and air are uniformly injected through a 5cm x 5cm honeycomb grid. The gases ignite, forming a uniform, thin flame sheet. Coal particles are injected through a narrow 3mm diameter tube in the center of the burner slightly above the tip of the flame sheet (Figure 5.1) at a velocity of approximately 2.6 m/s. Primary nitrogen was injected at a rate of 1.95 standard liters per minute and the CH<sub>4</sub> and air were injected in the secondary air at 5.47 and 40.18 standard liters per minute respectively. An equivalence ration of 1.3 was reported for this flame. The coal particles used in the experiment were sieved to maintain sizes between 75 and 63 μm. The hot product gases cause the coal to devolatilize without the occurrence of oxidation. A suction probe is placed above the

flame, which collects the char and soot. The char and soot are separated aerodynamically using a virtual impactor and cyclone system. Total soot yields were measured as a function of the height of the probe above the burner surface by Ma (1996; see also Ma et al, 1996a). These data include measured temperature profiles at various heights and axial positions, char and soot yields from the coal at various heights, and particle and gas velocity measurements at various locations. This apparatus was modeled with a 25x25x28 grid using PCGC-3, assuming laminar flow by not using the k- turbulence model. The cases modeled were the Pittsburgh #8, Illinois #6 and Utah Hiawatha coals at 1800 K. More details on the FFB are available in Appendix D. This case provided a means to test the soot formation model in PCGC-3 in a simple geometry without the complexity of oxidation. The other two cases (described next) include soot oxidation.

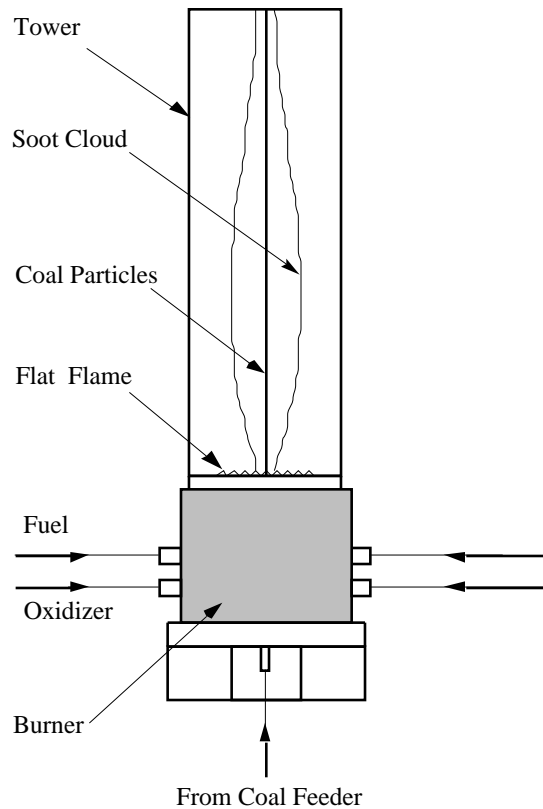


**Figure 5.1** A schematic of the flat flame burner (From Ma, 1996).

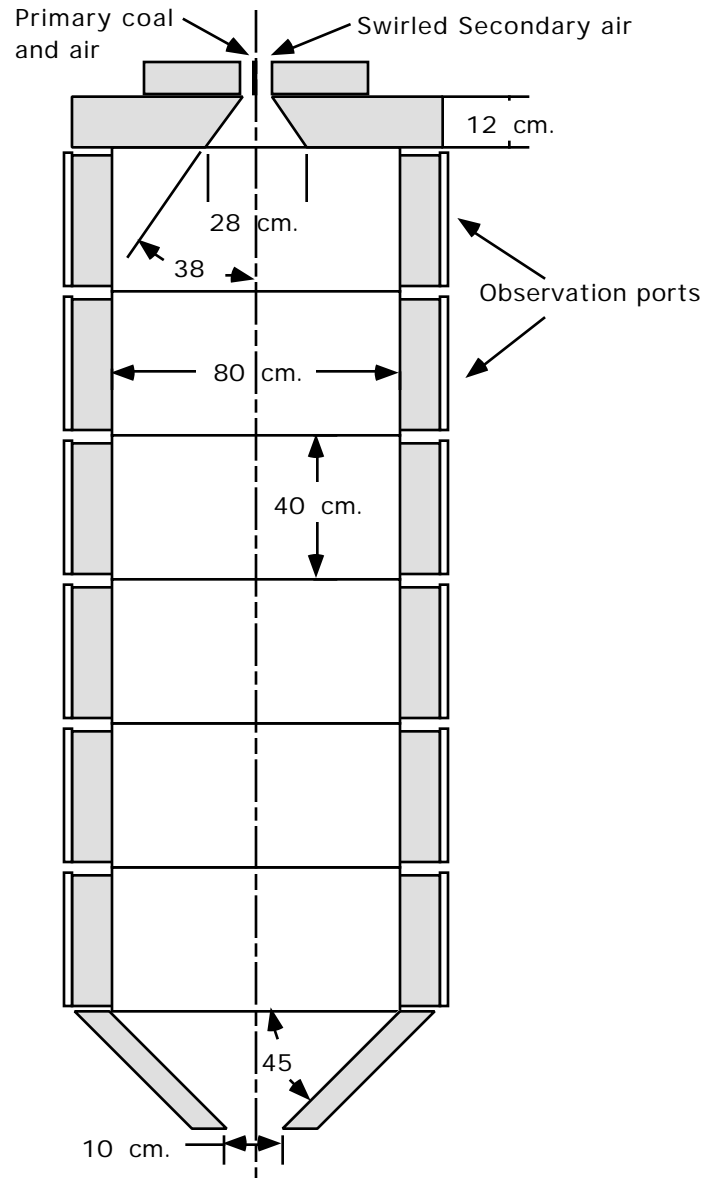


**Figure 5.2** A schematic of the controlled profile reactor.

### 5.2.2 Controlled Profile Reactor

The Controlled Profile Reactor (CPR) is a laboratory scale furnace that was designed specifically to measure coal flame parameters (Figure 5.2). The reactor is axi-

symmetric, which allows 2-dimensional model predictions. The symmetry potentially reduces the computational requirements. Measurements of various gas species concentrations in the CPR have been documented by Sanderson (1993). Also, Butler (1992) measured particle and gas temperature profiles in the CPR, as well as heat fluxes at various locations. This research has modeled Case 5 from these sources using a 49x49x69 grid. This lean case included a secondary swirl of 1.4, coal flow rate of 11.4 kg/hr, mass-mean particle size of 55 $\mu$ m, primary air flow rate at 289 K of 15 kg/hr, and secondary air flow rate at 533 K of 127 kg/hr. The fuel used was Utah Blind Canyon hvB bituminous coal. The CPR is further characterized in Appendix D.

### 5.2.3 Fireside Performance Test Facility

The ABB/CE Fireside Performance Test Facility (Figure 5.3) is a cylindrical laboratory scale furnace which was also used to make gas species concentration and temperature measurements (Thornock et al., 1993). Test 5, a lean ( $\phi = 0.83$ ) Ashland (West Virginia) hvA bituminous coal flame, was modeled using a 69x57x44 grid. The mass mean particle size was 41.9 $\mu$ m, coal feed rate was 118 kg/hr, primary air rate was 100kg/hr, and secondary air feed rate was 1360 kg/hr. The secondary air was modeled with a swirl number of 1.2. A major issue in the development of this grid was the inlet conditions. The tests were run with an insert in the secondary tube that constricted and then expanded the secondary flow between the swirl generators and the exit from the tube. An accurate representation of this configuration would have required a significantly finer grid resolution around the inlet area of the burner. This was not done in the interest

of both time and feasibility. The computers that were running this case were near the limits of memory, and adding the extra cells would have caused memory overflow on many of the machines and made the calculational time required significantly longer on the others. A more detailed characterization of the FPTF model is given in Appendix D.

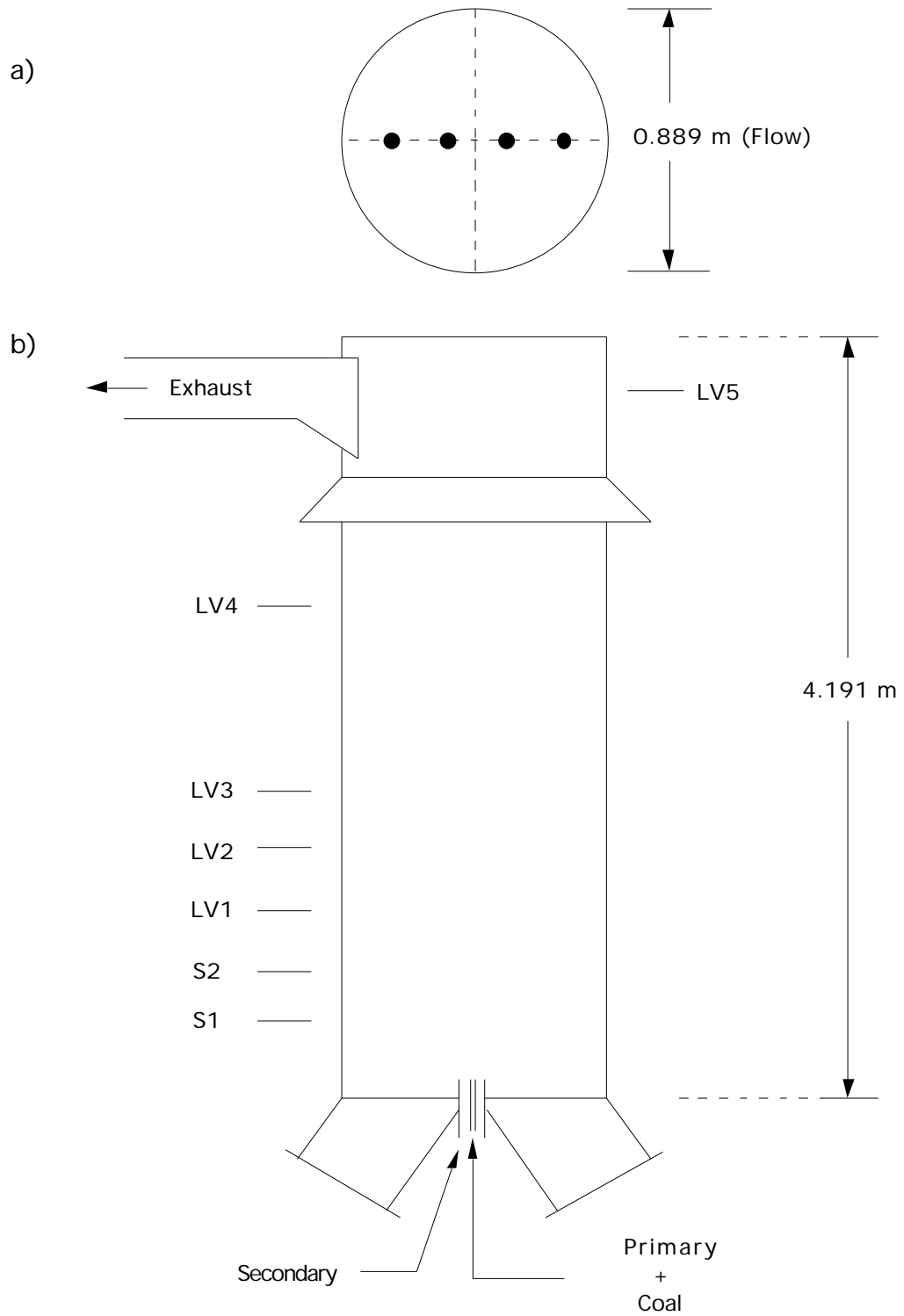


**Figure 5.3** A schematic of the fireside performance test facility (from Flores, 1996). The view labeled ‘a’ is a top view, with the major measuring points marked. View ‘b’ is a side view with measurement heights labeled.

## 6. RESULTS

### 6.1 Flat Flame Burner

The FFB model was by far the easiest of the three selected cases to model. Laminar fluid flow and the small, simple dimensions of the apparatus allowed for reasonably good predictions of the measured temperature profiles and velocities. A large source of error for this case is probably the predictions for the premixed methane-air secondary stream. Because PCGC-3 assumes the flames are mixing limited, as soon as these gases enter the flow field, they revert to equilibrium product form. In the actual burner, a flame sheet is formed above the honeycomb grid inlet which is several millimeters thick. Another possible source of error is the estimation of inlet temperatures. These were taken to be roughly room temperature. It is probable that some preheating of the gases occurred in the inlet section of the burner apparatus. Assumed wall temperatures, wall emissivities, and inlet velocities may be other sources for error. Walls in this reactor consisted of quartz windows, transparent in the visible spectrum. Since PCGC-3 is incapable of modeling transparent walls, the walls were modeled as solid 700 K walls with a 0.8 emissivity. Finally, the primary inlet was limited to one small node point. This may have caused some grid resolution problems which appeared in the predicted centerline temperature field. Figure 6.1 shows temperature measurements compared with the predicted temperatures at the centerline and two nodes to one side of the centerline node. Since the measurements would be incapable of

resolving a gradient in such a narrow geometric region (approximately 1.2 mm thick nodes), the temperatures from two adjacent nodes were weighted and averaged with the centerline temperature.

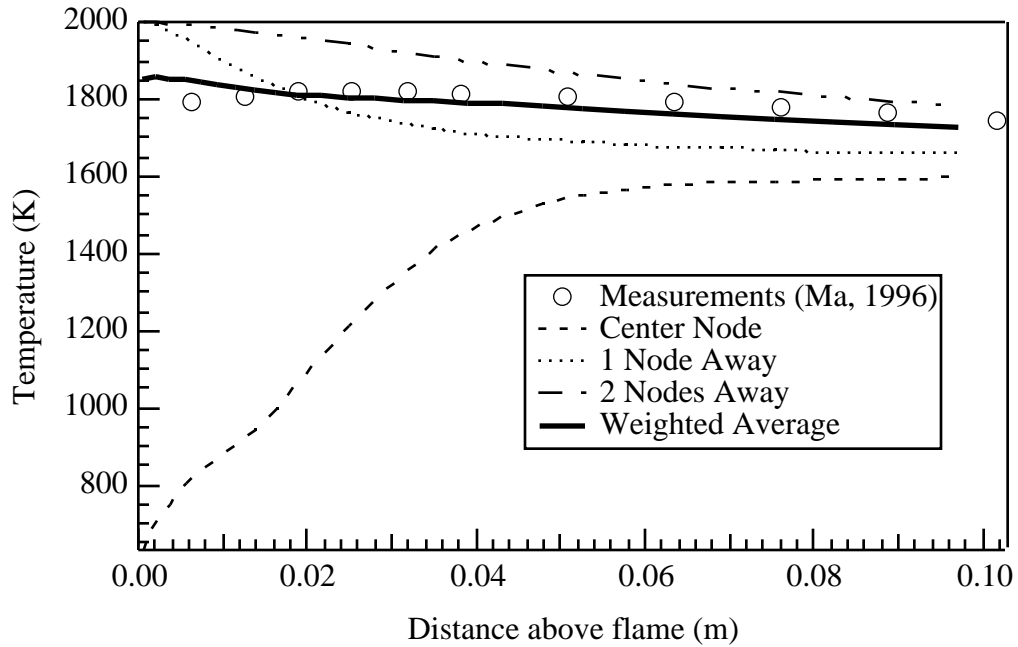


**Figure 6.1 A comparison of centerline temperature measurements and predictions for the FFB.**

With the noted exception at the centerline node, all predicted temperatures corresponded well to the measured temperatures from Ma (1996). The temperature measurements were taken without coal being injected into the burner, and the impact of the coal on the resulting temperature was assumed to be minimal. Modeling efforts confirmed this assumption. This case was modeled with and without considering soot, and the total radiative heat flux at the wall was observed to be equal to within 0.5 percent for either case. This is an indication that the gas temperatures and  $\text{NO}_x$  concentrations are not significantly affected by the inclusion of soot.

### 6.1.1 Soot Formation Predictions

Figures 6.2 to 6.6 illustrate the predicted and measured yields of soot from the three high volatile bituminous coals used in the experiments. Predictions of tar yield and soot plus tar have been plotted in these figures as well for illustrative purposes. <sup>13</sup>C NMR data were only available for the Pittsburgh #8 and the Illinois #6 coals. The correlation of Genetti and Fletcher (1997) was also used to make predictions for all three coals.

In Figures 6.2 to 6.6, the predictions close to the inlet are consistently below the measured values. This is probably due to the previously explained possibilities for error in the model. Another possible source is that the reported tar-to-soot conversion rate is slightly low. Also, soot samples were collected in a suction probe which was lowered into the flat flame burner reaction chamber. The probe used a nitrogen quench to cool the combustion products to a lower temperature which inhibited the chemical reactions, making measurements possible. The probe is lowered to the indicated height, but the quench may not actually take place until the nitrogen stream had mixed well with the combustion gases. Predictions, however, match the experimental data well at an axial position of greater than 0.05 m above the inlet, where the model predicts that the tar has largely reacted. The data and model both predict very little change in yield as a function of height after 0.05 m. The figures indicate that the model was capable of predicting the total soot yield within a maximum error of +/- 10 percent (absolute) for the cases performed using the correlation and within +/- 5 percent (absolute) for the cases performed using the raw NMR data for NMR input parameters to the CPD model.

The worst predictions are for the Pittsburgh #8 coal using the correlation. This is due to a significant variance in the predicted  $^{13}\text{C}$  NMR properties using the correlation of Genetti and Fletcher (1997) compared to the measured values for this coal. The Pittsburgh #8 coal was used to generate the correlation, and this coal was one of several coals that were not well described by the correlation. The best predictions are for the Illinois #6 coal using the measured  $^{13}\text{C}$  NMR data. The Pittsburgh #8 coal predictions using the measured NMR data, the Illinois #6 coal predictions using the correlation, and the Utah Hiawatha predictions using the correlation all predict reasonable soot yields when compared with the measurements.

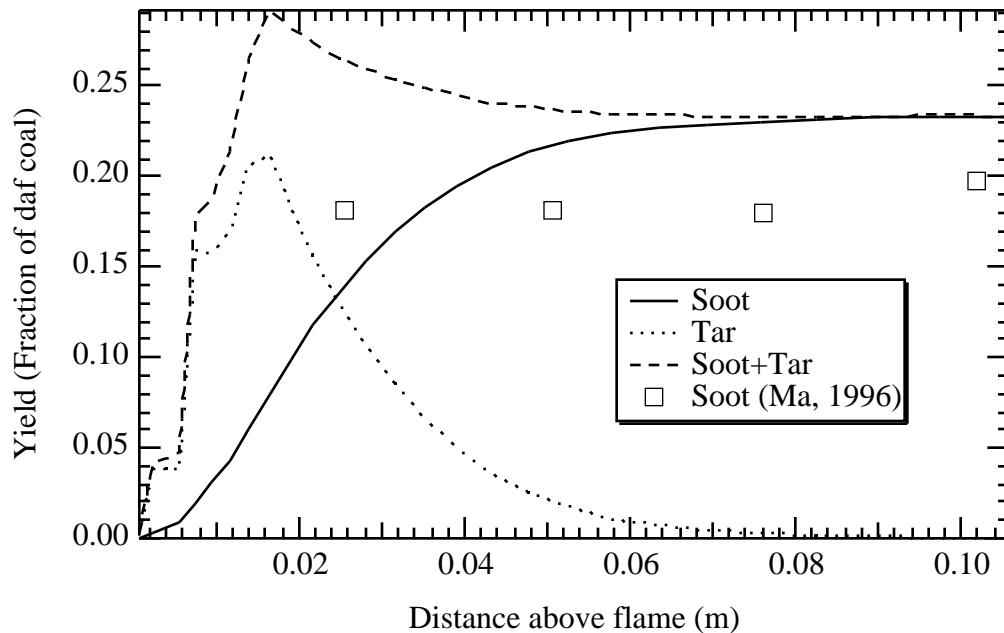


**Figure 6.2** A comparison of predicted and measured soot yields in the FFB for a Pittsburgh #8 coal using measured NMR parameters.

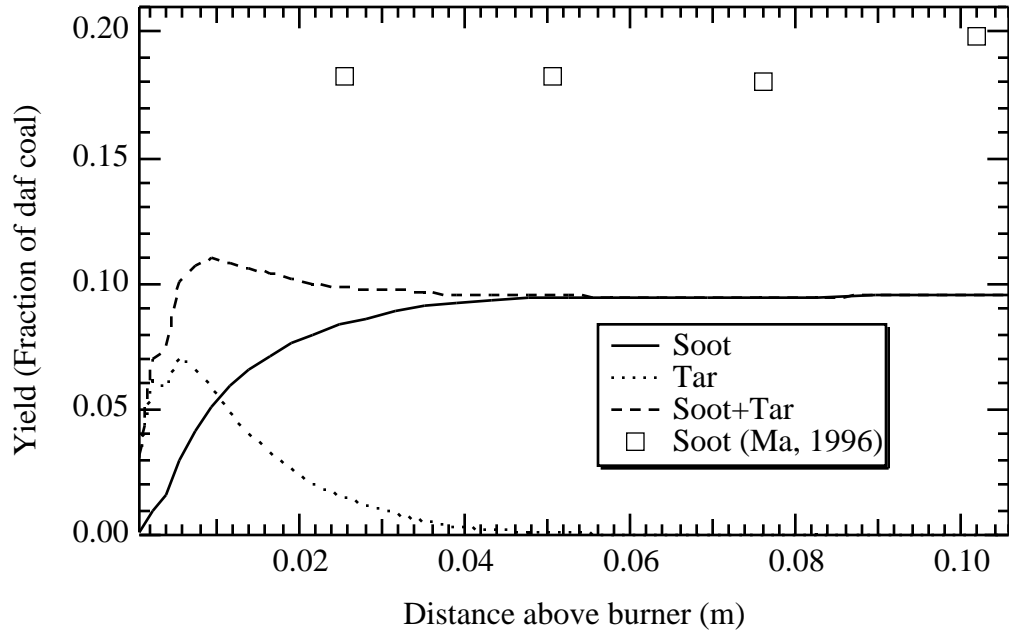


**Figure 6.3** A comparison of predicted and measured soot yields in the FFB for a Pittsburgh #8 coal using the correlation of Genetti et al. (1997).

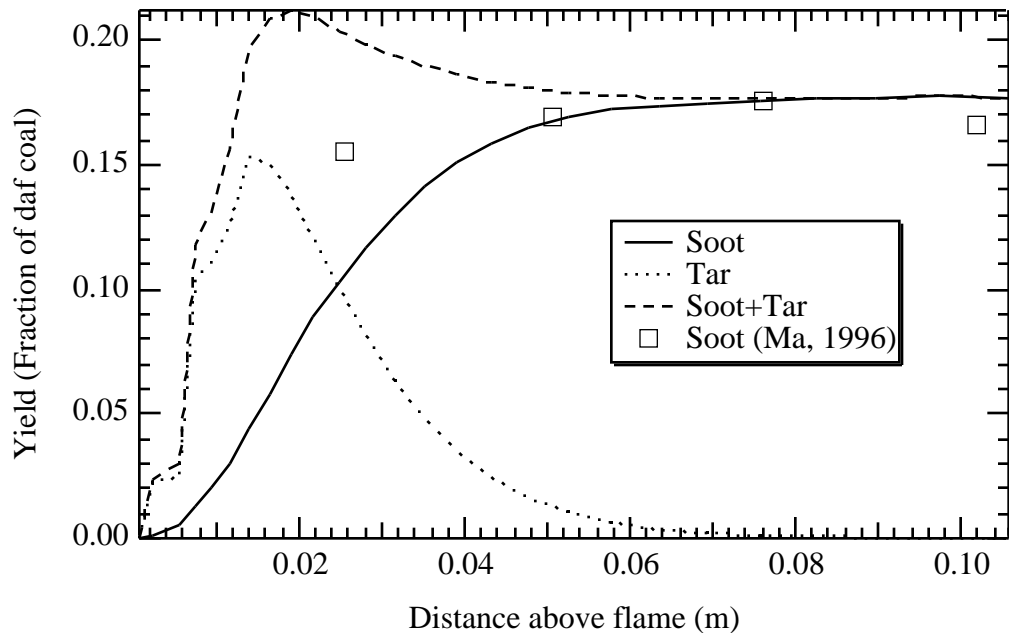


**Figure 6.4** A comparison of predicted and measured soot yields in the FFB for an Illinois #6 coal using measured NMR parameters.

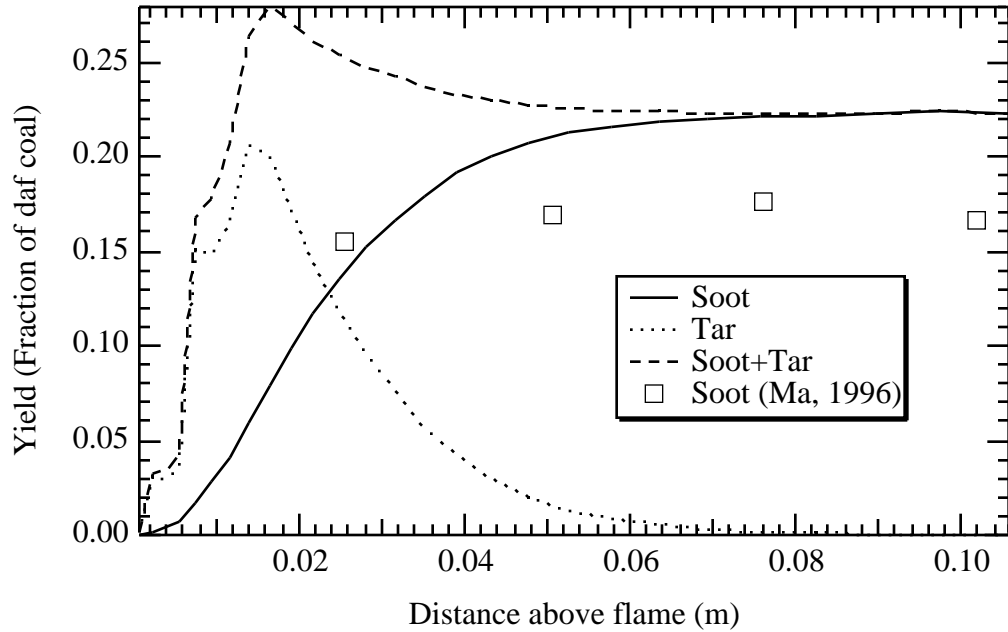


**Figure 6.5** A comparison of predicted and measured soot yields in the FFB for an Illinois #6 coal using the correlation of Genetti et al. (1997).

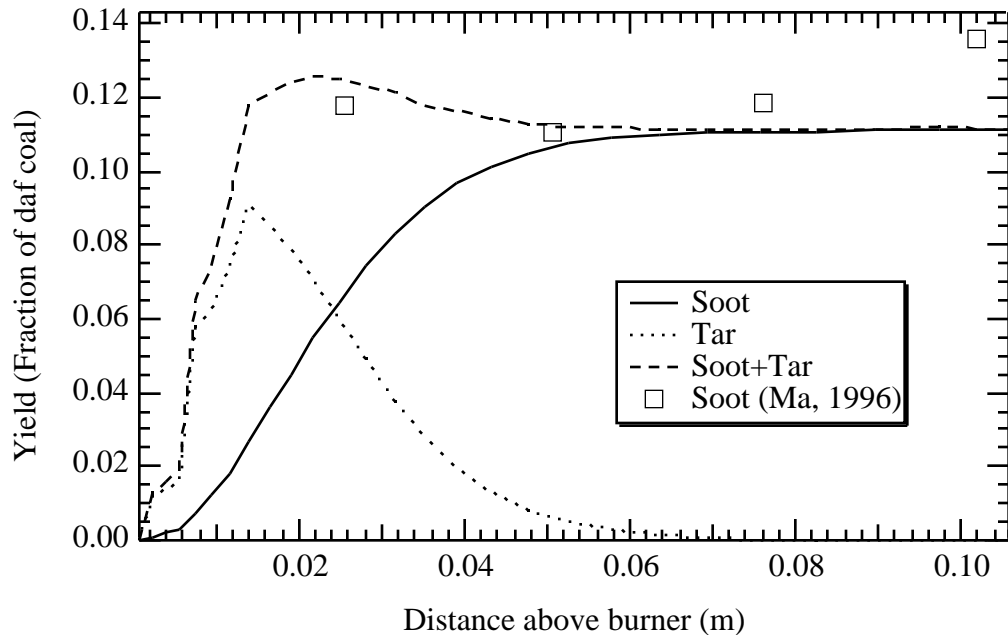


**Figure 6.6** A comparison of predicted and measured soot yields in the FFB for a Utah Hiawatha coal using the correlation of Genetti et al. (1997).

### 6.1.2 Soot Particle Size Predictions

The predicted values of the soot particles per unit mass ( $N_C$ ) in the FFB are interesting, even though  $N_C$  has no effect on the soot yield in this pyrolysis-only case. Mean particle sizes were not reported, but experimental data showed an increase in total yield of particles greater than 5  $\mu\text{m}$  with increasing height. For all coals, the mass fraction of soot greater than 5  $\mu\text{m}$  transitions from 0.0 at 2.54 cm to greater than 50.0 percent of the total soot yield at 10.2 cm. These data indicate that at some point between 2.54 cm and 10.2 cm the mass average particle diameter should approach or cross the 5  $\mu\text{m}$  threshold.

Based on the soot volume fraction ( $f_{v,C}$ ) and the soot particles per unit mass ( $N_C$ ), an average particle diameter ( $d$ ) can be calculated (Equations 3.12 and 3.13). Figures 6.7 to 6.9 show these calculations performed at the centerline in the FFB. The best available NMR parameters for the three modeled cases were used to generate these figures. The results indicate that the model for the soot particles per unit mass predicts the general expected trend based on the average soot diameter observations of Ma (1996). The other variables ( $f_{v,C}$  and  $N_C$ ) are plotted as well to indicate both centerline trends and typical predicted values for these variables.

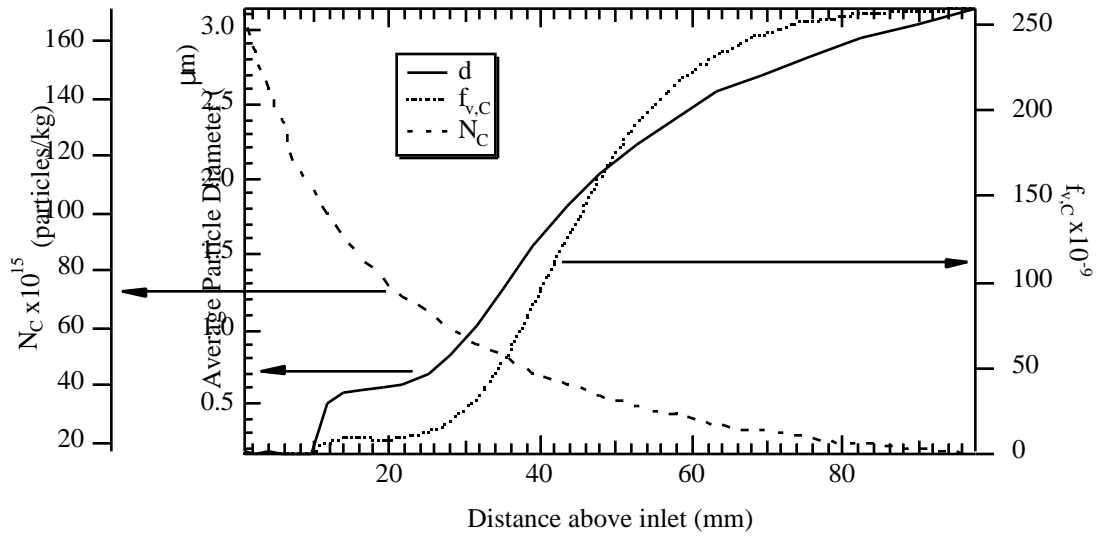


Figure 6.7 FFB centerline node  $d$ ,  $f_{v,C}$  and  $N_C$  predictions for a Pittsburgh #8 coal.

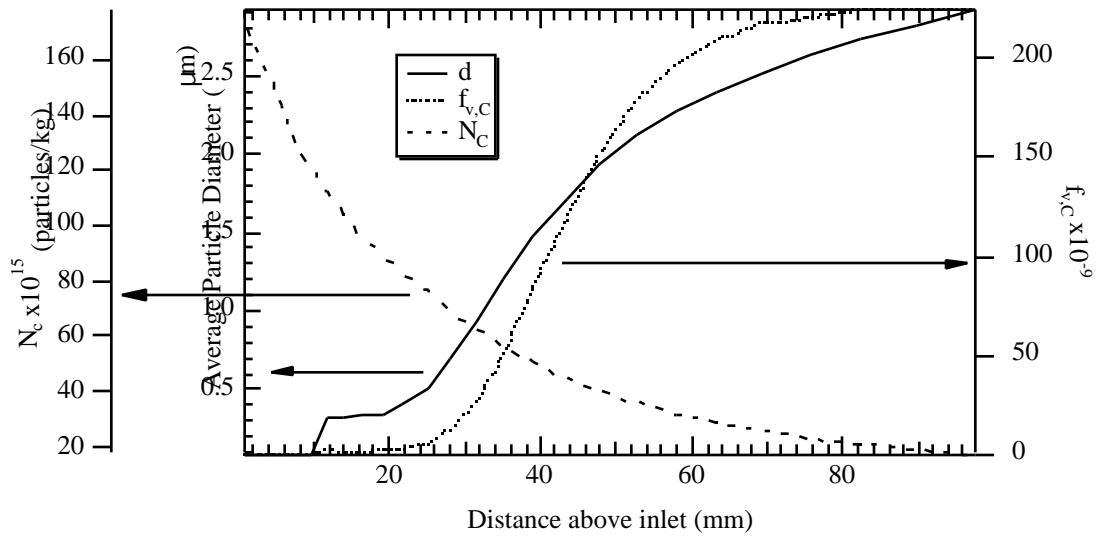
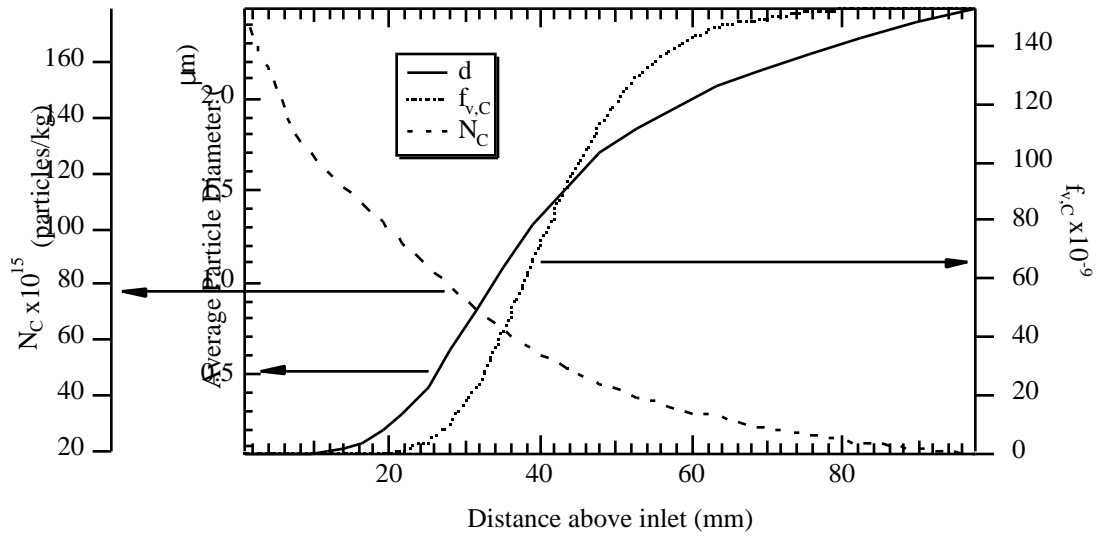


Figure 6.8 FFB centerline node  $d$ ,  $f_{v,C}$  and  $N_C$  predictions for an Illinois #6 coal.



**Figure 6.9** FFB centerline node  $d$ ,  $f_{v,C}$  and  $N_C$  predictions for a Utah Hiawatha coal.

In Figures 6.7 to 6.9, the predicted average particle diameters are close to the expected values based on the observations of Ma (1996). The calculated diameter is a number-based average as opposed to a mass-based average in the experiments; therefore, these predictions are thought to agree well with the available data. It is recognized that a distribution of soot agglomerate sizes exists in the experiment, but only a mean diameter is predicted in this research. The values for the soot particles per unit mass ( $N_C$ ) is within an expected range; since  $\rho_g$  is on the order of  $1.0 \text{ (kg/m}^3\text{)}$ , the average soot number density ( $\rho_g N_C$ ) is predicted to within two orders of magnitude of the  $1 \times 10^{16}$  assumed as an average from the measurements of Axelbaum et al. (1988).

### 6.1.3 Convergence Time

To quantify the convergence time penalty incurred on the comprehensive model predictions due to the inclusion of the soot model, the time this case required to perform one macro-iteration was observed. Due to the multi-tasking nature of the operating system, even under ideal conditions using identical starting conditions, times were not completely repeatable. Several runs were subsequently timed, and the averages of the times required to complete this macro-iteration are reported in Table 6.1. The total convergence time penalty may be under-represented by the estimates in this table. This would be the case if one of the soot variables were the most difficult to converge. Adding the most complete soot model in this timing test represents a 55 percent increase in run time.

**Table 6.1**

**Single Macro-iteration Run Times in the FFB.**

Model	Full (3 transport equation) Model	No Soot Considered
Time	10.74 Minutes	6.93 Minutes

### 6.1.4 Predicted Contours

A final result which validates the model is the predicted appearance of the soot cloud. Higher soot volume fractions would be characterized by higher luminescence. Ma (1996) reported the luminous soot cloud to be approximately 2.5 cm in diameter at the maximum point for the FFB. Figures 6.10 to 6.12 show predicted contours for the soot, tar, and  $N_C$  at a centerline cross section for an Illinois #6 coal using the correlation. The predicted soot cloud of 0.9 cm in width is narrower than the reported observation, possibly due to (a) the omission of the thermophoretic velocity term or (b) the failure to

consider radial velocities caused by rapid devolatilization or (c) both. These plots represent the predictions across a complete cross-section. Only slight variations exist between predictions on either side of the centerline (at about 0.0254 m). The soot particles per unit mass predictions in Figure 6.12 are unusually high in the near burner region and in the region near the wall where the value of the soot volume fraction in Figure 6.10 is predicted to be quite low. This is thought to be due to the omission of an important source term in the  $N_C$  transport equation. The problem is more apparent in the FPTF, and will be discussed in greater detail in that section.

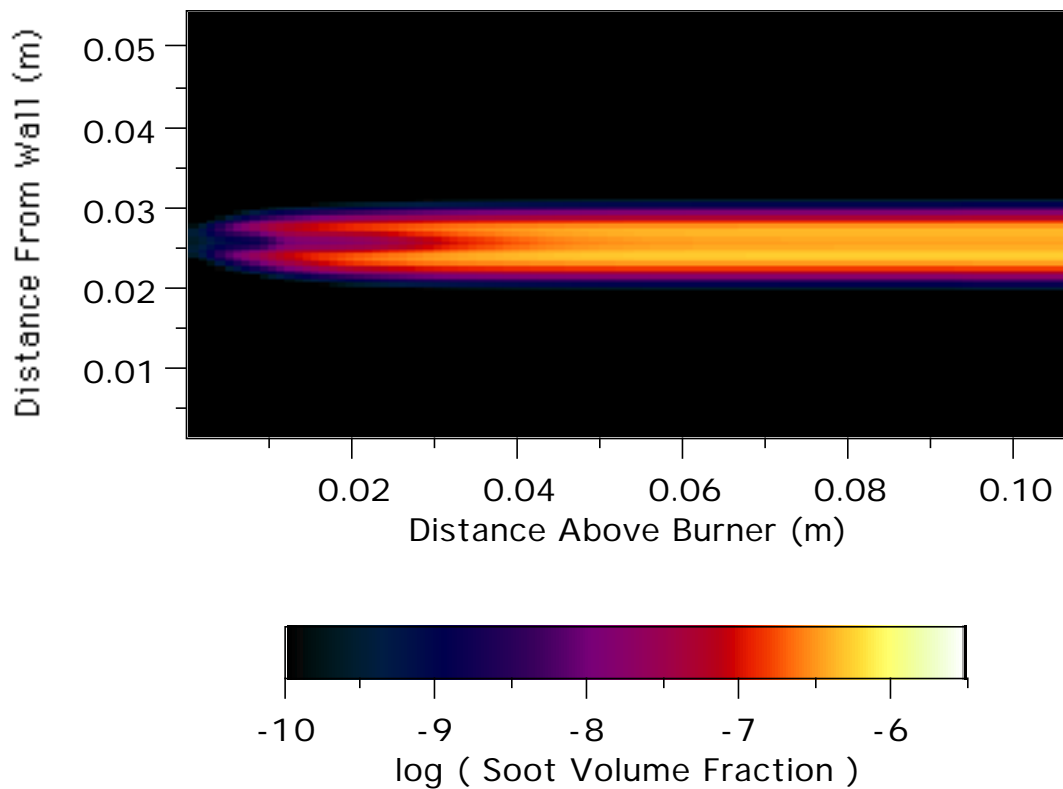


**Figure 6.10** A FFB soot cloud cross section prediction for an Illinois #6 coal.

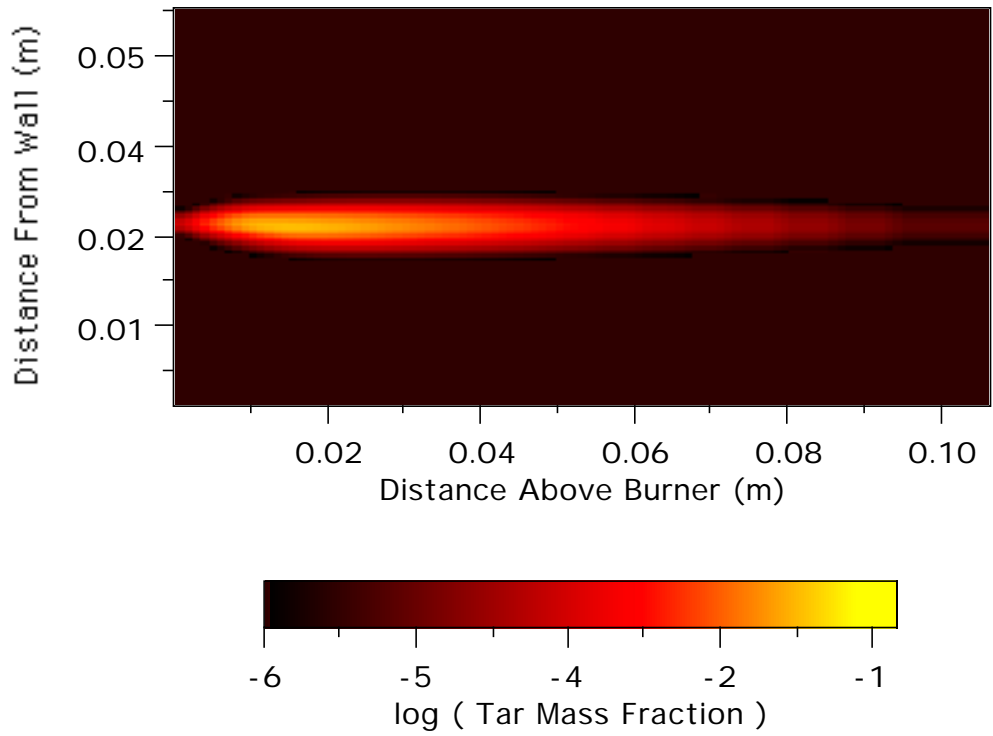


**Figure 6.11 FFB tar cloud cross section prediction for an Illinois #6 coal.**

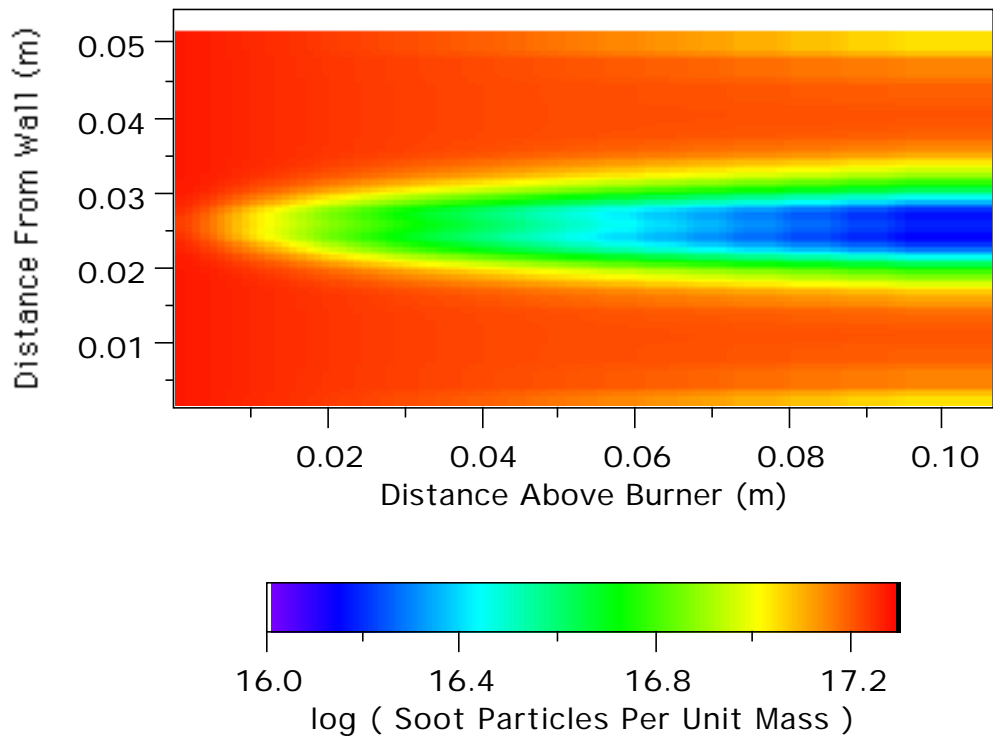


**Figure 6.12  $N_C$  contours at a cross section in the FFB for an Illinois #6 coal.**

## 6.2 Controlled Profile Reactor

Though no detailed soot measurements are available for these operating conditions for this apparatus, temperature and NO<sub>x</sub> predictions are affected by the radiation occurring from the soot present. Therefore, these parameters are examined in order to indicate not only the effect of soot on the resulting predictions, but also in an attempt to show how the addition of a soot model may improve the predictive capabilities of these parameters. Additionally, this test case may also be used to illustrate the characteristics of the soot model in a coal flame which is more typical of industrial use, and provides a means for comparing the variations of the new model with the Adams and Smith (1995) model.

Because there are several soot models being evaluated, a convention has been developed for reporting the results in the next two sections. Table 6.2 contains the key to the nomenclature used to describe all the conditions under which the predictions could possibly be performed. Case 1 is the most detailed case, which also includes the least empiricism. Predictions performed without considering soot are given as Case 2. In Case 3, the Adams and Smith (1995) model was used. Case 4 is identical to Case 1 except that an average soot number density was assumed. In Case 5, the empirical tar model, assuming an average soot number density following Kennedy et al. (1990), was used. In Case 6, the empirical tar formulation was used with transport equations for the two soot equations.

**Table 6.2****A Description of the Case Nomenclature.**

	<i>Soot</i>	<i>Tar</i>	<i>Particles Per Unit Mass</i>
Case 1	From Transport Equation	From Transport Equation	From Transport Equation
Case 2	None	None	None
Case 3	From Empirical Formulation	None	None
Case 4	From Transport Equation	From Transport Equation	Average Assumed
Case 5	From Transport Equation	From Empirical Formulation	Average Assumed
Case 6	From Transport Equation	From Empirical Formulation	From Transport Equation

The original intention was to illustrate the soot cloud and the impact of the soot predictions on the gas temperatures and NO<sub>x</sub> concentration predictions. After much work on model development, the axi-symmetric mode of PCGC-3 was abandoned in favor of a quartered symmetrical three-dimensional grid. Further evaluations led to the use of a full three-dimensional model. These fully three-dimensional models were incapable of predicting a symmetric flame for this reactor configuration, which most likely could be attributed to a) velocity predictions that would not converge, b) convergence to asymmetric solutions, or c) failure to achieve grid independence. This led to investigation into reasons for the asymmetric predictions. The reported inlet conditions for this experiment are suspect for this case. This is due to the fact that the primary inlet velocity is roughly twice the magnitude of the secondary inlet velocity (in the axial direction), a condition that is known to cause instabilities which are difficult to model (Kent and Bilger, 1972). PCGC-3 leaves out the time dependent term from the transport equations, so transient processes are assumed to represent a particular steady-state

condition. Turbulence fluctuations are modeled using mean and fluctuating flow variables. As the data were collected, measurements were taken to assure flame symmetry, but all the measurements were taken using suction probes which require a lengthy sampling time. The fluctuations observed in the model may be due to a) the inability of the turbulence model to properly characterize the transient flow conditions using the averaged steady-state code or b) the inability of the numerical scheme to distinguish between multiple steady-state solutions. Optical measurements in this burner (Hedman, 1997) support the theory that temperatures may significantly fluctuate, with standard deviations on the order of several hundred degrees Kelvin (see also Hedman and Warren, 1995).

Since repeated tests had given similar results, this led to the problem of how to interpret and present the asymmetric steady-state results obtained from this model. Solutions balance the total energy, so assuming the chemistry approaches a steady-state solution, the spatially averaged temperature predictions through the reactor should be similar to the measurements. Symmetry was therefore artificially imposed on an asymmetric converged solution by averaging all of the points at similar “radial locations.” Figure 6.13 illustrates the method used to generate the gas temperature and species concentration plots for the CPR. Points A-C are representative nodes in the prediction grid for the CPR. Predictions are plotted versus the distance from the centerline for all points in the grid at a given height  $z$ , and a distribution of all the individual predictions is represented by a cloud of prediction points. A 20th order polynomial curve fit is used to represent the predictions from a cross section of a given height as a function of radial distance. Figure 6.14 illustrates a typical field of temperature predictions and the resulting curve fit.

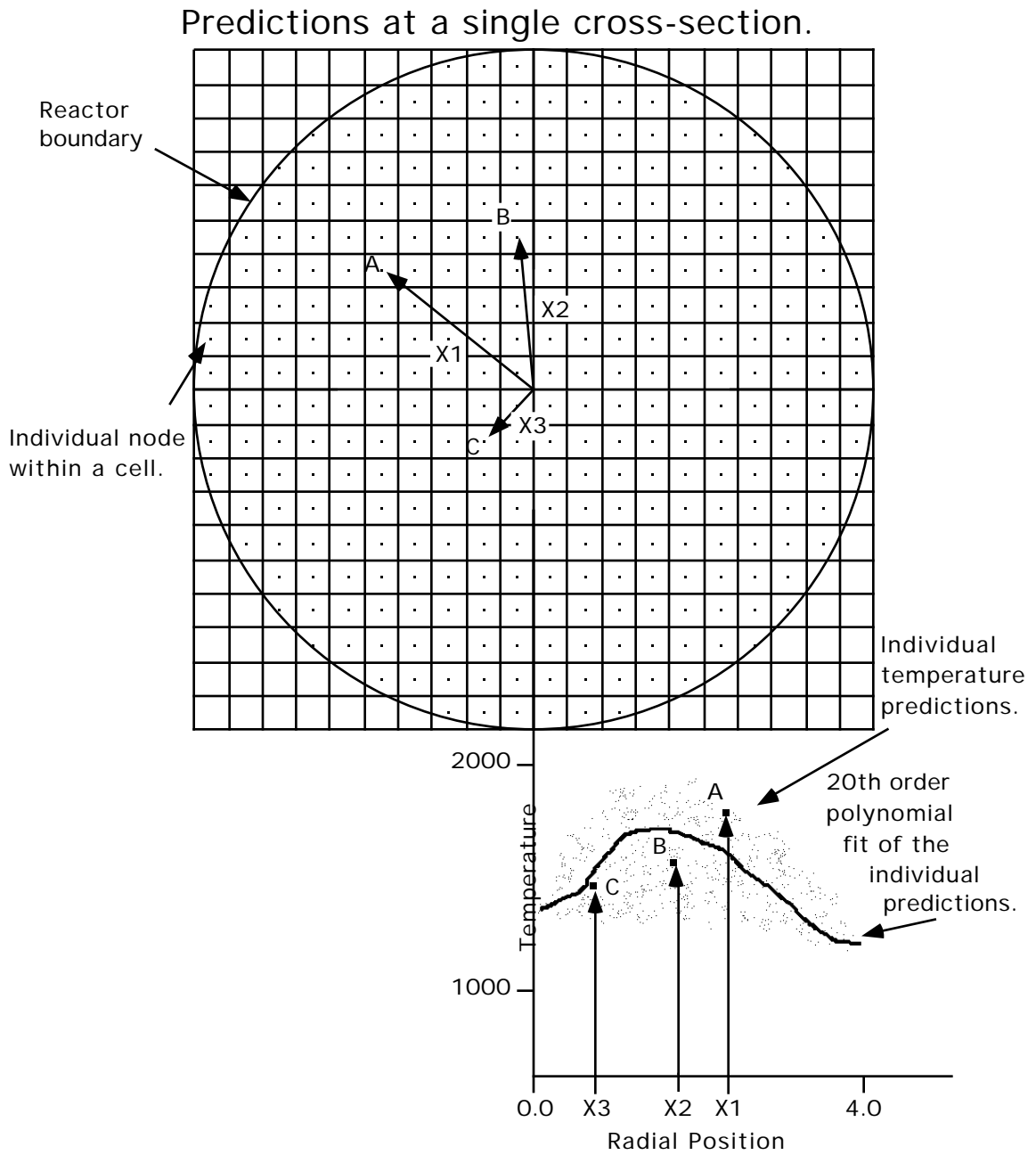


**Figure 6.13** An illustration of the technique used to represent the predictions for the CPR.

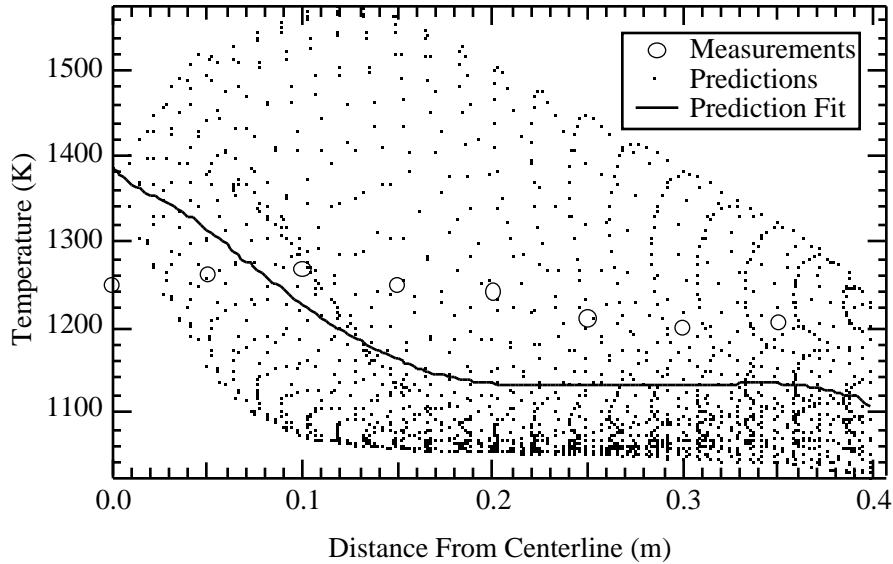


**Figure 6.14 An illustration of the typical CPR temperature predictions and curve fit versus measurements. Data are at 95 cm below the inlet.**

At the height of Figure 6.14, the temperature predictions at a given cross section vary as much as 500 K with an estimated standard deviation of  $\sim 180$  K. The spatially averaged prediction is within 100 K of the measurements, which is well within the typical bounds of experimental error for these kinds of suction probe temperature measurements. It is expected that the predictions near the centerline should be much less accurate than the predictions further away. This is because fewer nodes exist in the model at that location, and a polynomial curve fit tends to aggravate such a problem near the boundaries. Species predictions, such as  $\text{NO}_x$  can be represented with spatial averages in a similar manner.

In an attempt to eliminate these numerical instabilities in the CPR predictions, several other grid formulations were tried. However, refining the grid resolution from  $69 \times 49 \times 49$  to  $81 \times 69 \times 69$  produced similar results at the expense of significantly longer run

times. This indicated that grid independence may not be a significant factor. Velocity predictions would not converge for any of these model grids. Another possible cause for the numerical instabilities was grid biasing. In these predictions, grids are biased, or in other words they are set up such that areas of interest (such as the inlet) have smaller grid cells, while areas of lesser interest (such as the exit) have larger cells. Other grid biasing schemes were also tested. At the recommendation of an industrial researcher (Fiveland, 1997), the inlet grid resolution was relaxed by reducing the bias near the inlet, which led to the development of the grid used to generate the results in this section. Velocity convergence improved in the prediction with lower grid resolution in the inlet region, but the expected recirculation zones were absent. Primary inlet velocities were also slightly higher than with previous grids in order to maintain the same inlet mass flow rate. The resulting grid also developed an asymmetric flame, but because the “standard” PCGC-3 convergence criteria were satisfied, results were more presumed to be more meaningful. The asymmetry was more consistent as well; the velocity fluctuations observed in other grid configurations were not observed for this grid configuration. It is possible that the reduction in grid biasing in the near burner region resulted in grid dependence, which led to flow-field prediction errors that eliminated the recirculation zone and allowed for convergence. The resulting predictions were observed to give comparable asymmetry from one particle iteration to the next. Since the objective of this study was to examine the soot model, not asymmetric predictions, attempts to eliminate the instabilities were then stopped and the effects of soot in the asymmetric predictions were examined.

### 6.2.1 Temperature and Species Predictions

Figures 6.15 to 6.18 illustrate the spatially-averaged predictions at selected heights. More predictions have been made at other heights and are presented in Appendix E. All of the prediction lines for both the gas temperatures and  $\text{NO}_x$  concentrations represent twentieth order curve fits of many individual data points at different radial positions, as was illustrated in Figures 6.13 and 6.14. The scatter plots were omitted for convenience.

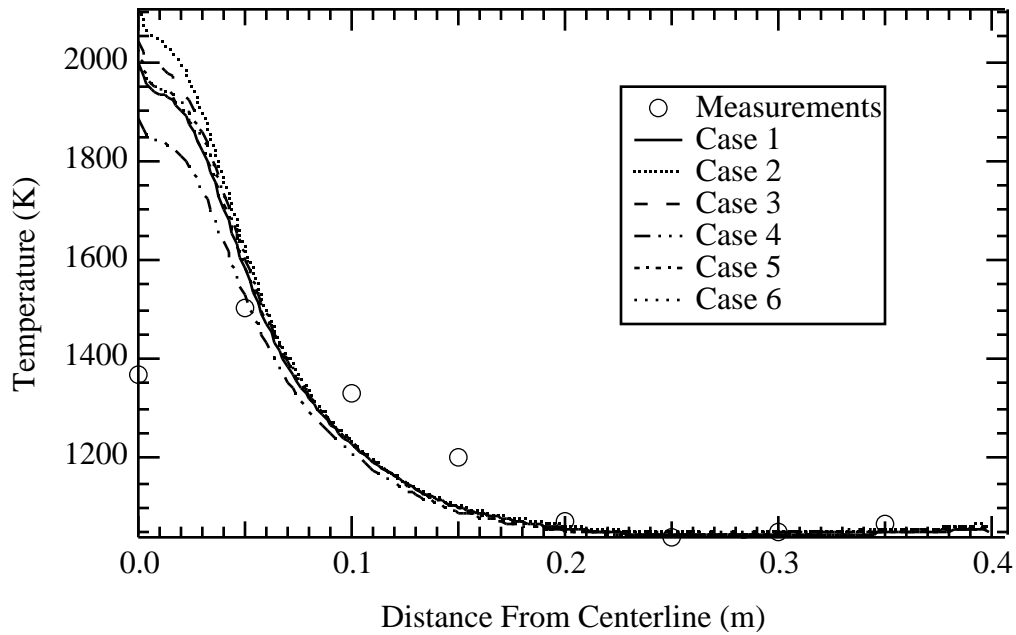


**Figure 6.15** Predicted and measured gas temperatures in the CPR at 30 cm below the inlet.

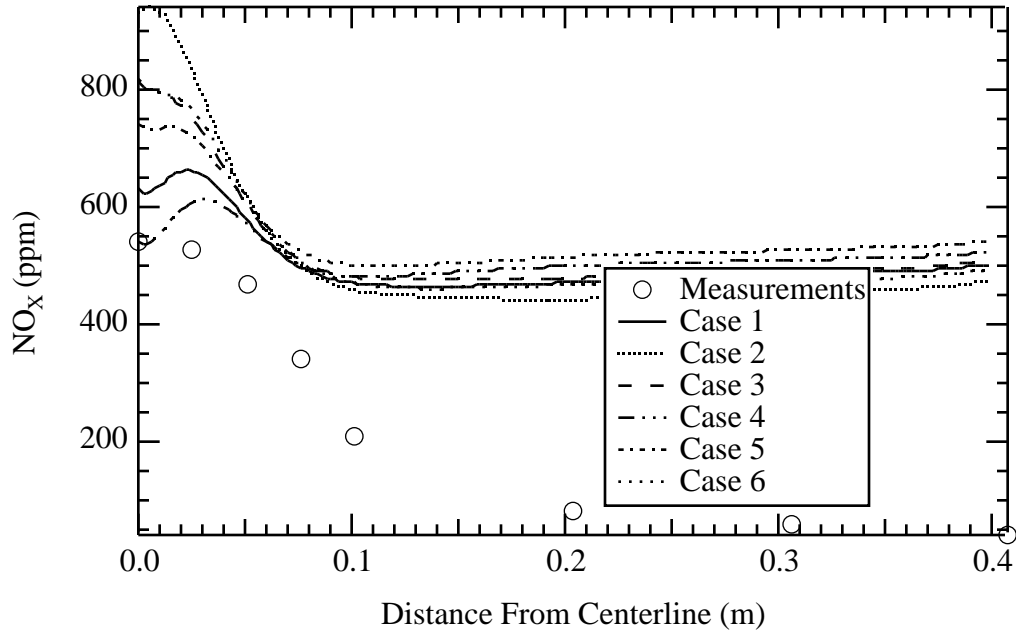


**Figure 6.16 Predicted and measured NO<sub>x</sub> concentrations in the CPR at 30 cm below the inlet.**

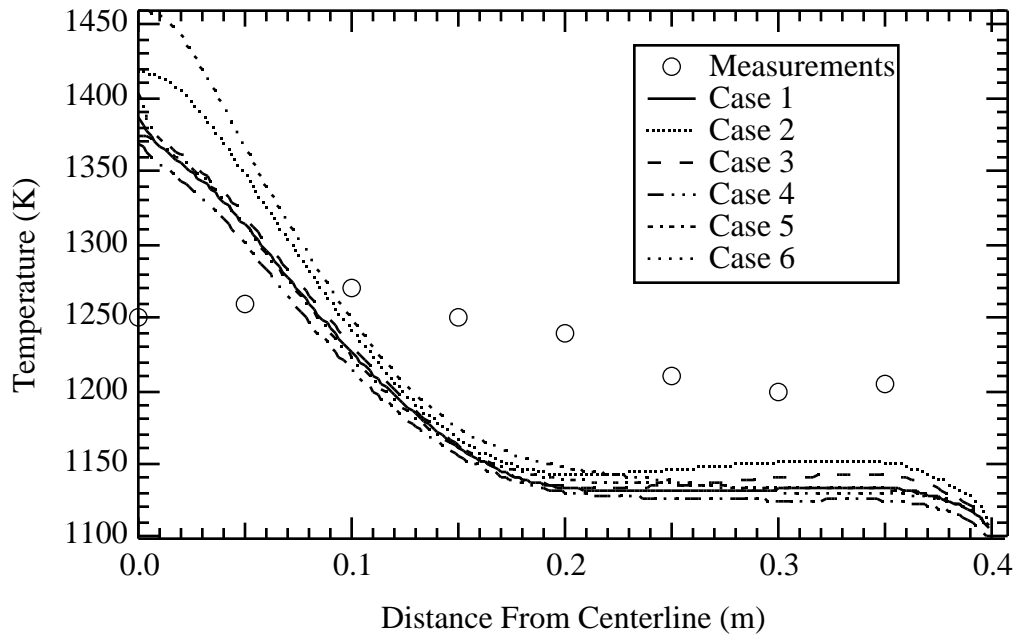


**Figure 6.17 Predicted and measured gas temperatures in the CPR at 95 cm below the inlet.**

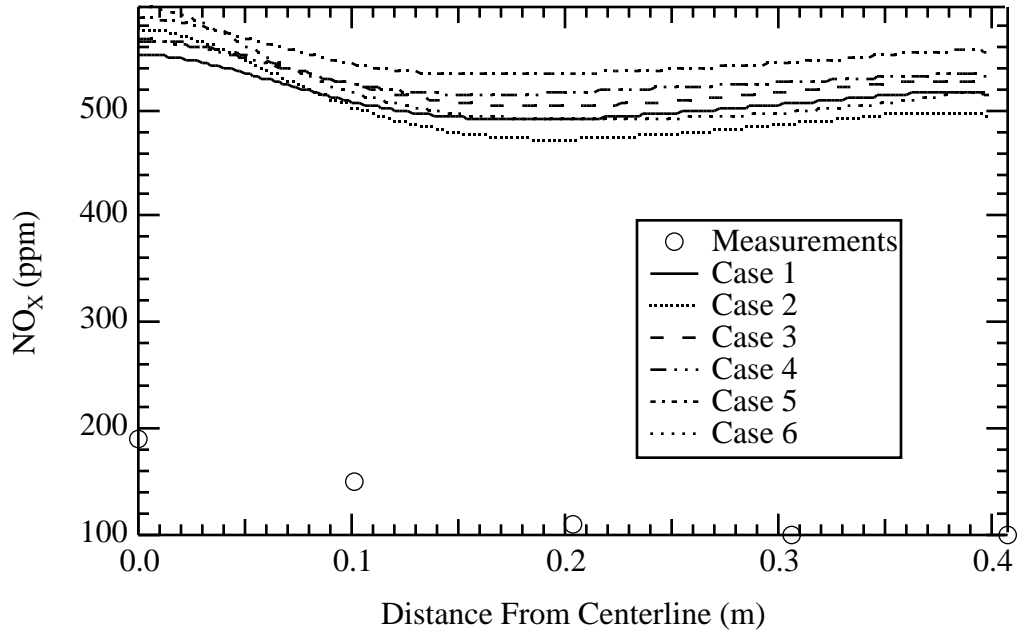


**Figure 6.18 Predicted and measured NO<sub>x</sub> concentrations in the CPR at 95 cm below the inlet.**

A surprising result for this case is the minimal effect the inclusion of the soot caused on the NO<sub>x</sub> concentration and gas temperature predictions. Figures 6.14 to 6.17 indicate that in general, the soot did not contribute enough to the radiative effects to demonstrate significant variation between Case 2 and the remaining soot cases. This can be attributed to the low soot yields predicted in this case. This is possibly caused by the lack of grid resolution in the near-burner region causing better mixing than would occur with finer resolution.

The profiles for the temperatures do not match up as well as might be expected with the measured profile. While this could be attributed to many parameters, it is suspected that the major difficulty comes from the inability to properly estimate the turbulent velocity flow field. This suspicion comes from both conversation with CPR operators regarding velocity profiles as well as an understanding of the inaccuracies

associated with the  $k$ - turbulence model. The  $k$ - turbulence model used in this case is known to give faulty predictions in adverse pressure gradient flows (Wilcox, 1993). Adverse pressure gradient flows are ones where  $dP/dx > 0.0$ . This is the case for the CPR, especially in the near burner region, which would indicate that the flow velocities might be incorrect. Another indication of this is the discrepancy in velocity flow fields for the various slightly modified geometry grids used to model the CPR. As previously indicated, strong recirculation regions found in measurements do not exist for the grid presented in this section.

Another glaring discrepancy is the fact that the code consistently over-predicts the  $NO_x$  measurements (Figures 6.16 and 6.18). The particular grid used to generate this data is probably to blame since other grids predicted  $NO_x$  more on the order of what the measurements were. This grid demonstrated a much lower propensity to recirculate along the centerline than did the other grids. The near-burner maximum temperature for this grid (Figure 6.15) is also somewhat higher than in other grid predictions, nearly reaching the adiabatic flame temperature. These two occurrences are likely to contribute to an over-prediction of  $NO_x$ . Despite the problems, these predictions are shown for two reasons. Some of the flow parameters matched the data well, and the likelihood of further reasonable modeling attempts to improve predictions was low due to numerical stability issues.

### 6.2.2 Soot Predictions

Figure 6.19 shows a plot of the predicted soot volume fraction at 30 cm below the inlet along a horizontal line of sight. Only Case 1, 3, and 6 were displayed in the

graph. Case 4 and Case 5, which were similar to Case 1 and Case 6 respectively, were omitted from the plot to improve the clarity of the figure. The average soot volume fraction predictions are low, and the regions of peak soot volume fraction are narrow. Soot therefore is not expected to contribute significantly to the radiative effects.

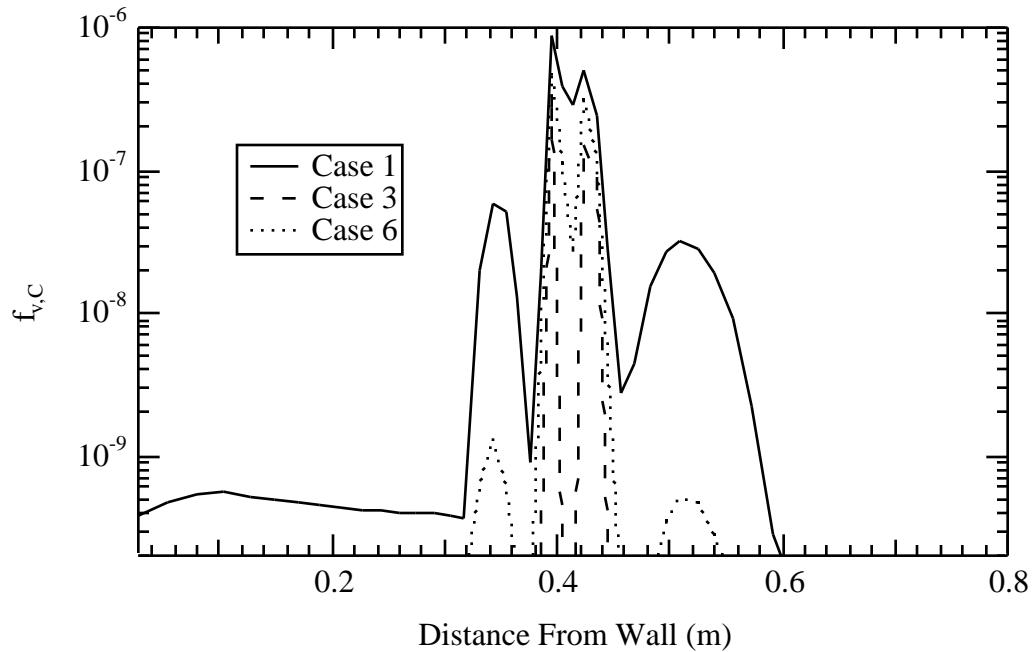


**Figure 6.19 Horizontal Line of sight soot volume fractions in the CPR at 30 cm below the inlet.**

Quite recently, line of sight soot measurements were performed in a similar experiment in the CPR (Haneberg, 1997). Average soot volume fractions were calculated from transmission measurements at various heights and operating conditions (swirl number = 1.5 and  $\beta = 0.9$ ). The coal used was a Wyoming Black Thunder subbituminous, similar in rank to the Utah Blind Canyon used in the experiments of Sanderson (1993) and Butler (1992). Some minor changes in the geometry within the reactor were made as well. Overall, they found that at similar operating conditions to the ones used in this research, the soot volume fraction measurement was too low to confidently distinguish the

measurements from the noise. The minimum average soot volume fraction considered for accurate detection in the experiment was  $5.0 \times 10^{-8}$ , and the measured average soot volume fraction fell just below this limit. Table 6.3 shows a comparison of predicted average line of sight soot volume fractions versus data from Haneberg's experiment. The predictions are the integrated soot volume fraction over the length of the furnace, and correspond to the average soot volume fractions measured by Haneberg. The predicted values are below the bounds of the experimental measurement threshold for all but Case 4, indicating that the average volume fraction would fall below the detectable region for these operating conditions as well.

**Table 6.3**

**A Comparison Between Predicted Line of Sight Soot Volume Fractions and Measurements for the CPR at 30 cm Below the Inlet.**

<i>Case</i>	<i>Average Soot Volume Fraction</i>
Measured	$<5.0 \times 10^{-8}$
Case 1	$3.34 \times 10^{-8}$
Case 3	$7.37 \times 10^{-9}$
Case 4	$8.46 \times 10^{-8}$
Case 5	$2.29 \times 10^{-8}$
Case 6	$1.35 \times 10^{-8}$

### **6.3 Fireside Performance Test Facility**

The Fireside Performance Test Facility (FPTF) is the largest of the three burners modeled in this research. Originally, this case was to be the large case used to show the impact of a soot model on larger scale predictions. Due to the difficulties encountered with modeling the CPR and the fact that the CPR conditions were not very representative of typical coal flames with higher sooting potentials, the FPTF case has become the principal case used to demonstrate the effect of soot in industrial sized coal flames.

Contour plots of the soot variables are included in this section in addition to comparisons of predicted and measured gas temperatures and concentrations. Predictions of this swirling burner exhibited a good tendency to stabilize and converge, in contrast to the CPR predictions.

An attempt was made to model the converging/diverging nozzle insert in the secondary inlet using a coarse grid. This model was abandoned, though, because a more simplistic inlet grid better predicted the O<sub>2</sub> measurements. The coarseness of the model at the inlet may contribute to the inaccuracies of the predictions. An improved model would require significantly more grid nodes near the inlet to accurately represent the true inlet geometry. Because this model is a turbulent, swirling case like the CPR, inaccuracies with the turbulence model may also exist.

### 6.3.1 Gas Temperature and Species Predictions

Although good information regarding gas velocity fields were not available, it is suspected that PCGC-3 accurately predicts the flow, based on the good correlation between predictions and measurements. Figure 6.20 and 6.21 show comparisons of predicted and measured O<sub>2</sub> concentrations at two different heights in the FPTF.

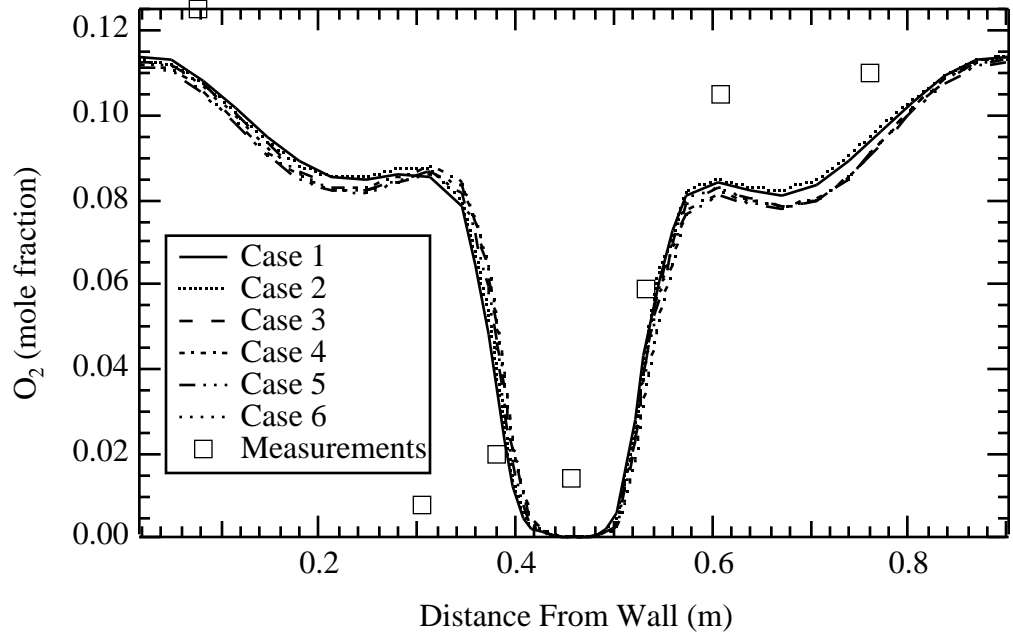


**Figure 6.20** Predicted and measured O<sub>2</sub> concentrations in the FPTF at 68.6 cm above the inlet.

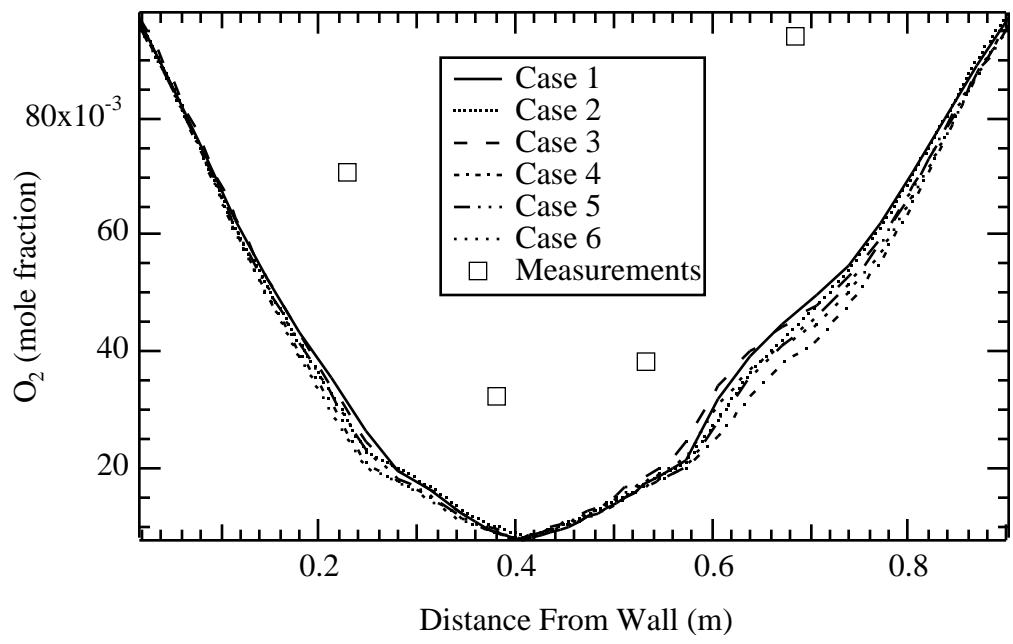


**Figure 6.21** Predicted and measured O<sub>2</sub> concentrations in the FPTF at 144.8 cm above the inlet.

O<sub>2</sub> predictions agree reasonably well with the measurements both in magnitude and in trends for this furnace. This indicates that the predicted flame location agrees with the actual flame location in the furnace. This would also indicate that the velocity field roughly represents what occurs in the furnace as well. Figures 6.22 to 6.25 show predicted and measured gas temperatures and NO<sub>x</sub> concentrations for this furnace at the same two heights. Additional plots of FPTF predictions and measurements at other heights are available in Appendix F.

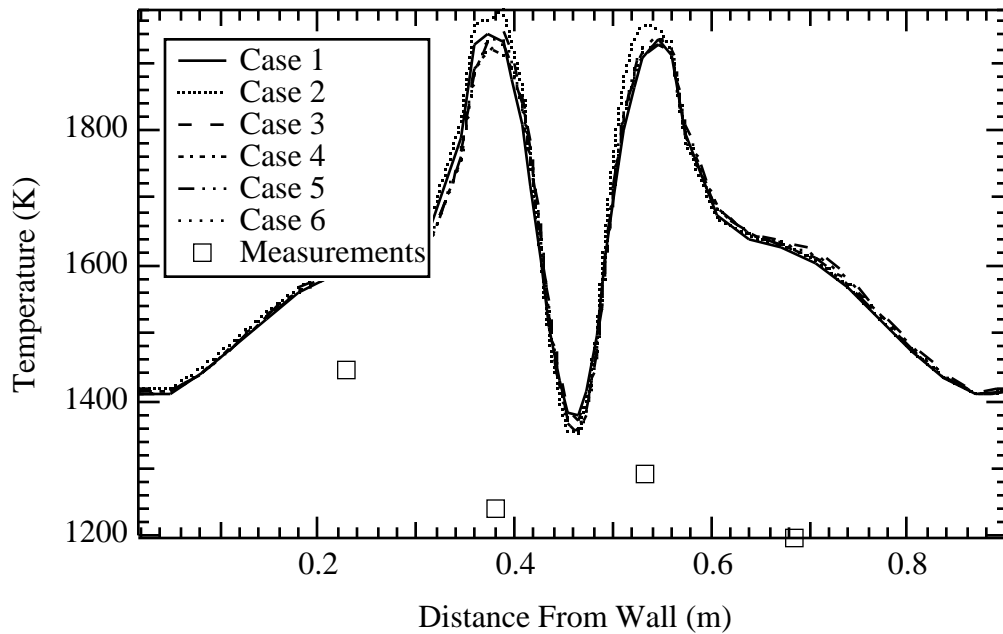


**Figure 6.22 Predicted and measured gas temperatures in the FPTF at 68.6 cm above the inlet.**

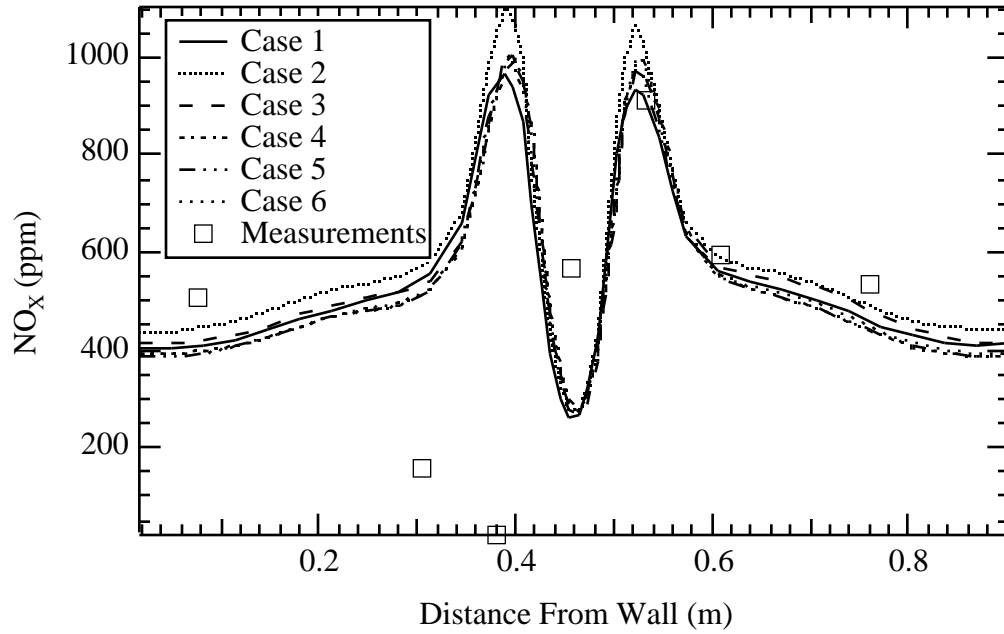


**Figure 6.23 Predicted and measured NO<sub>x</sub> concentrations in the FPTF at 68.6 cm above the inlet.**

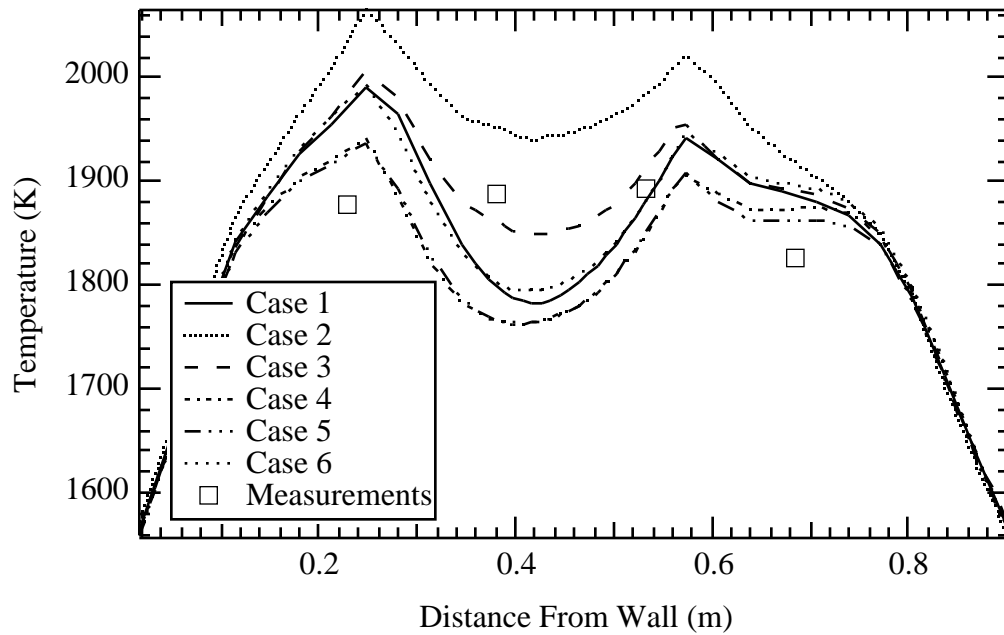


**Figure 6.24 Predicted and measured gas temperatures in the FPTF at 144.8 cm above the inlet.**

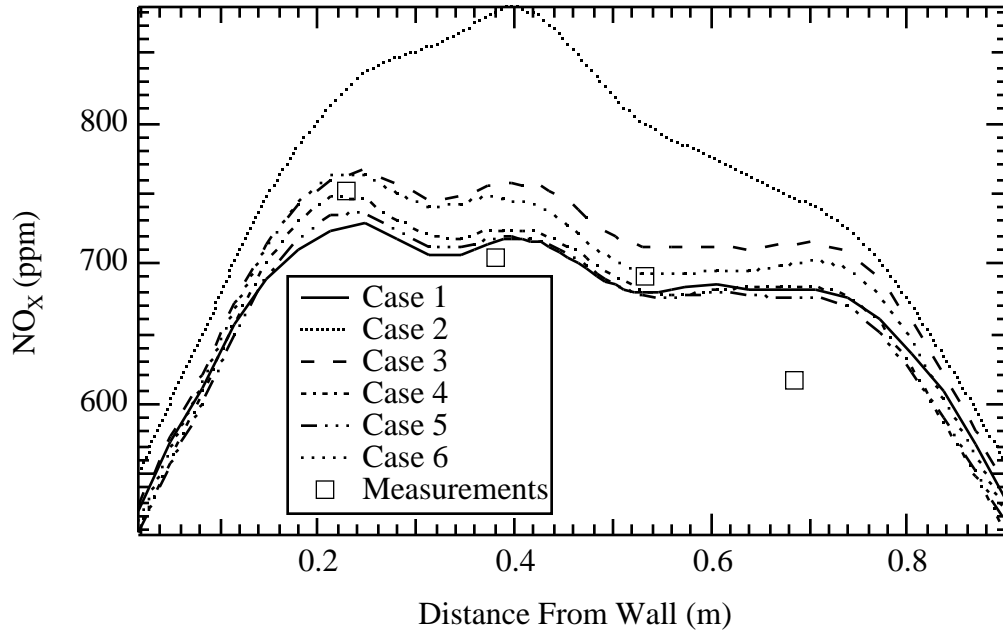


**Figure 6.25 Predicted and measured NO<sub>x</sub> concentrations in the FPTF at 144.8 cm above the inlet.**

Figures 6.21 and 6.22 illustrate the predictions in the region nearer to the burner. In the center region of the predictions near the burner, only slight variations exist in the predicted gas temperatures and NO<sub>x</sub> concentrations for the different cases. Further away from the furnace inlet at the positions of Figures 6.24 and 6.25, the predictions from the various cases have a more significant impact on the predicted NO<sub>x</sub> concentrations and gas temperatures. In Figure 6.24, the largest difference between the gas temperature predictions of the several cases was approximately 200 K. The largest NO<sub>x</sub> concentration difference in Figure 6.25 was nearly 200 ppm. The maximum gas temperatures and NO<sub>x</sub> concentrations were from Case 2, the case where soot is not considered. Also, in Figures 6.24 and 6.25, the cases where soot is considered more closely match the measurements.

Table 6.4 indicates the maximum observed differences between Case 2 gas temperature and NO<sub>x</sub> concentration predictions and the lowest predicted values from the cases in which soot is considered. At a height of 182.9, the maximum gas temperature difference of nearly 300 K is observed. At a height of 106.7, the maximum observed NO<sub>x</sub> concentration difference of almost 250 ppm is observed.

**Table 6.4**

**Maximum Difference Between Gas Temperature and NO<sub>x</sub> Concentration Predictions With and Without Soot at Various Heights.**

<i>Height Above the Burner (cm)</i>	<i>Maximum Gas Temperature Difference (K)</i>	<i>Maximum NO<sub>x</sub> Concentration Difference (ppm)</i>
30.5	54.1	115.4
68.6	92.9	188.0
106.7	109.6	234.2
144.8	183.8	206.9
182.9	281.8	196.9
259.1	138.2	153.3

Good convergence was achieved for all of the flow variables with the revised grid with the exception of the soot particles per unit mass (N<sub>C</sub>) variable. The residual values for this variable would drop to a level considered unconverged and fluctuate. Because this variable is large in magnitude which causes numeric scaling problems, it was assumed that the variable was converged when the residual ceased to decrease in value.

**6.3.2 Contour Plots**

The predicted contour plots for the FPTF provide insight into the soot predictions for this case; trends may be similar in comparable flames from other coal fired

furnaces. There are no data on the magnitude and form that these variables should take, but these plots illustrate the predictions for the various models in a typical coal-fired flame. Comparisons between the different cases show the impact of using various levels of empiricism on the resulting predictions. Contour plots also provide detail that would otherwise be difficult to interpret from standard one-dimensional plots.

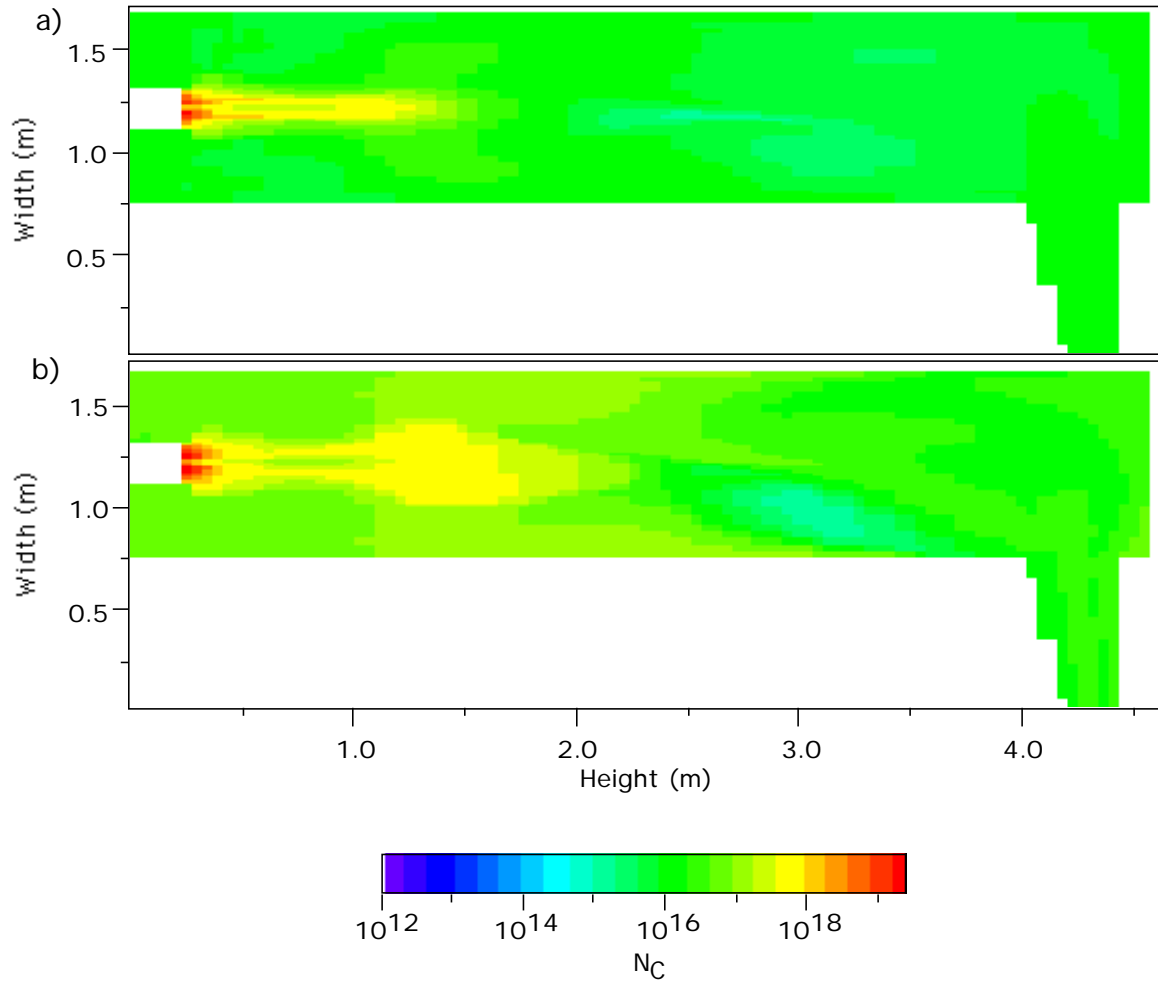


**Figure 6.26**  $N_C$  contour predictions in the FPTF using the transport equation. The plot labeled a) is from Case 1 and the plot labeled b) is from Case 6.

There were several problems with the transport equation method for determining  $N_C$  in the FPTF. Like in the CPR results, the FPTF predictions for this variable did not

converge very well. This is thought to be a result of the large numbers predicted for this variable, an effect that could be counteracted by scaling the variable. Scaling was considered but not attempted due to the complexity of the problem. Although the residuals were high, the predictions were consistent, so convergence was assumed. An additional problem was the violation of the upper constraint. As is evident in Figure 6.26, the  $N_C$  predictions in the region nearest the burner for some reason tended towards the maximum allowed value. This is unusual because tar is nearly non-existent in that region, as well as is the soot. Another unusual observation apparent in these plots is the prediction of a high number of soot particles throughout the reactor. It is reasonable to assume that the high number of soot particles does not exist in many of these regions. It is also reasonable to assume that the predicted average soot diameter based on these predictions is smaller than the minimum soot diameter. This high soot particle number prediction can be attributed to the failure to include a term that oxidizes soot particles or evaporates soot particles with low molecular weights back to gas phase hydrocarbons. The only pathway for a reduction in the number of soot particles in the current model is through agglomeration. Interpreting the soot particles per unit mass equation as being valid only in regions where the predicted average soot diameter is above a minimum value (i.e.  $0.005 \mu\text{m}$ ) may be a reasonable assumption in the absence of a mechanism to describe the gasification or oxidation of soot particles.

$N_C$  predictions in regions of high tar are typically higher than in regions of lower tar. This is a direct result of the formation mechanism.  $N_C$  predictions are the highest near the burner and decrease within the regions of high soot as they move away from the

burner, exhibiting the expected trend towards agglomeration. Overall, the  $N_C$  predictions were within a few orders of magnitude of the comparable assumed soot number density.

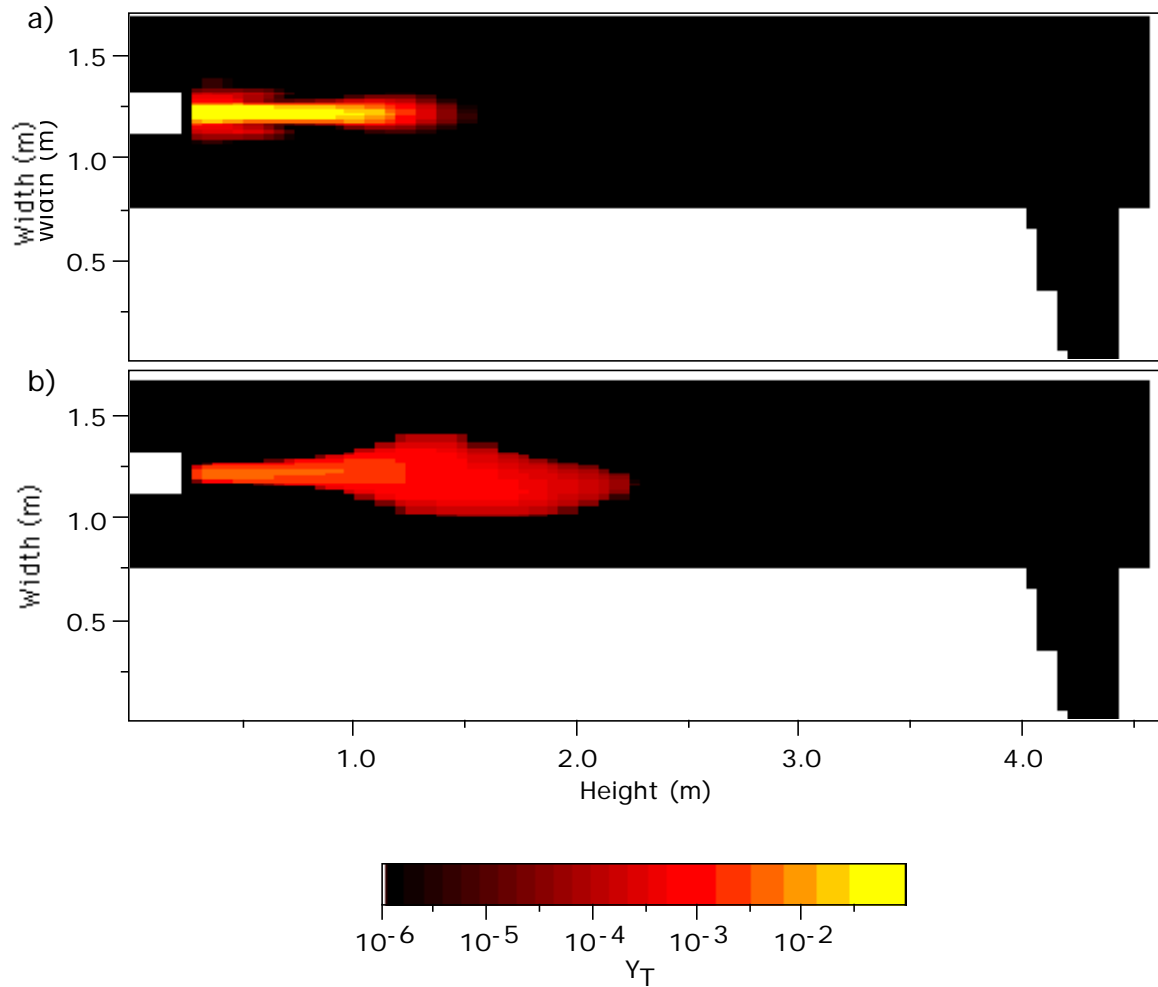


**Figure 6.27**  $Y_T$  contour predictions in the FPTF. The plot labeled a) is from Case 1 and the plot labeled b) is from Case 6.

$Y_T$  predictions for Case 1 and Case 6 are illustrated in Figure 6.27. Tar predictions for Cases 4 and 5 were omitted because they were nearly identical to the corresponding predictions from Case 1 and 6. This indicates that the impact of the  $N_C$  variable on the tar predictions is negligible. Tar predictions are significantly different

depending on the method of calculation. The empirical method for predicting tar predicts a much larger tar region away from the burner, but with a significantly lower maximum value near the burner compared to the transport equation method. Although no data exist to validate these predictions, the transport equation predictions are expected to better represent the actual tar formation due to the source term originating from the CPD model and the closer relation to the more theoretical Lagrangian particle predictions.

Predictions of the soot volume fraction ( $f_{v,C}$ ) are shown in Figures 6.28 and 6.29. The soot volume fraction ( $f_{v,C}$ ) is used to represent the quantity of soot rather than the soot mass fraction ( $Y_C$ ) because soot is usually quantified for radiative purposes in terms of the soot volume fraction. Soot mass fraction contours are similar to the soot volume fraction contours, except on a different scale (several orders of magnitude higher).

Comparing in Figures 6.28 and 6.29 Case 1 and 4 predictions to Case 5 and 6 predictions illustrates the differences incurred on the transport equation soot predictions due to the type of tar formation model used. Surprisingly, after noting the significant difference between the two tar models, only subtle differences exist between the soot predictions using the empirical and transport equation based tar models. The transport equation based tar model yielded slightly higher overall soot volume fraction predictions than did the empirical tar model. Additionally, the peak region of soot volume fraction using the empirical tar model was slightly further away from the burner than with the semi-empirical tar model predictions.

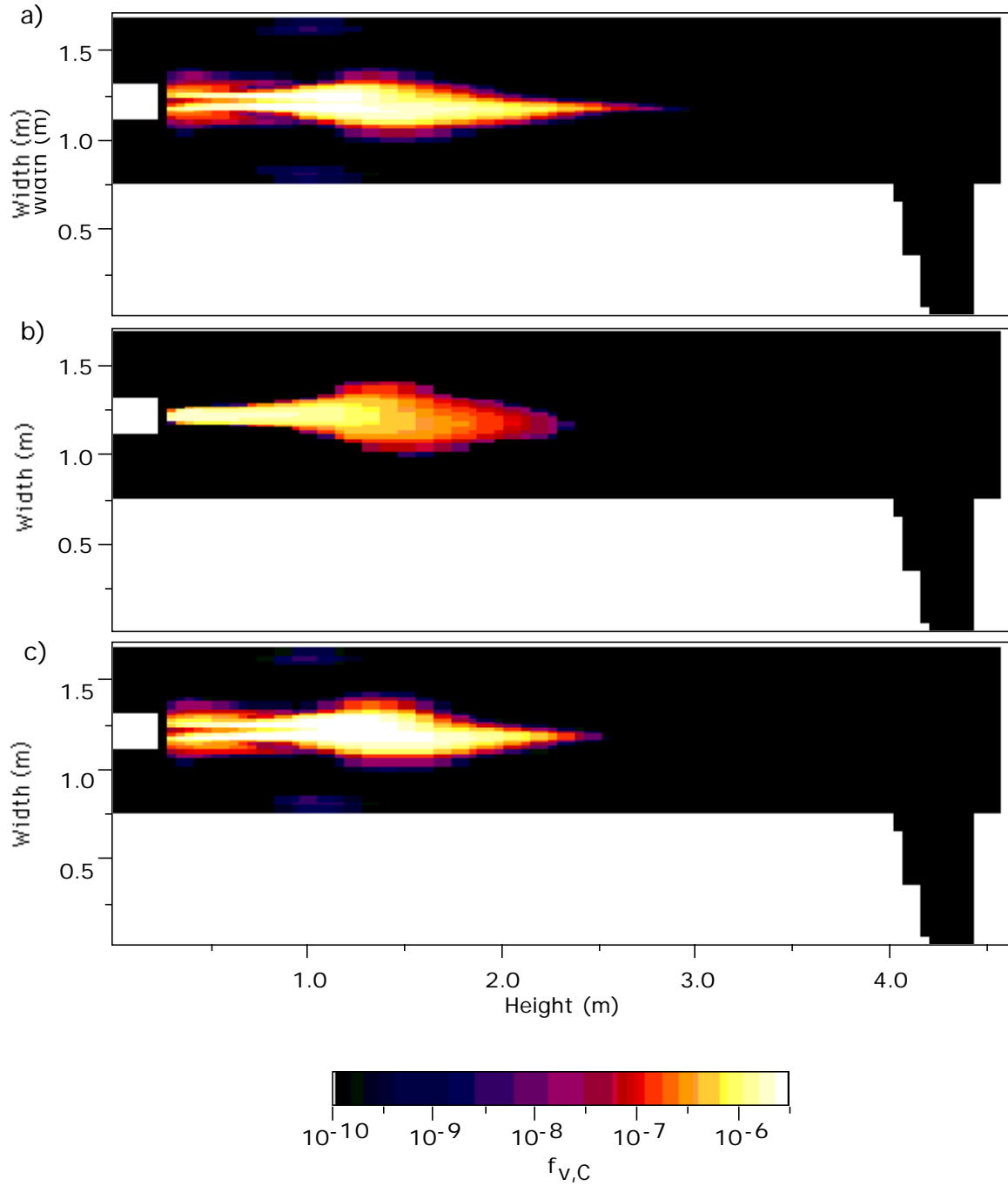


**Figure 6.28**  $f_{v,C}$  contour predictions in the FPTF. The plot labeled a) is from Case 1, the plot labeled b) is from Case 3, and the plot labeled c) is from Case 4.

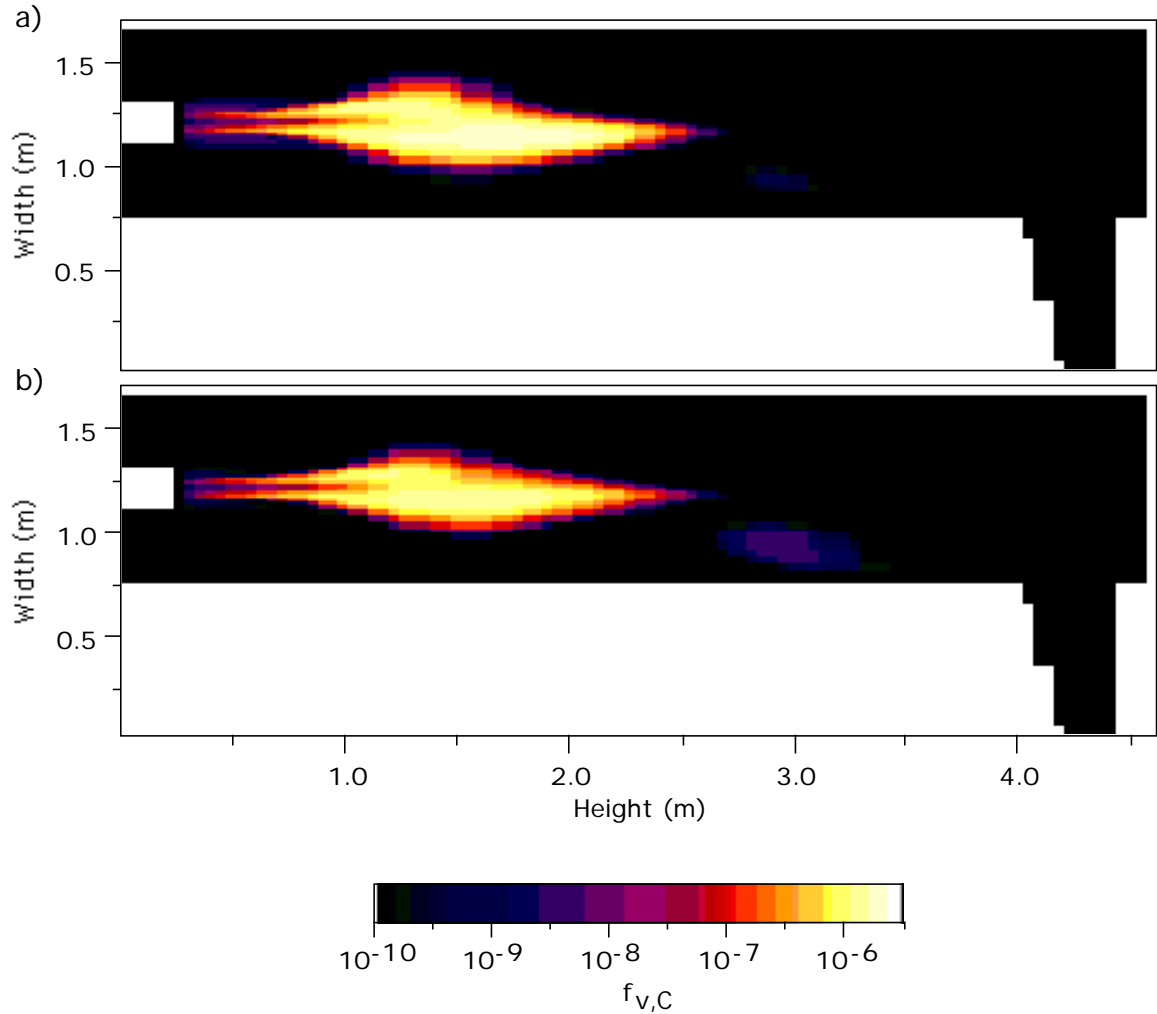


**Figure 6.29**  $f_{v,C}$  contour predictions in the FPTF. The plot labeled a) is from Case 5 and the plot labeled b) is from Case 6.

Comparing Case 1 predictions to Case 4 predictions and Case 5 predictions to Case 6 predictions, the overall impact of the soot particles per unit mass ( $N_C$ ) equation on the soot volume fraction ( $f_{v,C}$ ) results are illustrated. Including the soot particles per unit mass ( $N_C$ ) equation did not result in significant differences in the soot volume fraction predictions. Finally, Figure 6.28 (b) shows predictions using the empirical soot model of Adams and Smith (1995). While the predicted maximum soot volume fraction is close in magnitude to the maximums for the other semi-empirical soot cases, the predicted peak

region is located much closer to the burner. A significantly lower soot volume fraction exists for the empirical soot predictions in regions of maximum soot than predicted in the other cases.

## 7. DISCUSSION

### 7.1 Flat Flame Burner Predictions

Agreement between the predictions and experimental data in the FFB support many of the assumptions and equations used in generating this model. Although discrepancies exist, particularly in the near burner regions, these problems could be a result of the inability of parts of the combustion code (apart from the soot model) to describe the apparatus. Yields away from the burner are quite accurate. As best as can be distinguished from the available data, the  $N_C$  variable can be used to accurately predict the expected soot particle diameters. The observed visible soot cloud also conforms reasonably well to the predicted soot volume fraction locations.

The agreement between the predicted and measured soot yields is considered to be very good. This suggests that the assumptions involved in the formation mechanisms for soot from tar may be reasonable. Results from the Adams and Smith (1995) empirical model were not reported for this case. Their model relies on the assumption that the equivalence ratio is a function of only the coal volatiles and the oxidizer. Due to the premixed methane in the secondary inlet, and because the entire reactor is fuel-rich, the Adams-Smith model is incapable of predicting soot yields in this flame.

Temperature and  $NO_x$  predictions were not examined in the FFB calculations due to the low particle loading. Soot present in the FFB did not significantly influence the temperature predictions for this case. This is due to the small geometry of the FFB and

the low soot volume fractions. Because the impact of soot on energy transport in this case was small,  $\text{NO}_x$  measurements were omitted for this apparatus as well.

Less accurate soot yield predictions resulted from using the correlation for the  $^{13}\text{C}$  NMR parameters as opposed to measured values. Using the correlation resulted in reasonable predictions for the Illinois #6 and Utah Hiawatha coal, but resulted in poor predictions for the Pittsburgh #8 coal when compared with measurements. FFB predictions illustrate the importance of obtaining proper characterization of the coal to the accurate prediction of soot. Because measured  $^{13}\text{C}$  NMR parameters result in improved predictions in the cases examined, the correlation should be used only in instances where measured parameters are unavailable.

Due to the lack of oxygen in the FFB environment, the oxidation mechanism for this model had minimal contribution to the overall result. These data therefore can not be used to evaluate the oxidation mechanism. Also, the comparative impact between using the average number density and using the  $N_C$  equation may not be evaluated for similar reasons. A major obstacle to this work is the lack of data regarding coal-derived soot in an oxidizing environment. Additional soot measurement data which included soot oxidation effects would be necessary to provide the basis for a good characterization of the entire soot model.

The additional time required to run the soot model is evaluated based on a single macro-iteration. This gives a fairly good worst-case representation of the impact of including soot predictions on the total convergence time in a laminar flame. The added time cost for practical flames is likely to be a smaller percentage of the time when the turbulence models are included. Also, the soot model does not need to be run until the

flow velocity, pressure, and mixing variables have converged. The major impact of the soot will be on the enthalpy equation and starting with most of the other flow parameters converged should reduce the computational load. Though the time penalty for using the new soot model is difficult to quantify, it is apparent that the soot calculations represent a significant addition to computational requirements for a burner calculation.

## **7.2 Controlled Profile Reactor Predictions**

Overall, the predictions of the CPR case selected were not very satisfactory. The ability to model this specific turbulent flow appeared to be the principal difficulty with matching predictions to the measurements. Discrepancies are evident in the  $\text{NO}_x$  concentration predictions being consistently high, and variations within the gas temperature measurements. The coal and conditions used were not very conducive to soot formation, resulting in only minor changes in the predictions due to the inclusion of soot. Recent measurements at similar conditions indicate that the soot predictions may be reasonable for this case. Using a modified grid, inlet conditions, and the proper coal would provide better means for comparing the soot measurements to the predictions. Modeling the more recently improved geometry and inlet conditions for the CPR (Haneberg, 1997) may also alleviate some of the modeling problems evident in the predictions based on the operating conditions of Sanderson (1993) and Butler (1992).

The predicted near-burner centerline gas temperatures are suspected to be a major problem in this case. This may be a result of only a few nodes existing near the centerline for the curve fit or a grid resolution problem resulting in incorrect flow patterns and high predictions near the burner. High gas temperature predictions could be the reason  $\text{NO}_x$

concentrations are over-predicted; excessively high temperatures could result in higher  $\text{NO}_x$  concentration predictions in the flame region. The  $\text{NO}_x$  is then transported to the colder flow regions. More examination into the development of a reliable CPR model would be required to better evaluate the soot model using this furnace.

Some of the developed CPR model predictions did not converge. Velocities were observed to fluctuate in known regions of recirculation. This may be a result of modeling an unsteady flow with steady-state code. It may also represent problems with the turbulence model or with the inability to model the CPR without significant further refinement of the grid. Additionally, the code may be simulating the instabilities through the iteration steps. Cases that did converge predicted asymmetric flames, contrary to the averaged measurements from this furnace. Curve fits of the asymmetric gas temperature predictions were on the order of the measurements and the expected standard deviation of the predictions. The method used for representing asymmetric predictions in an axisymmetric burner would properly represent a flame that moved symmetrically about the centerline, provided that the steady-state code achieved a converged instantaneous solution. The chances of this being the case as well as the merit of predicting an unsteady flow with steady-state code are both questionable. Using a code developed for transient flow to model the CPR may provide insight to better evaluate the predictions from this burner. Regardless of the source of the predictive problems, it is apparent that further investigation is needed to develop an adequate model for the CPR at the test conditions modeled in this experiment.

### 7.3 Fireside Performance Test Facility Predictions

Because of the good convergence and accurate predictions achieved with the FPTF, these predictions are good for evaluation of the different combinations of theories represented by the different cases for this facility.

Soot volume fraction predictions for the various cases illustrate the impact of the different  $Y_T$  and  $N_C$  models on the  $Y_C$  equation as well as the differences between the empirical predictions of Adams and Smith (1993) and the new models. Excluding the  $N_C$  equation (Cases 4 and 5) did not significantly impact the resulting soot volume fraction predictions. Large iterative codes do not necessarily make identically the same predictions if slight variations are made in the input and operating conditions. It would be difficult to distinguish from the FPTF results the effect of the  $N_C$  equation on soot volume fraction predictions from this iteration to iteration variability. This suggests that assuming an average soot number density is not a bad assumption for this case; using the  $N_C$  equation may not be worth the extra computational time required to solve this variable. However, a possible benefit of using this equation may be more accurate particle size predictions which could be used for a scattering model, or for other applications which would require detailed predictions of particle sizes.

The empirical tar equation predicts significantly lower quantities of tar in the maximum regions, but the tar is spread out over a longer region. Overall, this results in predictions of similar quantities of soot to the complete model, and similar soot contours. While the use of the CPD model for tar source term predictions is likely to result in more accurate tar predictions, results from this model suggest that in the absence of such a model (CPD), the empirical tar formulation may serve as a reasonable approximation.

This result is one of the most surprising results from this research, especially since the somewhat arbitrarily assumed  $C_1$  variable did not need to be modified from the assumed value for the empirical soot model. Although the equations used to predict the empirical tar formation understandably represent the coal volatiles to a certain extent, the reason that distinct tar predictions would result in such similar soot volume fraction predictions remains without a good theoretical explanation. The good soot volume fraction results from the empirical tar equation may be case dependent. Further testing is recommended to determine the extent of the accuracy of this empirical assumption for tar formation.

The good agreement between the data and the numerical predictions for this case illustrates the necessity for including a model that will accurately predict the soot field and account for the radiative effects. Just as in the CPR predictions, it is difficult to know the accuracy of the turbulence model, which may be the most significant contributing factor to the inaccuracies presented in the data. Despite these modeling problems, the predictions represent well the measurements in the test facility. The results also seem to indicate an improvement in the overall predictions due to the inclusion of the soot models.

#### **7.4 General Discussion**

An important result of this research is the improved capability to predict soot formation in coal flames. Predictions of soot characteristics in the FFB showed good agreement with the measurements for all the different coals modeled. This agreement helps support the proposed formation and oxidation mechanisms for soot and tar. It is also apparent from the FFB results that the soot particles per unit mass equation can be

used to predict particle diameters similar to what was measured in the experimental apparatus. Soot cloud plots conform well to the observed characteristics from the experiments as well. Overall, the FFB case provides a good test of the soot formation mechanism, and the model agrees well with the data. Results from the CPR also show reasonable correlation between soot measurements and predictions, but the model used did not prove to be sufficient for accurate comparisons. More work is needed on the development of a CPR model to adequately evaluate the soot model based on this burner.

A major benefit of the new soot model is that it represents a reduction in empiricism compared to the previous modeling efforts. Reduction in empiricism is likely to result in improved robustness as well as more accurate predictions. The improved robustness of the new model is demonstrated in the fact that the empirical models are incapable of predicting soot in the FFB case. Because the newly developed method is similar to soot modeling efforts in similar hydrocarbon flames, the inclusion of a model to account for acetylene, benzene or soot derived from similar sources would be simply a matter of adding source terms to the existing equations.

Attempts to distinguish the accuracy of the individual soot models were hampered by difficulties with turbulence and other CFD modeling issues. Although sufficient data did not exist to ascertain the increased accuracy between the empirical and transport equation based models in existing experiments, results from the FPTF indicate a possible improvement. More testing would be required to validate the improvement in predictions. The improved accuracy using the transport equations can only be assumed based on the closer relation between the transport equation based models and the transport and kinetic theory.

Despite the somewhat limited agreement with the data for oxidizing flames, the model demonstrates the necessity for consideration of soot in comprehensive coal prediction codes. An increase in the amount of predicted soot causes a change in predicted gas temperatures and NO<sub>x</sub> concentrations. The fact that inclusion of a soot model lowers the predicted local gas temperature in the flame zone by as much as 300 K and NO<sub>x</sub> concentration by as much as 250 ppm in the FPTF adds credence to the assertion that including a soot model is important. Additionally, it appears from the FFB, CPR, and FPTF results that the effects of soot increase with the larger sized furnaces. Since the furnaces modeled were smaller test scale models, the effect of accounting for soot would be expected to be even more important for the large industrial scale furnaces.

## **7.5 Recommendations**

It is recommended that research be conducted in several major areas in order to improve this model. A primary difficulty with this project was the lack of reliable soot and tar measurements taken in coal flames. Having detailed and reliable data would provide an improved means through which the various models may be evaluated and improved. More than anything, this could be remedied by the development of a method to make such measurements, overcoming the inherent interference from coal, char, and ash particles present during the burning of the coal. Also, the oxidation term for the tar is not considered to be very reliable. The tar oxidation rate was derived from different coals than were used in the furnaces modeled, and the rate was for the light gas volatiles in addition to the tar. The predicted tar yield is sensitive to the tar kinetics, and

uncertainties in predicted tar yields may detract from the reliability of the soot model. Soot oxidation is a function of the soot particles per unit mass, which has been shown to yield questionable results under the conditions present in the FPTF. Although the particle count appears to have a minimal effect on the resulting soot volume fraction, the development of more accurate source terms for the  $N_C$  equation would provide important details regarding soot particle sizes.

The variety of methods existing for calculating coal derived soot provide various degrees of empiricism. The most developed model is capable of predicting particle sizes. The accuracy of these predictions appears to be good based on results from the FFB, but needs improvement to properly model regions of low soot volume fraction. Including a source term to account for oxidation and gasification of soot particles may improve the  $N_C$  model. Assuming an average soot number density does not significantly affect the ultimate soot volume fraction predictions in any of the cases considered, and may be a reasonable assumption. Using the transport equation for calculating  $N_C$  is recommended for cases where specific soot particle size predictions are required. Excluding the  $N_C$  equation is recommended to reduce the cost in computer run time. The empirical tar equation method predicts significantly different tar contours in the FPTF than the transport equation method. Although both tar equations result in a similar soot contour predictions in the FPTF and similar gas temperature and species concentrations in the FPTF and CPR, the less empirical transport equation method is recommended where accurate tar source terms are possible. Since the CPD model more closely represents coal devolatilization, the less empirical transport equation method is recommended for soot.

Other possible improvements are suggested which relate indirectly to the soot model. A big challenge in CFD codes is accurately predicting turbulence, as was apparent in the CPR and FPTF results. It is thought that the turbulence impacts soot chemistry and distribution; no attempt was made here to describe these effects. Particle scattering from soot agglomerates might influence predictions as well. More accurate radiative properties could also contribute to overall predictive capabilities. Resorting to Lagrangian statistical methods may be necessary for accurate predictions if the transport equation method is shown to be insufficient. Modeling tar ejection velocities may also be important, especially for laminar single particle cases such as the FFB. Finally, the consideration of OH as an oxidizer instead of just O<sub>2</sub> may prove necessary for accurate predictive capabilities.

## 8. CONCLUSIONS

A model of soot formation from coal tar was incorporated into a 3-D comprehensive coal combustion code (PCGC-3). Soot oxidation and agglomeration were also included. The model was tested versus data from a high temperature pyrolysis reactor and two laboratory scale coal combustors. Based on the predictions made, the following conclusions were reached.

1. The soot model is capable of predicting soot behavior in both non-oxidizing and oxidizing environments based on predicted tar yields from the CPD model.
2. Good agreement was achieved with the high temperature pyrolysis data from a flat flame burner, including gas temperatures, total soot yields, and qualitative diameter characteristics.
3. Fairly good agreement with data from the Fireside Performance Test Facility was achieved.
4. Good predictions for the Controlled Profile Reactor were not achieved, despite significant effort to model this reactor. Further research into the development of more accurate predictions for the Controlled Profile Reactor is needed.
5. Computational analysis on the impact of including a soot model indicates that the gas temperatures are lowered by as much as 300 K, and  $\text{NO}_x$  concentrations are lowered by as much as 250 ppm. The most significant differences were observed in the predictions of the Fireside Performance Test Facility, which was the largest furnace modeled. Because the impact of soot is shown to be significant in a large furnace,

modeling soot in coal-fired flames is thought to be important to assure accurate predictions.

6. Including a soot model in comprehensive coal combustion modeling code appears to improve the gas temperature and NO<sub>x</sub> concentration predictions. Uncertainties exist, but it is difficult to distinguish these uncertainties due to the limited capabilities of the code in modeling turbulence effects and the problems with developing adequate model grids.
7. Proper characterization of the coal is vital to the accurate prediction of tar release. This has a direct impact on the resulting soot predictions.
8. The average soot particle diameter was calculated accurately in this research in regions of high soot. These calculations are based on the soot particles per unit mass equation. Calculating the soot particles per unit mass equation is recommended to provide predictions of the average soot particle diameter. Assuming an average soot number density appears from the modeling results in this research to be a reasonable alternative to save computation time without significant reduction in the accuracy of the soot volume fraction predictions.
9. Although tar yields may be adequately represented through an empirical formula, using the more theoretical and accurate network particle devolatilization models are recommended over the empirical formula for tar predictions.
10. The developed soot model represents a significant additional time expense to model convergence. The full model may add as much as fifty percent to the time required to converge. Added convergence time requirements may be reduced by starting the soot

model after flow parameters such as velocities and pressures have approached convergence, or else by using the quicker, more empirical models.

11. Additional data on coal-derived soot would greatly increase the ability to perform detailed validation tests.
12. Future related research areas involve the including the effects of soot particle gasification, modeling soot oxidation by OH, improving soot optical properties, improving turbulence models, modeling tar ejection velocities, accounting for scattering of agglomerates, and accounting for the interaction between soot and turbulence.

## REFERENCES

- Adams, B. R., "Computational Evaluation of Mechanisms Affecting Radiation in Gas-and Coal-Fired Industrial Furnaces," Ph.D. Dissertation University of Utah (1993).
- Adams, B. R., and P. J. Smith, "Modeling Effects of Soot and Turbulence-Radiation Coupling on Radiative Transfer in Turbulent gaseous Combustion," *Combustion Science and Technology*, 109, 121-140 (1995).
- Ahluwalia, R. K. and K. H. Im, "Spectral Radiative Heat-Transfer in Coal Furnaces using a Hybrid Technique", *Journal of the Institute of Energy*, 67, 23-29, March (1994).
- Axelbaum, R. L., W. L. Flower and C. K. Law, "Dilution and Temperature Effects of Inert Addition on Soot Formation in Counterflow Diffusion Flames," *Combustion Science and Technology*, 61, 51-73, (1988).
- Bartok, W. and A. F. Sarofim, "Fossil Fuel Combustion," John Wiley & Sons, Inc., (1991).
- Boardman, R. D., C. N. Eatough and G. J. Germane, "Comparison of Measurements and Predictions of Flame Structure and Thermal NO<sub>x</sub>, in a Swirling, Natural Gas Diffusion Flame," *Combustion Science and Technology*, 93, 1-6, 193-210, (1993).
- Brewster, B. S., S. C. Hill, P. T. Radulovic, and L. D. Smoot, "Comprehensive Modeling." Chapter 8 *Fundamentals of Coal Combustion for Clean and Efficient Use*, edited by Smoot, L. D., 567-706 (1993).
- Butler, B. W., "An Experimental Evaluation of Radiant Energy Transport in Particle-Laden Flames," Ph.D. Dissertation, Brigham Young University (1992).
- Chen, J, "Effect of Secondary Reactions on Product Distribution and Nitrogen Evolution from rapid Coal Pyrolysis," Ph.D. Dissertation, Stanford University, (1991).
- Coelho, P. J., and M. G. Carvalho, "Modeling of Soot Formation in Turbulent Diffusion Flames." ASME paper, HTD-Vol. 272, *Heat Transfer in Fire and Combustion Systems* (1994).
- Fairweather, M., W. P. Jones and R. P. Lindstedt, "Predictions of Radiative Transfer from a Turbulent Reacting Jet in a Cross-Wind," *Combustion and Flame*, 89, 45-63 (1992).
- Fiveland, W., personal communication, (1997).

- Fiveland, W., "Discrete Ordinates Solutions of the Radiative Transport Equation for Rectangular Enclosures," *Journal of Heat Transfer*, vol. 106, no. 4, 699-706, (1984).
- Fletcher, T. H., A. R. Kerstein, R. J. Pugmire, M. S. Solum and D. M. Grant, "Chemical Percolation Model for Devolatilization. 3. Direct Uses of C NMR Data To Predict Effects of Coal Type," *Energy & Fuels*, 6, 4, 414-431 (1992).
- Frenklach, M., "Development of Predictive Reaction Models of Soot Formation", Annual Technical Report, Grant No. AFOSR 91-0129, January 31, (1991).
- Genetti, D. B., and T. H. Fletcher, "Predicting  $^{13}\text{C}$  NMR Measurements of Chemical Structure of Coal Based on Elemental Composition and Volatile Matter Content," *ACS Division of Fuel Chemistry*, Preprints, 42:1, 194-198 (1997).
- Grant, D. M., R. J. Pugmire, T. H. Fletcher, and A. R. Kerstein, "Chemical Model of Coal Devolatilization Using Percolation Lattice Statistics," *Energy & Fuels*, 3:175-186, (1989).
- Haneberg, A. L., "Soot Volume Fraction Determined by Two-Color Extinction in a Practical Scale Pulverized Coal Flame," Masters Thesis, Brigham Young University, (1997).
- Hedman, P. O., personal communication, (1997).
- Hedman, P. O., and D. L. Warren, "Turbulent Velocity and Temperature Measurements from a Gas-Fueled Technology Combustor with a Practical Fuel Injector," *Combustion and Flame*, 100: 185-192, (1995).
- Hill, S. C., L. D. Smoot and P. J. Smith, "Prediction of Nitrogen Oxide Formation in Turbulent Coal Flames," *Twentieth Symposium (International) on Combustion/The Combustion Institute*, 1391-1400, (1984).
- Honnery, D. R., and J. H. Kent, "Soot Mass Growth Modeling in Laminar Diffusion Flames." *Twenty-Fourth Symposium (International) on Combustion/The Combustion Institute*, 1041-1047 (1992).
- Hottel, H. C. and A. F. Sarofim, *Radiative Transfer*, McGraw-Hill, New York (1967).
- Kennedy, I. M., W. Kollmann and J. Y. Chen, "A Model for Soot Formation in a Laminar Diffusion Flame," *Combustion and Flame*, 73-85, July (1990).
- Kent, J. H., and R. W. Bilger, "Turbulent Diffusion Flames," *Fourteenth Symposium (International) on Combustion/The Combustion Institute*, 1041-1047 (1972).

- Kent, J. H., and D. R. Honnery, "A Soot Formation Map for a Laminar Ethylene Diffusion Flame," *Combustion and Flame*, 79, 287-298 (1990).
- Kollmann, W., I. M. Kennedy, M. Metternich and J.-Y. Chen, "Application of a Soot Model to a Turbulent Ethylene Diffusion Flame," *Springer Series in Chemical Physics*, 59, 503-526 (1994).
- Lee, K. B., M. W. Thring and J. M. Beer, "On the Rate of Combustion of Soot in a Laminar Soot Flame," *Combustion and Flame*, 6, 3, Sep. (1962).
- Leung, K. M., P. Lindstedt and W. P. Jones, "A Simplified Reaction Mechanism for Soot Formation in Nonpremixed Flames," *Combustion and Flame*, 87, 289-305 (1991).
- Ma J., "Soot Formation and Secondary Reactions During Coal Pyrolysis," Ph.D. Dissertation, Brigham Young University (1996).
- Magnussen, B. F. and B. H. Hjertager, "On Mathematical Modelling of Turbulent Combustion with Special Emphasis on Soot Formation and Combustion," *Sixteenth Symposium (International) on Combustion, the Combustion Institute*, 719-728, (1977).
- Majidi, V., N. Xu and K. Saito "Probing Soot Particles Using Laser Based Techniques," *SPIE* 2122, 146-152 (1994).
- McLean, W. J., D. R. Hardesty, and J. H. Pohl, "Direct Observations of Devolatilizing Pulverized Coal Particles in a Combustion Environment," *Eighteenth Symposium (International) on Combustion, the Combustion Institute*, 1239 (1980).
- Mengüç, M. P. and B. W. Webb, "Radiative Heat Transfer," Chapter 5 *Fundamentals of Coal Combustion for Clean and Efficient Use*, edited by Smoot, L. D., 375-431 (1993).
- Moss, J. B., C. D. Stewart and Syed, K. J., "Flowfield Modelling of Soot Formation at Elevated Pressure," *Twenty-Second Symposium (International) on Combustion, The Combustion Institute, Pittsburgh*, 413-423 (1988).
- Moss, J. B., C. D. Stewart and K. J. Young, "Modeling Soot Formation and Burnout in a High Temperature Laminar Diffusion Flame Burning Under Oxygen-Enriched Conditions," *Combustion and Flame*, 101:491-500, (1995).
- Nagel, J. and R. F. Strickland-Constable, "Oxidation of Carbon Between 1000°-2000°C," *Proceedings of the 5th Conference on Carbon*, Pergamon, 1, 154, (1961).
- Nenniger, R. D., J. B. Howard and A. F. Sarofim, "Sooting Potential of Coals," *Proceedings of the 1983 International Conference on Coal Science*, 521 (1983).

- Niksa, S., and A. R. Kerstein, "Flashchain Theory for Rapid Coal Devolatilization Kinetics," *Energy & Fuels*, 5:647-655, (1991).
- Patankar, S. V., *Numerical Heat Transfer and Fluid Flow*, Hemisphere Publishing Corporation, (1980).
- PCGC-3 Users Manual*, Published by the Advanced Combustion Engineering Research Center, Brigham Young University (1993).
- Puri, R., R. J. Santoro, and K. C. Smyth, "The Oxidation of Soot and Carbon Monoxide in Hydrocarbon Diffusion Flames," *Combustion and Flame*, 97, 125-144 (1994).
- Rigby, J. "Experimentally Determined Optical Properties, Volume Fraction and Temperature Measurements of Coal Soot in a Slot Flame Reactor," Ph.D. Dissertation, Brigham Young University (1996).
- Sanderson, D. K., "Composition of Combustion Gases and Particles in a Pulverized Coal-Fired Reactor," M. S. Thesis, Brigham Young University (1993).
- Seeker, W. R., G. S. Samuelson, M. P. Heap, and J. D. Trolinger, "Thermal Decomposition of Pulverized Coal Particles," *Eighteenth Symposium (International) on Combustion*, 1213 (1980).
- Shaw, D. W., X. Zhu, M. K. Misra, and R. H. Essenhigh, "Determination of Global Kinetics of Coal Volatiles Combustion," *Twenty-Third Symposium (International) on Combustion*, 1155-1162 (1990).
- Siegel, R. and J. R. Howell, *Thermal Radiation Heat Transfer Third Edition*, Hemisphere Publishing Corporation (1992).
- Sivathanu, Y. R., and J. P. Gore, "Coupled Radiation and Soot Kinetics Calculations in Laminar Acetylene/Air Diffusion Flames." *Combustion and Flame*, 97, November, 161-172 (1994).
- Smith, K. L., L. D. Smoot, T. H. Fletcher and R. J. Pugmire, *The Structure and Reaction Processes of Coal*, Plenum Chemical Engineering Series, (1994).
- Smoot, L. D. and P. J. Smith, *Coal Combustion and Gasification*, Plenum Press (1985).
- Solomon, P. R., D. G. Hamblen, R. M. Carangelo, M. A. Serio, and G. V. Desphande, "Models of Tar Formation During Coal Devolatilization," *Energy & Fuels*, 2:405-422, (1988).
- Thornock, D. E., P. J. Grandia, and B. F. Griffith, "Combustion Modeling: A Combustion Data Set Taken in the Pilot-Scale Fireside Performance Test

Facility”, Company Confidential, ABB Power Plant Laboratories, 5, March (1993).

Ulrich, G. D., “Theory of Particle Formation and Growth in Oxide Synthesis Flames,” *Combustion Science and Technology*, Vol. 4, 47-57, (1971).

Villasenor, R., and I. M. Kennedy, “Soot Formation and Oxidation in Laminar Diffusion Flames,” *Twenty-Fourth Symposium (International) on Combustion*, 1023-1030 (1992).

Wilcox, D. C., “Comparison of Two-Equation Turbulence Models for boundary Layers With Pressure Gradient,” *AIAA Journal*, Vol. 31, No. 8, August, (1993).

Wornat, M. J., A. F. Sarofim, and J. P. Longwell, “Changes in the Degree of Substitution of Polycyclic Aromatic Compounds from Pyrolysis of a High-Volatile Bituminous Coal,” *Energy and Fuels*, Vol. 1, 431, (1987).

## **APPENDIX**

## Appendix A. PCGC-3 Modifications Required for the Soot Model

Including the soot model in PCGC-3 required the modification of several of the major subroutines. It also required the creation of several new subroutines to determine the soot volume fraction and to calculate the impact of the soot on the absorption coefficient. Table A.1 contains a list of the subroutines modified and created as part of this research. Additionally, a program listing of the new subroutines has been included in Appendix B.

**Table A.1**

### Changes to PCGC-3 Required for the Soot Model.

<i>Modified Subroutines</i>	<i>New Subroutines</i>
eolp.f	calcnu.f
init.f	calcyc.f
output.f	calfv.f
psict.f	caltar.f
radtn.f	caltra.f
restrt.f	radst.f
setup.f	
threed.f	
unders.f	

## Appendix B. Program Listing of New Soot Subroutines

```

SUBROUTINE CALCNU
C-----
C      THREE-DIMENSIONAL VERSION
C CALCN ASSEMBLES THE COEFFICIENTS FOR THE FINITE DIFFERENCE SPECIES
C CONTINUITY EQUATION ACCORDING TO A CONTROL VOLUME APPROACH. LISOLV
C IS CALLED TO SOLVE FOR THE MEAN NU CONCENTRATIONS AT EACH NODE.
C
C-----
C      AFC          IS THE ARRHENIUS PRE-EXPONENTIAL FOR SOOT FORMATION
C      AOC          IS THE ARRHENIUS PRE-EXPONENTIAL FOR SOOT OXIDATION
C      CACOLL       IS THE COLLISION CONSTANT FOR SOOT
C      CPIP         IS THE # OF CARBON ATOMS PER INCIPIENT SOOT PARTICLE
C      EFC          IS THE ACTIVATION ENERGY FOR SOOT FORMATION
C      EOC          IS THE ACTIVATION ENERGY FOR SOOT OXIDATION
C      KBOLTZ       IS BOLTZMAN'S CONSTANT
C      MWC          IS THE MOLECULAR WEIGHT OF CARBON
C      ZNA          IS AVAGADROS NUMBER
C      RGC          IS THE IDEAL GAS CONSTANT
C      RHOC         IS THE AVERAGE SOOT DENSITY
C      RHONUA       IS THE AVERAGE SOOT PARTICLE NUMBER DENSITY
C-----
      INCLUDE 'dimen.i'
      INCLUDE 'paraml.i'
      INCLUDE 'COEFLOG.I'
      INCLUDE 'GEOM.I'
      INCLUDE 'LOGPSOU.I'
      INCLUDE 'MISC2.I'
      INCLUDE 'MISC4.I'
      INCLUDE 'MISC6.I'
      INCLUDE 'SOOTDAT.I'
      INCLUDE 'PFLOW.I'
      INCLUDE 'EFVAR.I'
      INCLUDE 'CPARAF0.I'
      INCLUDE 'C.I'
      INCLUDE 'PHICOE.F.I'

      DIMENSION AC(NX,NY,NZ),OLD(NX,NY,NZ),TRES(NX,NY,NZ)
      TCONS = 0.0
      IF (LCONS) TCONS = 1.0
      DATA EFC/198.9/,AFC/5.02E8/,RGC/0.0083144/,CPIP/9.0E4/,
&      MWC/12.011/,ZNA/6.022E26/
      DATA RHOC/1950.0/,PIC/3.1415927/,BOLTZK/1.381E-23/,CACOLL/3.0/
      NNUL0 = 0
      NNUG1 = 0
C-----
C      STORE OLD VALUES
C-----
      DO 75 K = 1,NK
        DO 50 J = 1,NJ
          DO 25 I = 1,NI
            OLD(I,J,K) = YNU(I,J,K)
          25 CONTINUE
        50 CONTINUE
      75 CONTINUE
C-----
C      ASSEMBLY OF COEFFICIENTS
C-----
      DO 220 K = 2,NKM1
        DO 210 J = 2,NJM1

```

```

DO 203 I = 2,NIM1
C-----
C   CALCULATE COEFFICIENTS
C-----
      CALL CALPHI(PRNU,I,J,K)
C-----
C   ASSURE FEASIBLE CALCULATIONS
C-----
      IF(YNU(I,J,K).LT.0.0)THEN
        YNU(I,J,K) = 0.0
        NNULO = NNULO + 1
      ENDIF
      IF(YNU(I,J,K).GT.1.0E20)THEN
        YNU(I,J,K) = 5.0E19
        NNUG1 = NNUG1 + 1
      ENDIF
C-----
C   ASSEMBLE SOURCE COEFFICIENTS
C-----
      SU(I,J,K) = CPO*YNU(I,J,K)+SU(I,J,K)
      IF (LTEST) SU(I,J,K) = SU(I,J,K) + FSU(I,J,K)*VOL
      SP(I,J,K) = -CP-SPM(I,J,K)
C-----
C   SOURCE TERMS FROM FAIRWEATHER ET AL. (1992) AND DERIVED BY
C   ALEX BROWN, 1996 FOR COAL SOOT.
C-----
C   *****      FORMATION      *****
C   CPIP IS THE CARBON PARTICLES PER INCIPIENT SOOT PARTICLE
C-----
      SU(I,J,K) = SU(I,J,K) + AFC * EXP(-EFC / (RGC *
&   TG(I,J,K))) * TAR(I,J,K) * DEN(I,J,K) * VOL / (CPIP * MWC / ZNA)
C-----
C   *****      AGGLOMERATION      *****
C   CACOLL IS THE COLLISION CONSTANT
C   KBOLTZ IS BOLTZMAN'S CONSTANT
C-----
      SP(I,J,K) = SP(I,J,K) - VOL * 2 * CACOLL *
&   (6.0 * MWC / (PIC * RHOC) ) ** 0.16666666666667 *
&   (6.0 * BOLTZK * TG(I,J,K) / RHOC) ** 0.5
&   * DEN(I,J,K) ** 2 * ( ABS( YC(I,J,K) ) / MWC) ** 0.16666666667 *
&   YNU(I,J,K) ** 0.833333333
203   CONTINUE
      DO 206 I = 2,NIM1
        IF (PCELL(I,J,K).EQ.WALL) THEN
          SU(I,J,K) = GREAT*0.0
          SP(I,J,K) = -GREAT
        ENDIF
206   CONTINUE
210   CONTINUE
220   CONTINUE
C-----
C   PROBLEM MODIFICATIONS
C-----
      CALL MODPHI(YNU)
C-----
C   FINAL ASSEMBLY AND RESIDUAL SOURCE CALCULATION
C-----
      RESNU = 0.0
      TRNNU = 0.0
      DO 420 K = 2,NKM1
        DO 410 J = 2,NJM1
          DO 400 I = 2,NIM1
            AP(I,J,K) = AE(I,J,K)+AW(I,J,K)+AN(I,J,K)+AS(I,J,K)+

```

```

&          AT(I,J,K)+AB(I,J,K)-SP(I,J,K)+AC(I,J,K)
RESOR = AE(I,J,K)*YNU(I+1,J,K)+AW(I,J,K)*YNU(I-1,J,K)+
&          AN(I,J,K)*YNU(I,J+1,K)+AS(I,J,K)*YNU(I,J-1,K)+
&          AT(I,J,K)*YNU(I,J,K+1)+AB(I,J,K)*YNU(I,J,K-1)-
&          AP(I,J,K)*YNU(I,J,K)+SU(I,J,K)
TRUNC = AP(I,J,K)*YNU(I,J,K)
IF (-SP(I,J,K).GT.0.5*GREAT) THEN
    RESOR = RESOR/GREAT
    RESOR = 0.0
    TRUNC = TRUNC/GREAT
ENDIF
RESNU = RESNU+ABS(RESOR)
TRNNU = TRNNU + ABS(TRUNC)
C-----
C          UNDERRELAXATION OF YNU
C-----
    AP(I,J,K) = AP(I,J,K)/URFNU
    SU(I,J,K) = SU(I,J,K) + (1.0-URFNU)*AP(I,J,K)*YNU(I,J,K)
400    CONTINUE
410    CONTINUE
420    CONTINUE
C-----
C          SOLUTION OF DIFFERENCE EQUATIONS
C-----
    IST = 2
    JST = 2
    KST = 2
    DO 600 N = 1,NSWPNU
        LSWPWE = .TRUE.
        LSWPSN = .TRUE.
        LSWPBT = .TRUE.
        CALL LISOLV(IST,JST,KST,NI,NJ,NK,YNU)
        RTOT = 0.0
        DO 520 K = 2,NKM1
            DO 510 J = 2,NJM1
                DO 500 I = 2,NIM1
                    RSIDNU = AE(I,J,K)*YNU(I+1,J,K)+AW(I,J,K)*YNU(I-1,J,K)+
&                    AN(I,J,K)*YNU(I,J+1,K)+AS(I,J,K)*YNU(I,J-1,K)+
&                    AT(I,J,K)*YNU(I,J,K+1)+AB(I,J,K)*YNU(I,J,K-1)-
&                    AP(I,J,K)*YNU(I,J,K)+SU(I,J,K)
                    IF (-SP(I,J,K).GT.0.5*GREAT) RSIDNU = 0.0
                    RTOT = RTOT + ABS(RSIDNU)
500                CONTINUE
510            CONTINUE
520        CONTINUE
        ISPNU = N
        IF (RTOT.LE.0.003*RESNU) GO TO 800
600    CONTINUE
    IF (RTOT/RESNU .GT. 1.0 .AND. .NOT.LTEST) THEN
        PRINT *, ' YNU DIVERGING BY: ',RTOT/RESNU,' USING OLD VALUES '
        DO 550 K=1,NK
            DO 540 J=1,NJ
                DO 530 I=1,NI
                    YNU(I,J,K) = OLD(I,J,K)
530                CONTINUE
540            CONTINUE
550        CONTINUE
    ENDIF
800    CONTINUE
    IF (LRESID) THEN
        DO 950 K=2,NKM1
            DO 940 J=2,NJM1
                DO 930 I=2,NIM1
                    VRESID(I,J,K) = TRES(I,J,K)

```

```

930     CONTINUE
940     CONTINUE
950     CONTINUE
      LRESID = .FALSE.
      ENDIF
C-----
C   IS TRUNCATION ERROR IN LISOLV OR HERE?
C-----
C     IF (CONVL*TRNCF.NE.0.0) RESNU = MIN(CONVL*TRNNU,RESNU)
C-----
C   INDICATE NUMBER OF CORRECTIONS MADE IF ANY
C-----
      IF (NNULO.GT.0.OR.NNUG1.GT.0)
&   WRITE(6,*)'# TIMES YNU<0:',NNULO,
&   ' , NU>1E20:',NNUG1
      RETURN
      END

      SUBROUTINE CALCYC
C-----
C   THREE-DIMENSIONAL VERSION
C CALCYC ASSEMBLES THE COEFFICIENTS FOR THE FINITE DIFFERENCE SPECIES
C CONTINUITY EQUATION ACCORDING TO A CONTROL VOLUME APPROACH. LISOLV
C IS CALLED TO SOLVE FOR THE MEAN YC (SOOT MASS FRACTION) AT EACH NODE.
C-----
C-----
C   AFC           IS THE ARRHENIUS PRE-EXPONENTIAL FOR SOOT FORMATION
C   AOC           IS THE ARRHENIUS PRE-EXPONENTIAL FOR SOOT OXIDATION
C   EFC           IS THE ACTIVATION ENERGY FOR SOOT FORMATION
C   EOC           IS THE ACTIVATION ENERGY FOR SOOT OXIDATION
C   NTLO          COUNTS THE # OF TIMES TAR IS LESS THAN ZERO
C   NYCL0         COUNTS THE # OF TIMES YC IS LESS THAN ZERO
C   NYCG1         COUNTS THE # OF TIMES YC IS GREATER THAN 1
C   RGC AND ROC   ARE IDEAL GAS CONSTANTS
C   RHOC          IS THE AVERAGE SOOT DENSITY
C   RHONUA        IS THE AVERAGE SOOT PARTICLE NUMBER DENSITY
C-----
      INCLUDE 'dimen.i'
      INCLUDE 'param1.i'
      INCLUDE 'param2.i'
      INCLUDE 'COEFLOG.I'
      INCLUDE 'GEOM.I'
      INCLUDE 'LOGPSOU.I'
      INCLUDE 'MISC4.I'
      INCLUDE 'MISC6.I'
      INCLUDE 'MISC2.I'
      INCLUDE 'SOOTDAT.I'
      INCLUDE 'EFVAR.I'
      INCLUDE 'PFLOW.I'
      INCLUDE 'CINDEX.I'
      INCLUDE 'CPARAF0.I'
      INCLUDE 'C.I'
      INCLUDE 'PHICOE.F.I'

      DIMENSION AC(NX,NY,NZ),OLD(NX,NY,NZ),TRES(NX,NY,NZ)
      INTEGER NTLO,NYCL0,NYCG1
      TCONS = 0.0
      IF (LCONS) TCONS = 1.0
      NTLO = 0
      NYCL0 = 0
      DATA RGC/0.0083144/,EFC/198.9/,AFC/5.02E8/
      DATA PIC/3.1415927/,RHOC/1950/,AOC/1.085E5/,EOC/39300/,ROC/1.9872/
      DATA RHONUA/1E16/

```

```

C-----
C   STORE OLD VALUES
C-----
      DO 75 K = 1,NK
        DO 50 J = 1,NJ
          DO 25 I = 1,NI
            OLD(I,J,K) = YC(I,J,K)
          25   CONTINUE
        50   CONTINUE
      75   CONTINUE
C   LTZ = 0
C   GTM = 0
C-----
C   ASSEMBLY OF COEFFICIENTS
C-----
      DO 220 K = 2,NKM1
        DO 210 J = 2,NJM1
          DO 203 I = 2,NIM1
C-----
C   CALCULATE COEFFICIENTS
C-----
          CALL CALPHI(PRYC,I,J,K)
C-----
C   ASSURE FEASIBLE CALCULATIONS
C-----
          IF(TAR(I,J,K).LT.0.0)THEN
            TAR(I,J,K) = 0.0
            NTL0 = NTL0 + 1
          ENDIF
          IF(YC(I,J,K).LT.0.0)THEN
            YC(I,J,K) = 0.0
            NYCL0 = NYCL0 + 1
          ENDIF
          IF(YC(I,J,K).GT.1.0)THEN
            YC(I,J,K) = 0.5
            NYCG1 = NYCG1 + 1
          ENDIF
C-----
C   ASSEMBLE SOURCE COEFFICIENTS
C-----
          IF (PCELL(I,J,K).NE.FFIELD) THEN
            SU(I,J,K) = GREAT*0.0
            SP(I,J,K) = -GREAT
          ELSE
            SU(I,J,K) = CPO*YC(I,J,K)+SU(I,J,K)
            IF (LTEST) SU(I,J,K) = SU(I,J,K) + FSU(I,J,K)*VOL
            SP(I,J,K) = -CP-SPM(I,J,K)
C-----
C   ***** FORMATION *****
C-----
            SU(I,J,K) = SU(I,J,K) + AFC *
            & EXP(- EFC / (RGC * TG(I,J,K) ) ) * TAR(I,J,K)* DEN(I,J,K) * VOL
            IF (ABS(YC(I,J,K)).GT.0.0) THEN
C-----
C   ***** OXIDATION: LEE ET AL. MODEL *****
C-----
            IF(LCNU) THEN
C-----
C   THE FIRST TWO LINES ARE THE SURFACE AREA OF THE SOOT FROM
C   KENNEDY ET AL. (1990).
C   THE NEXT TWO ARE THE REST OF THE LEE ET AL. OXIDATION MODEL.
C-----
            SP(I,J,K)=SP(I,J,K)-VOL*(6.0/ RHOC*DEN(I,J,K))*0.666666666667*
            & (PIC/YC(I,J,K)*DEN(I,J,K))*0.33333333*(YNU(I,J,K))*0.33333333

```

```

&      *AOC*SPECIE(I,J,K,IDO2)*EXP(-EOC/(ROC*TG(I,J,K)))
&      *TG(I,J,K)**-0.5
      ELSE
C-----
C      THE FIRST TWO LINES ARE THE SURFACE AREA OF THE SOOT FROM
C      KENNEDY ET AL. (1990).
C      THE NEXT TWO ARE THE REST OF THE LEE ET AL. OXIDATION MODEL.
C-----
      SP(I,J,K)=SP(I,J,K)-VOL*(6.0/RHOC*DEN(I,J,K))**0.66666666667
&      *(RHONUA*PIC/YC(I,J,K))**0.333333333333333
&      *AOC*SPECIE(I,J,K,IDO2)*EXP(-EOC/(ROC*TG(I,J,K)))
&      *TG(I,J,K)**-0.5
      ENDIF
      ENDIF
      ENDIF
203      CONTINUE
      DO 206 I = 2,NIM1
        IF (PCELL(I,J,K).EQ.WALL) THEN
          SU(I,J,K) = GREAT*0.0
          SP(I,J,K) = -GREAT
        ENDIF
206      CONTINUE
210      CONTINUE
220      CONTINUE

C-----
C      PROBLEM MODIFICATIONS
C-----
      CALL MODPHI(YC)
C-----
C      FINAL ASSEMBLY AND RESIDUAL SOURCE CALCULATION
C-----
      RESYC = 0.0
      TRNYC = 0.0
      DO 420 K = 2,NKM1
        DO 410 J = 2,NJM1
          DO 400 I = 2,NIM1
            AP(I,J,K) = AE(I,J,K)+AW(I,J,K)+AN(I,J,K)+AS(I,J,K)+
&              AT(I,J,K)+AB(I,J,K)-SP(I,J,K)+AC(I,J,K)
&      RESOR = AE(I,J,K)*YC(I+1,J,K)+AW(I,J,K)*YC(I-1,J,K)+
&              AN(I,J,K)*YC(I,J+1,K)+AS(I,J,K)*YC(I,J-1,K)+
&              AT(I,J,K)*YC(I,J,K+1)+AB(I,J,K)*YC(I,J,K-1)-
&              AP(I,J,K)*YC(I,J,K)+SU(I,J,K)
            TRUNC = AP(I,J,K)*YC(I,J,K)
            IF (-SP(I,J,K).GT.0.5*GREAT) THEN
              RESOR = RESOR/GREAT
              RESOR = 0.0
              TRUNC = TRUNC/GREAT
            ENDIF
            RESYC = RESYC+ABS(RESOR)
            TRNYC = TRNYC + ABS(TRUNC)
          ENDIF
        ENDIF
      ENDIF
C-----
C      UNDERRELAXATION OF YC
C-----
      AP(I,J,K) = AP(I,J,K)/URFYC
      SU(I,J,K) = SU(I,J,K) + (1.0-URFYC)*AP(I,J,K)*YC(I,J,K)
400      CONTINUE
410      CONTINUE
420      CONTINUE

C-----
C      SOLUTION OF DIFFERENCE EQUATIONS
C-----
      IST = 2
      JST = 2

```

```

KST = 2
DO 600 N = 1,NSWPYC
  LSWPWE = .TRUE.
  LSWPSN = .TRUE.
  LSWPBT = .TRUE.
  CALL LISOLV(IST,JST,KST,NI,NJ,NK,YC)
  RTOT = 0.0
  DO 520 K = 2,NKM1
    DO 510 J = 2,NJM1
      DO 500 I = 2,NIM1
        RSIDYC = AE(I,J,K)*YC(I+1,J,K)+AW(I,J,K)*YC(I-1,J,K)+
&                AN(I,J,K)*YC(I,J+1,K)+AS(I,J,K)*YC(I,J-1,K)+
&                AT(I,J,K)*YC(I,J,K+1)+AB(I,J,K)*YC(I,J,K-1)-
&                AP(I,J,K)*YC(I,J,K)+SU(I,J,K)
        IF (-SP(I,J,K).GT.0.5*GREAT) RSIDYC = 0.0
        RTOT = RTOT + ABS(RSIDYC)
500      CONTINUE
510    CONTINUE
520  CONTINUE
C-----
C      ESTIMATE SOOT VOLUME FRACTION BASED ON MASS FRACTION
C-----
      DO 521 K = 2,NK
        DO 511 J = 2,NJ
          DO 501 I = 2,NI
            FV(I,J,K) = DEN(I,J,K)/1950.0*YC(I,J,K)
501      CONTINUE
511    CONTINUE
521  CONTINUE

      ISPYC = N
      IF (RTOT.LE.0.003*RESYC) GO TO 800
600 CONTINUE
      IF (RESYC.NE.0.0) THEN
      IF (RTOT/RESYC .GT. 1.0 .AND. .NOT.LTEST) THEN
        PRINT *, ' YC DIVERGING BY: ',RTOT/RESYC, 'USING OLD VALUES'
        DO 550 K=1,NK
          DO 540 J=1,NJ
            DO 530 I=1,NI
              YC(I,J,K) = OLD(I,J,K)
530      CONTINUE
540    CONTINUE
550  CONTINUE
      ENDIF
      ENDIF
800 CONTINUE
      IF (LRESID) THEN
        DO 950 K=2,NKM1
          DO 940 J=2,NJM1
            DO 930 I=2,NIM1
              VRESID(I,J,K) = TRES(I,J,K)
930      CONTINUE
940    CONTINUE
950  CONTINUE
          LRESID = .FALSE.
      ENDIF
C-----
C      INDICATE NUMBER OF CORRECTIONS MADE IF ANY
C-----
      IF (NTL0.GT.0.0.OR.NYCL0.GT.0.OR.NYCG1.GT.0.0)
&    WRITE(6,*)'# TIMES TAR INCREASED TO 0:',NTL0,', YC:',NYCL0,
&    ' YC.GT.1:',NYCG1
      RETURN
      END

```

```

*****
C This code is the soot formation model proposed
C by Adams. Modified to run with PCGC-3 on 9/28/95 by
C Alex Brown.
C Last modification: 6/6/96
*****
      SUBROUTINE CALFV
*****
C CPARAF0.I contains BF1, BF0
C CINDEXT.I contains ILC
C GEOM.I contains DEN()
C EFVAR.I contains F() and ETA()
C C.I contains BCT()
C PFLOW.I contains E() and TG()
C SOOTDAT.I contains FV()
*****
      REAL EDLT,C4
      INCLUDE 'dimen.i'
      INCLUDE 'param1.i'
      INCLUDE 'param2.i'
      INCLUDE 'GEOM.I'
      INCLUDE 'CPARAF0.I'
      INCLUDE 'CINDEX.I'
      INCLUDE 'EFVAR.I'
      INCLUDE 'C.I'
      INCLUDE 'PFLOW.I'
      INCLUDE 'SOOTDAT.I'
      INCLUDE 'LOGBUG.I'

      RHOSOOT = 1950.
      C3 = 0.10
      ECRIT = 1.0
      EDLT = 1.0
      DO 75 K = 1,NK
        DO 50 J = 1,NJ
          DO 25 I = 1,NI
C-----
C   CALCULATE THE AMOUNT OF CARBON IN THE CELL
C-----
          IF (LCALE2) THEN
            BC = DEN(I,J,K)
            & * ((BF1(ILC)*F(I,J,K) + BF0(ILC)*(1.-F(I,J,K)))
            & *(1.0-ETA(I,J,K)) + BCT(ILC)*ETA(I,J,K))*(1.
            & -ETA2(I,J,K))+ ETA2(I,J,K)*BCT2(ILC)
          ELSE
            BC = DEN(I,J,K)
            & * ((BF1(ILC)*F(I,J,K) + BF0(ILC)*(1.-F(I,J,K)))
            & *(1.0-ETA(I,J,K)) + BCT(ILC)*ETA(I,J,K))
          ENDIF
C-----
C   DETERMINE THE OXIDATION CONSTANT
C-----
          C4 = MAX(0.0,MIN((E(I,J,K)-ECRIT),EDLT))/EDLT
C-----
C   ESTIMATE THE SOOT VOLUME FRACTION
C-----
          FV(I,J,K) = C3 * BC * 12.0 * C4 / RHOSOOT
25      CONTINUE
50      CONTINUE
75      CONTINUE

```

RETURN  
END

SUBROUTINE CALTAR

```
C-----  
C      THREE-DIMENSIONAL VERSION  
C CALTAR ASSEMBLES THE COEFFICIENTS FOR THE FINITE DIFFERENCE SPECIES  
C CONTINUITY EQUATION ACCORDING TO A CONTROL VOLUME APPROACH. LISOLV  
C IS CALLED TO SOLVE FOR THE MEAN TAR MASS FRACTIONS AT EACH NODE.  
C  
C-----  
C      AFC          IS THE ARRHENIUS PRE-EXPONENTIAL FOR SOOT FORMATION  
C      AGT          IS THE ARRHENIUS PRE-EXPONENTIAL FOR TAR GASIFICATION  
C      AOT          IS THE ARRHENIUS PRE-EXPONENTIAL FOR TAR OXIDATION  
C      EFC          IS THE ACTIVATION ENERGY FOR SOOT FORMATION  
C      EGT          IS THE ACTIVATION ENERGY FOR TAR GASIFICATION  
C      EOT          IS THE ACTIVATION ENERGY FOR TAR OXIDATION  
C      RGC AND ROT  ARE IDEAL GAS CONSTANTS  
C      MWC          IS THE MOLECULAR WEIGHT OF CARBON  
C-----  
      INCLUDE 'dimen.i'  
      INCLUDE 'param1.i'  
      INCLUDE 'param2.i'  
      INCLUDE 'COEFLOG.I'  
      INCLUDE 'GEOM.I'  
      INCLUDE 'LOGPSOU.I'  
      INCLUDE 'MISC4.I'  
      INCLUDE 'MISC6.I'  
      INCLUDE 'MISC2.I'  
      INCLUDE 'RATEPOL.I'  
      INCLUDE 'SOOTDAT.I'  
      INCLUDE 'EFVAR.I'  
      INCLUDE 'PFLOW.I'  
      INCLUDE 'CPARAF0.I'  
      INCLUDE 'C.I'  
      INCLUDE 'CINDEX.I'  
      INCLUDE 'PHICOE.F.I'  
  
      DIMENSION AC(NX,NY,NZ),OLD(NX,NY,NZ),TRES(NX,NY,NZ)  
      TCONS = 1.0  
      IF (LCONS) TCONS = 2.0  
      DATA RGC/0.008314/,EFC/198.9/,AFC/5.02E8/,EGT/286.9/,AGT/9.77E10/  
      DATA AOT/1870508/,EOT/12.50/,ROT/.0019872/,MWO2/32.0/  
C-----  
C      STORE OLD VALUES  
C-----  
      DO 75 K = 1,NK  
        DO 50 J = 1,NJ  
          DO 25 I = 1,NI  
            OLD(I,J,K) = TAR(I,J,K)  
25          CONTINUE  
50          CONTINUE  
75          CONTINUE  
C-----  
C      ASSEMBLY OF COEFFICIENTS  
C-----  
      DO 220 K = 2,NKM1  
        DO 210 J = 2,NJM1  
          DO 203 I = 2,NIM1  
C-----  
C      CALCULATE COEFFICIENTS  
C-----
```

```

CALL CALPHI(PRTAR,I,J,K)
C-----
C ASSEMBLE SOURCE COEFFICIENTS
C-----
IF (PCELL(I,J,K).NE.FFIELD) THEN
    SU(I,J,K) = GREAT*0.0
    SP(I,J,K) = -GREAT
ELSE
    SU(I,J,K) = CPO*TAR(I,J,K)+SU(I,J,K)
    IF (LTEST) SU(I,J,K) = SU(I,J,K) + FSU(I,J,K)*VOL
    SP(I,J,K) = -CP-SPM(I,J,K)
C-----
C ***** FORMATION *****
C SPTAR IS THE TAR FROM THE PARTICLE PHASE EQUATIONS.
C THE NEXT TWO LINES ARE THE LOSS OF TAR TO SOOT.
C THE FINAL LINE IS THE RATE OF TAR GASIFICATION.
C-----
SU(I,J,K) = SU(I,J,K) + SPTAR(I,J,K)
SP(I,J,K) = SP(I,J,K) - AFC *
& EXP(-EFC / (RGC * TG(I,J,K))) *VOL*DEN(I,J,K) - AGT *
& EXP(-EGT / (RGC * TG(I,J,K))) *VOL*DEN(I,J,K)
C-----
C ***** OXIDATION *****
C (SHAW ET AL. 1990)
C [C(O2)]=MWO2*SPECIE(O2)*WTM
C [C(V)] = TAR
C A=1870508 M^3/KG/S E=12.5 KCAL/MOL
C-----
SP(I,J,K) = SP(I,J,K) -MWO2*VOL*DEN(I,J,K)**2*SPECIE(I,J,K,IDO2)*
& WTM(I,J,K)*AOT*EXP(-EOT/(ROT*TG(I,J,K)))
ENDIF
203 CONTINUE
DO 206 I = 2,NIM1
    IF (PCELL(I,J,K).EQ.WALL) THEN
        SU(I,J,K) = GREAT*0.0
        SP(I,J,K) = -GREAT
    ENDIF
206 CONTINUE
210 CONTINUE
220 CONTINUE
C-----
C PROBLEM MODIFICATIONS
C-----
CALL MODPHI(TAR)
C-----
C FINAL ASSEMBLY AND RESIDUAL SOURCE CALCULATION
C-----
RESTAR = 0.0
TRNTAR = 0.0
DO 420 K = 2,NKM1
    DO 410 J = 2,NJM1
        DO 400 I = 2,NIM1
            AP(I,J,K) = AE(I,J,K)+AW(I,J,K)+AN(I,J,K)+AS(I,J,K)+
& AT(I,J,K)+AB(I,J,K)-SP(I,J,K)+AC(I,J,K)
            RSID = AE(I,J,K)*TAR(I+1,J,K)+AW(I,J,K)*TAR(I-1,J,K)+
& AN(I,J,K)*TAR(I,J+1,K)+AS(I,J,K)*TAR(I,J-1,K)+
& AT(I,J,K)*TAR(I,J,K+1)+AB(I,J,K)*TAR(I,J,K-1)-
& AP(I,J,K)*TAR(I,J,K)+SU(I,J,K)
            TRUNC = AP(I,J,K)*TAR(I,J,K)
            IF (-SP(I,J,K).GT.0.5*GREAT) THEN
                RSID = RSID/GREAT
                RSID = 0.0
                TRUNC = TRUNC/GREAT
            ENDIF
        ENDDO
    ENDDO
ENDDO

```

```

                ENDIF
                RESTAR = RESTAR+ABS(RSID)
                TRNTAR = TRNTAR + ABS(TRUNC)
C-----
C                UNDERRELAXATION OF TAR
C-----
                AP(I,J,K) = AP(I,J,K)/URFTAR
                SU(I,J,K) = SU(I,J,K) + (1.0-URFTAR)*AP(I,J,K)*TAR(I,J,K)
400        CONTINUE
410        CONTINUE
420        CONTINUE
C-----
C                SOLUTION OF DIFFERENCE EQUATIONS
C-----
                IST = 2
                JST = 2
                KST = 2
                DO 600 N = 1,NSPTAR
                LSWPWE = .TRUE.
                LSWPSN = .TRUE.
                LSWPBT = .TRUE.
                CALL LISOLV(IST,JST,KST,NI,NJ,NK,TAR)
                RTOT = 0.0
                DO 520 K = 2,NKM1
                DO 510 J = 2,NJM1
                DO 500 I = 2,NIM1
                TAR(I,J,K) = AMIN1(TAR(I,J,K), 1.0)
                TAR(I,J,K) = AMAX1(0.0,TAR(I,J,K))
                RSID = AE(I,J,K)*TAR(I+1,J,K)+AW(I,J,K)*TAR(I-1,J,K)+
&                    AN(I,J,K)*TAR(I,J+1,K)+AS(I,J,K)*TAR(I,J-1,K)+
&                    AT(I,J,K)*TAR(I,J,K+1)+AB(I,J,K)*TAR(I,J,K-1)-
&                    AP(I,J,K)*TAR(I,J,K)+SU(I,J,K)
                IF (-SP(I,J,K).GT.0.5*GREAT) RSID = 0.0
                TRES(I,J,K) = RSID
                RTOT = RTOT + ABS(RSID)
500        CONTINUE
510        CONTINUE
520        CONTINUE
                ISPTAR = N
                IF (RTOT.LE.0.003*RESTAR) GO TO 800
600        CONTINUE
                IF(RTOT/RESTAR .GT. 1.0 .AND. .NOT.LTEST) THEN
                PRINT *, ' TAR DIVERGING BY: ',RTOT/RESTAR,' USING OLD VALUES'
                DO 550 K=1,NK
                DO 540 J=1,NJ
                DO 530 I=1,NI
                TAR(I,J,K) = OLD(I,J,K)
530        CONTINUE
540        CONTINUE
550        CONTINUE
                ENDIF
800        CONTINUE
                IF (LRESID) THEN
                DO 950 K=2,NKM1
                DO 940 J=2,NJM1
                DO 930 I=2,NIM1
                VRESID(I,J,K) = TRES(I,J,K)
930        CONTINUE
940        CONTINUE
950        CONTINUE
                LRESID = .FALSE.
                ENDIF
C-----
C                IS TRUNCATION ERROR IN LISOLV OR HERE?

```

```

C-----
C      IF (CONVL*TRNCF.NE.0.0) RESTAR = MIN(CONVL*TRNTAR,RESTAR)
C      RETURN
C      END

*****
C This code is the soot formation model proposed
C by Adams. Modified to run with PCGC-3 on 9/28/95 by
C Alex Brown. Rerived for tar correlation on 6/14/96
C Last modification: 9/26/96
*****
      SUBROUTINE CALTRA
*****
C CPARAF0.I contains BF1, BF0
C CINDEX.I contains ILC
C EFVAR.I contains F() and ETA()
C C.I contains BCT()
C PFLOW.I contains E() and TG()
C SOOTDAT.I contains FV()
*****
      REAL EDLT,C4
      INCLUDE 'dimen.i'
      INCLUDE 'param1.i'
      INCLUDE 'param2.i'
      INCLUDE 'GEOM.I'
      INCLUDE 'CPARAF0.I'
      INCLUDE 'CINDEX.I'
      INCLUDE 'EFVAR.I'
      INCLUDE 'C.I'
      INCLUDE 'PFLOW.I'
      INCLUDE 'SOOTDAT.I'
      INCLUDE 'LOGBUG.I'

C-----
C      THIS C3 PARAMETER THE FORMATION CONSTANT.
C-----
      C3 = 0.10
      ECRIT = 1.0
      EDLT = 1.0

C-----
C      LOOP OVER THE FLOWFIELD
C-----
      DO 75 K = 1,NK
        DO 50 J = 1,NJ
          DO 25 I = 1,NI

C-----
C      CALCULATE THE CARBON MASS-ATOMS
C-----
          IF(LCALE2) THEN
            BC = ((BF1(ILC)*F(I,J,K)+BF0(ILC)*(1.-F(I,J,K)))
&              *(1.0-ETA(I,J,K))+BCT(ILC)*ETA(I,J,K))*(1.-ETA2(I,J,K))
&              + ETA2(I,J,K)*BCT2(ILC)
          ELSE
            BC = ((BF1(ILC)*F(I,J,K)+BF0(ILC)*(1.-F(I,J,K)))
&              *(1.0-ETA(I,J,K)) + BCT(ILC)*ETA(I,J,K))
          ENDIF

C-----
C      DETERMINE OXIDATION WEIGHTING BASED ON THE EQUIVALENCE RATIO
C-----
          C4 = MAX(0.0,MIN((E(I,J,K)-ECRIT),EDLT))/EDLT

C-----
C      COMBINE TO FORM TAR
C-----

```

```

          TARA(I,J,K) = C3 * BC * 12.0 * C4 *DEN(I,J,K)
25      CONTINUE
50      CONTINUE
75      CONTINUE

```

```

      RETURN
      END

```

```

*****
C This code is the soot radiation model proposed
C by Adams and Smith (1995). Modified to run with
C PCGC-3 on 9/28/95 by Alex Brown.
C Last modification: 5/7/96
*****

```

```

      SUBROUTINE RADST (I,J,K,OPL)
*****

```

```

C GEOM.I contains ABSKT()
C CPARAF0.I contains BF1, BF0
C CINDEXT.I contains ILC
C EFVAR.I contains F() and ETA()
C C.I contains BCT()
C PFLOW.I contains E() and TG()
*****

```

```

      INTEGER I,J,K
      INCLUDE 'dimen.i'
      INCLUDE 'param1.i'
      INCLUDE 'param2.i'
      INCLUDE 'GEOM.I'
      INCLUDE 'PFLOW.I'
      INCLUDE 'RAD.I'
      INCLUDE 'SOOTDAT.I'
      REAL EMISS

```

```

C-----
C USE THE CORRELATION BY SAROFIM AND HOTTEL (1978) TO FIND
C THE EMISSIVITY
C-----

```

```

      EMISS = 1-(1.0+350.0*FV(I,J,K)*TG(I,J,K)*OPL)**-4

```

```

C-----
C CONVERT THE EMISSIVITY TO AN ABSORPTION COEFFICIENT AND ADD IT
C TO THE TOTAL ABSORPTION COEFFICIENT.
C-----

```

```

      ABSKT(I,J,K) = ABSKT(I,J,K) + MIN( 8.0, ((4.0/OPL)
& *ALOG(1.0+350.*FV(I,J,K)*TG(I,J,K)*OPL)))
      RETURN
      END

```

**Appendix C. Characteristic Parameters for the Coals Modeled.**

**Table C.1**

**Characteristics of the Various Coals Modeled (percent daf).**

	<i>Illinois #6</i>	<i>Pittsburgh #8</i>	<i>Utah Hiawatha</i>	<i>Ashland</i>	<i>Utah Blind Canyon</i>
Carbon	76.65	84.71	80.53	84.00	80.87
Hydrogen	4.93	5.4	5.96	6.00	6.06
Oxygen	10.01	7.26	11.71	7.60	10.96
Nitrogen	1.47	1.71	1.33	1.80	1.57
Sulpher	6.93	0.92	0.47	0.60	0.54
ASTM Volatile Matter	38.69	37.1	38.78	N/A	N/A

**Table C.2**

**<sup>13</sup>C NMR Data for the Coals Modeled.**

	<i>Illinois #6</i>	<i>Pittsburgh #8</i>	<i>Ashland</i>	<i>Utah Blind Canyon</i>
p0	0.52	0.45	0.44	0.49
c0	0.0	0.0	0.0	0.0
sigp1	5.5	5.0	5.3	5.1
mw1	402.00	420.23	420 .0	366 .0
mdel	39.0	34.0	44.3	36.0

**Table C.3****<sup>13</sup>C NMR Predictions from the Correlation of Genetti et al. (1997).**

	<i>Illinois #6</i>	<i>Pittsburgh #8</i>	<i>Utah Hiawatha</i>
p0	0.442567	0.6186545	0.582797
c0	0.0295573	0.045167	0.053853
sigp1	5.40411	4.93975	5.11437
mw1	431.1418	310.2762	330.7694
mdel	37.83503	25.25827	30.16151

## Appendix D. Additional Characterization of the Burners Modeled

**Table D.1**

**Characteristic Parameters of the Facilities Modeled.**

Case	Axial Scale (m)	Radial Scale (m)	Coal Feed Rate (kg/hr)	Equivalent Heating Rate (KWatts) *	Assumed Wall Emissivity	Average Wall Temp. (K)
FFB	0.016	~0.254	0.0015	0.01279	0.8	700
CPR	2.820	0.40	5.17	38.19	0.8	1000
FPTF	4.191	0.445	117.93	1035.0	0.9	1450

\* Assuming all the coal burned.

### A Data File Listing from the Flat Flame Burner Model

```

5,                                     !NSAY..(SAY(I),I=1,NSAY) follows:
***** PGC-3 *****
Flat Flame Burner Model
4 inches above the burner.
Pittsburgh #8 coal.
Modeled by Alex Brown.
T      T      F      T
F      F      T      F
T      F      F      F      T
T      T      F      T      F
F      F      F      F
T      T      F      F
T      T      T      F      F
F      F      F      F      F
T      T      F      T
0.80      ,      0.70      ,      0.98
0.60      ,      0.60      ,      0.85
0.00000E+00, 0.00000E+00, 0.00000E+00
-9.8000E+00, 0.00000E+00, 0.00000E+00
1000      ,      10      ,      1      ,      0
1      ,      1      ,      1
5      ,      50      ,      100
0.9000E+00, 0.0 0 ,
9.66e-7, 1.0, 0.0, 0.00, 0.0032, 0.000
9.99e-4, 0.0, 0.0, 0.00, 0.0231, 0.000
0.000 , 0.0 , 1.0, 0.00, 0.01 , 0.00
1.79000E-05, 86128.0 , 7.00000E+02
!LRSRT,LRDGD,LRDPR,LFLOW
!LPRIN,LCORD,LSMPR,LSMPT
!LCALF,LCALG,LFSOU,LCREE,LMETCEC
!LCLET,LCLGE,LCALE2,LCALH,LHPVW
!LKETM,LNLKM,LMLTM,LRLAM
!LCALN,LPRST,LTBUG,lcons
!LRAD,LPART,LCOAL,LSSF,L3REACT
!LPRDKK,LPRDJK,LNOX,LSORB,POLLUT
!LSOOT,LCTAR,LEMPST,LCNU
!URFUVW,URFKEM,URFP
!URFFGM,URFETG,URFH
!SOR,YSCENT,ZSCENT
!GX,GY,GZ
!MAXIT,INDOUT,IJKPR
!ISKIP,JSKIP,KSKIP
!INITPR,INDRST,INDPAR
!SORMAX,SORMIN
!FLOWPR,FPR,E2PR,TINPR,PRLS,SWNPR
!FLOWSC,FSC,E2SC,TINSC,SCLS,SWNSC
!FLOWTR,FTR,E2TR,TINTR,TRLS,SWNTR
!VISCOS,PRES,TWALL
!
(blank line)
ELEMENTS
THERMO
!The react. sect. is formatted
REACTANTS 1
298.00000
!TMP (unformatted)
N 2.00000 0.00000 0.00000 0.00000N2
1.00000M G
!
(blank line)
REACTANTS 2
298.00000
!TMP (unformatted)
O 2.00000 0.00000 0.00000 0.00000O2
0.17726M G
N 2.00000 0.00000 0.00000 0.00000N2
0.70782M G
C 1.00000H 4.00000 0.00000 0.00000CH4
0.11492M G
!
(blank line)

```

```

      T      F      T      T      F
100 5.00000E-03 1 1 3.00000E-01      !LSCAT,LWSSG,LH2O,LCO2,LCNVL(RADTN)
0.00000E+00 2.00000E+04      !MAXITR,QACCU,NBNS,NG,URFRAD
8.00000E-01      !RETA(ME), ME=1, NBNS+1
      10, 1, 26, 80, 15000,      !EMWALL(ME), ME=1, NBNS
0.4310, 0.0E+00, 0.0, 4.0E-01, 0.0E+00, !NSL,NPS,MAXITP,MINITP,NPMAX
ParticleDiameter      !PLODPR,PLODSC,PLODTR,URFNJ,SPRANG
6.900E-05 ,
ParticleDensity
1.340E+03 ,
ParticleVelocityLag
      1.0 ,
ParticleTemperatureLag
      1.0 ,
ParticleSizeMassFraction
1.000E+00 ,
ParticleSchmidtNumber
3.500E+03 ,
ParticleAbsorbCoefs
1.177E+00 ,
ParticleScatterCoefs
1.378E+00 ,
2.404E+00 ,
3.613E+00 ,
4.475E+00 ,
Last
1
      !NCARD
      COAL0.F INPUT All Particles have the same properties
      1, 1, 5, 0, 1,      !NCRXN,NHRXN,NPROP,IEUCK,KEQ,NSHRNK
2000.0000, 800.0000, 0.7000, 1.1000, 0, 0.100000
!RHOEHEL,RHOMIN,THETAC,SWELL,NFRAG,GAMMA
0.010000, 0.000001, 0.500000, 0.300000, 0.500000, !DELTPJ,DELRRJ,URFPM,URFPH,URFPV
0.55,FALSE      !fracv,lfracv
      T      F      F      !lcpd,LSNDCH,LNMRE
0.98, 0.93      !(fvolk(K) K=2,3) i.e. H, O
0.50, 0.75      !(fvolk(K) K=4,5) i.e. N, S
1.00000      !XI(J)
0.00000E+00, 3.73150E+02,      !QHC(J),TNBP
9.77170E-01, 0.00000E+00, 2.28300E-02,      !OMEGAC(J),OMEGAH(J),OMEGAA(J)
0.00000E-02,      !OMEGAW(J)
3.70000E+05, 7.36300E+07, 3.90000E-01,      !AMJ(J,M),EMJ(J,M),YY(J,M)
0.00000E+00, 0.00000E+00,      !HGV(J,M),SIGDEV(J,M)
      2.3 , 9.29E+07 , 1.0000 ,      !ALJ(J,L),EL(J,L),EMM(J,L)
      0.5 , 3.E8 , 2.512E8      !XORD(J,L),ACOCO2(J,L),ECOCO2(J,L)
-9.218E+06,-3.28E7      !HGH(J,L,1),HGH(J,L,2)
8.47100E-01, 5.40000E-02, 7.26000E-02,      !WIC(J,K)
1.71000E-02, 9.20000E-03,      !WIC(J,K)
H2O      H2O(L)      !SLRCMP
O2      !OXYD(L),L = 1,NHRXN
2.00000E+00,      !PHIL(L),L = 1,NHRXN
0.45      !p0
0.0      !c0
5.0      !sigpl
420.23      !mw1
34.0      !mdel
0.371      !ASTMVM
2.602e15      !ab
2.31794e8      !eb0
7.5312e6      !ebsig
0.9      !ac
0      !ec0
3.e15      !ag
2.88696e8      !eg0
3.389e7      !egsig
3.e15      !acr
2.7196e8      !ecr
      12, 6, 5, 12, 9,      !NTZ,NC,NTX,NTW,NE2
      0.0, 1.0, 0.0, 1.0, 0.0, 1.0, -1.0, 1.0, 0.0, 1.0,
!FMIN,FMAX,EMIN,EMAX,E2MIN,E2MAX,HLMIN,HLMAX,PIMIN,PIMAX
      1,      !NSAYNX..(SAYNX(I),I=1,NSAYNX) follows:
      ***** PCNOX *****
      2      !FUELNO FLG =1 S; =2 W; =3 MT; =0 no fuelno
      0      !THRMNO FLG =1 f&r; =2 f only; =0 no calc
      1, 0.5, 0, 0,      !RADOXY,EQTEST,RADOH,OHADJ
0.90, 0.90, 0.90, 0.05, 0.80, 0.000,      !PRNOX,PRHCN,PRNH3,FCTNO,FCTHCN,FCTNH3
      90, 2, 100, 1,      !MXITNX,ITYNX,INDPNX,ICALCN
      1.0000, 1.0000, 0.5, 2.0,      !XIANOX,ZEDA,FN2PRT,MAXRES
0.90, 0.90, 0.75,      !URFNOX,URFHCN,URFNH3
F      T      T      !LRSTNO,LPLTNX,LNHTNX

```

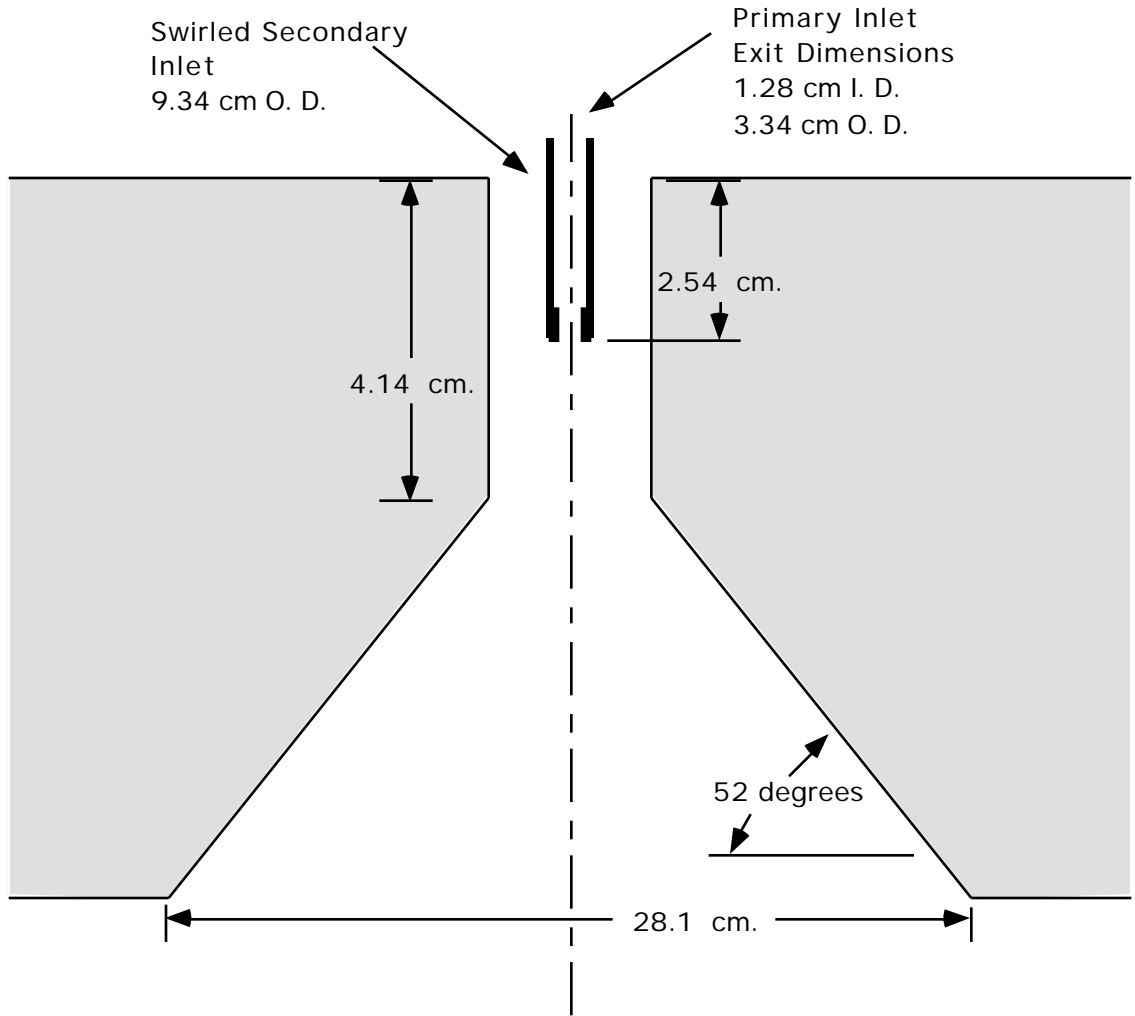


**Figure D.1 The Controlled Profile Reactor Inlet.**

**A Data File Listing from the Controlled Profile Reactor Model**

```

5,
***** PCGC-3 ***** !NSAY..(SAY(I),I=1,NSAY) follows:
>>>> Controlled Profile Reactor Case <<<<<
      3-Dimensional Version
      Sanderson's Case #5 (Swirl No. = 1.4)
      Alex Brown
T      T      T      T      !LRSRT,LRDGD,LRDPR,LFLOW
F      F      T      F      !LPRIN,LCORD,LSMPR,LSMPT
T      T      F      T      F      !LCALF,LCALG,LFSOU,LCREE,LMETCEC
T      T      F      T      T      !LCLET,LCLGE,LCALE2,LALH,LHPVW
T      T      F      T      !LKETM,LNLKM,LMLTM,LRLAM
T      T      F      T      !LCALN,LPRST,LTBUG,LCONS
T      T      T      F      F      !LRAD,LPART,LCOAL,LSSF,L3REACT
F      F      T      F      F      !LPRDKK,LPRDJK,LNOX,LSORB,POLLUT
T      T      F      T      !LSOOT,LCTAR,LEMPST,LCNU
0.70   ,      0.70   ,      0.98   !URFUVW,URFKEM,URFP
0.70   ,      0.70   ,      0.90   !URFFGM,URFETG,URFH
0.50   ,      0.70   ,      0.30   !URFTAR,URFYC,URFNU
0.000  ,      0.0000  ,      0.0000  !SOR,YSCENT,ZSCENT
9.8    ,      0.0    ,      0.0    !GX,GY,GZ

```

```

5000      , 100      , 2      , 0      !MAXIT,INDOUT,IJKPRT,IOPFMT
2         , 2         , 1         !ISKIP,JSKIP,KSKIP
5         , 100        , 100        !INITPR,INDRST,INDPAR
2.50     , 0.0000000 ,          !SORMAX,SORMIN
4.1667E-03, 1.0, 0.0, 0.10, 1.28E-02, 0.0      !4.1667E-
03FLOWPR,FPR,E2PR,TINPR,PRLS,SWNPR
35.28E-03, 0.0, 0.0, 0.10, 2.313E-02, 1.4 !35.28E-03FLOWSC,FSC,E2SC,TINSC,SCLS,SWNSC
0.001 , 0.0 , 1.0, 0.10, 0.01 , 0.00 !FLOWTR,FTR,E2TR,TINTR,TRLS,SWNTR
1.790E-05 , 101325.0 ,1000.0 !VISCOS,PRES,TWALL
!
! (Blank line)
ELEMENTS
THERMO !The react. sect. is formatted
REACTANTS 1
289.00, !TMP (unformatted)
O 2.00 0.00 0.00 0.00 O2 0.20948M G
N 2.00 0.00 0.00 0.00 N2 0.79052M G
!
! (Blank line)
REACTANTS 2
533.00, !TMP (unformatted)
O 2.00 0.00 0.00 0.00 O2 0.20948M G
N 2.00 0.00 0.00 0.00 N2 0.79052M G
!
! (Blank line)
T F T T F
100, .005, 1, 0, 0.5,
0., 20000.
0.8
20, 5, 6, 40, 15000, !NSL,NPS,MAXITP,MINITP,NPIMAX
0.760, 0.0, 0.0, 0.5, 0.0, !PLODPR,PLODSC,PLODTR,URFVNJ,SPRANG
ParticleDiameter
1.700E-06 , 6.500E-06 , 4.000E-05, 10.50E-05 ,
19.50E-05 ,
ParticleDensity
1340.0 , 1340.0 , 1340.0 , 1340.0 ,
1340.0 ,
ParticleVelocityLag
1.0 , 1.0 , 1.0 , 1.0 ,
1.0 ,
ParticleTemperatureLag
1.0 , 1.0 , 1.0 , 1.0 ,
1.0 ,
ParticleSizeMassFraction
0.0024 , 0.0126 , 0.510 , 0.366 ,
0.109 ,
ParticleSchmidtNumber
0.35 , 0.35 , 0.35 , 0.35 ,
0.35 ,
ParticleAbsorbCoefs
0.9300,0.8600,0.8200,0.8200,0.8200, !(QAB(IPS),IPS = 1,NPS)
ParticleScatterCoefs
1.350E-00 , 1.330E-00 , 1.310E-00 , 1.300E-00 , 1.290E-00 ,
2.490E-00 , 2.520E-00 , 2.550E-00 , 2.620E-00 , 2.710E-00 ,
3.980E-00 , 4.090E-00 , 4.160E-00 , 4.300E-00 , 4.450E-00 ,
5.320E-00 , 5.570E-00 , 5.710E-00 , 5.940E-00 , 6.160E-00 ,
Last
1, !NCARD
COAL0.F INPUT All Particles have the same Properties
1, 1, 5, 1, 0, 0, !NCRXN,NHRXN,NPROP,IEUCK,KEQ,NSHRNK
2000.0,800.0,0.7,1.0,0,0.1 !RHOHEL,RHOMIN,THETAC,SWELL,NFRAG,GAMMA
.01, 0.000001, 0.40, 0.4 , 0.4, !DELTPJ,DELRRJ,URFPM,URFPH,URFPV
0.55,FALSE !fracv,lfracv
T F F !lcpd,LSNDCH,LNMRE
0.8, 0.82 ! (fvolk(K) K=2,3) i.e. H, O
0.42, 0.12 ! (fvolk(K) K=4,5) i.e. N, S
1.0000 !XI(J)
0.0, 373.15, !QHC(J),TNBP
0.85590 , 0.00000E+00, 1.44100E-01, !OMEGAC(J),OMEGAH(J),OMEGAA(J)
0.00000E+00, !OMEGAW(J)
4.30000E+14, 2.29000E+08, 0.40000 , !AMJ(J,M),EMJ(J,M),YY(J,M)
0.00000E+00, 0.00000E+00, !HGV(J,M),SIGDEV(J,M)
2.3 , 9.29E+07 , 1.0000 , !ALJ(J,L),EL(J,L),EMM(J,L)
0.5 , 3.E8 , 2.512E8 !XORD(J,L),ACOCO2(J,L),ECOCO2(J,L)
-9.218E+06,-3.28E7 !HGH(J,L,1),HGH(J,L,2)
0.8087 , 0.0606 , 0.1096 , ! (WIC(J,K) K = 1,3)
0.0157 , 0.0054 , ! (WIC(J,K) K = 4,NLM)
H2O !SLRCMP
O2 !OXYD(L),L = 1,NHRXN
1.74, !PHIL(L) L = 1,NHRXN
0.49 !p0
0.0 !c0
5.1 !sigpl
366 .0 !mw1

```

```

36.0                                !mde1
0.45                                !ASTMVM
2.602e15                            !ab
2.31794e8                           !eb0
7.5312e6                             !ebsig
0.9                                  !ac
0                                    !ec0
3.e15                                !ag
2.88696e8                            !eg0
3.389e7                              !egsig
3.e15                                !acr
2.7196e8                             !ecr
12, 6, 5, 12, 9,                   !NTZ,NC,NTX,NTW,NE2
0.0, 1.0, 0.0, 1.0, 0.0, 1.0, -1.0, 1.0, 0.0, 1.0,
!FMIN,FMAX,EMIN,EMAX,E2MIN,E2MAX,HLMIN,HLMAX,PIMIN,PIMAX
4,                                  !NSAYNX..(SAYNX(I),I=1,NSAYNX) follows:
***** PCNOX *****
**** NOX POLLUTANT CALCULATION USING OUTPUT FROM PCGC-3 FOR THE ****
**** PHASE AND PARTICLE PROPERTIES THROUGHOUT THE FLOW FIELD ****
***** BASECASE *****
2                                !FUELNO FLG =1 S; =2 W; =3 MT; =0 no fuelno
0                                !THRMNO FLG =1 f&r; =2 f only; =0 no calc
1, 0.5, 0, 0,                   !RADOXY,EQTEST,RADOH,OHADJ
0.90, 0.90, 0.90, 0.05, 0.80, 0.000, !PRNOX,PRHCN,PRNH3,FCTNO,FCTHCN,FCTNH3
30, 2, 100, 1,                 !MXITNX,ITYNX,INDPNX,ICALCN
1.0000, 1.0000, 0.5, 2.5,      !XIANOX,ZEDA,FN2PRT,MAXRES
0.15,                            !chrno
0.90, 0.90, 0.75,              !URFNOX,URFHCN,URFNH3
T T T                            !LRSTNO,LPLTNX,LNHTNX

```

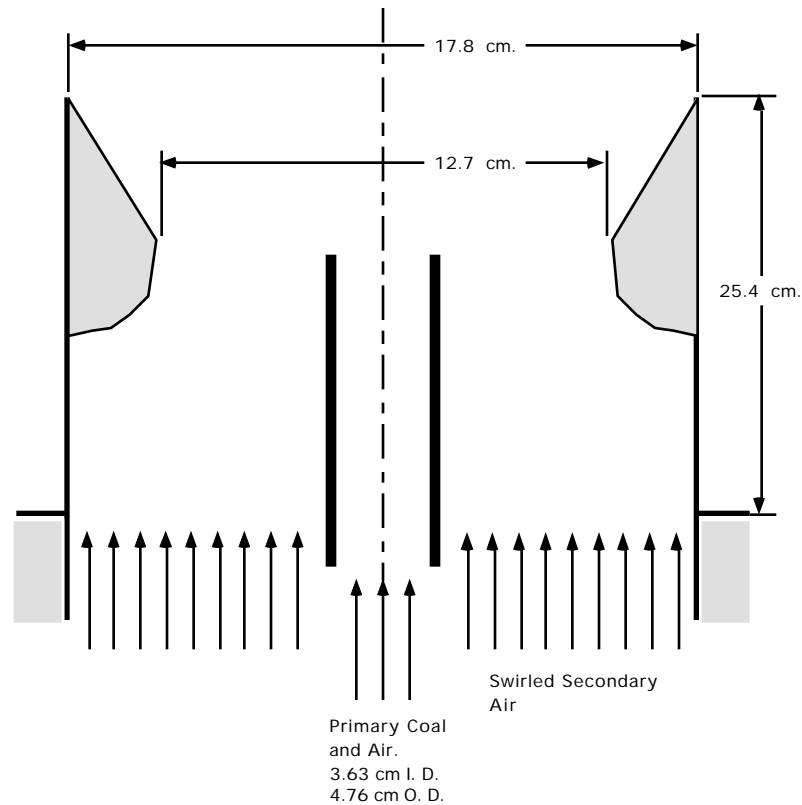


**Figure D.2 The Fireside Performance Test Facility Inlet.**

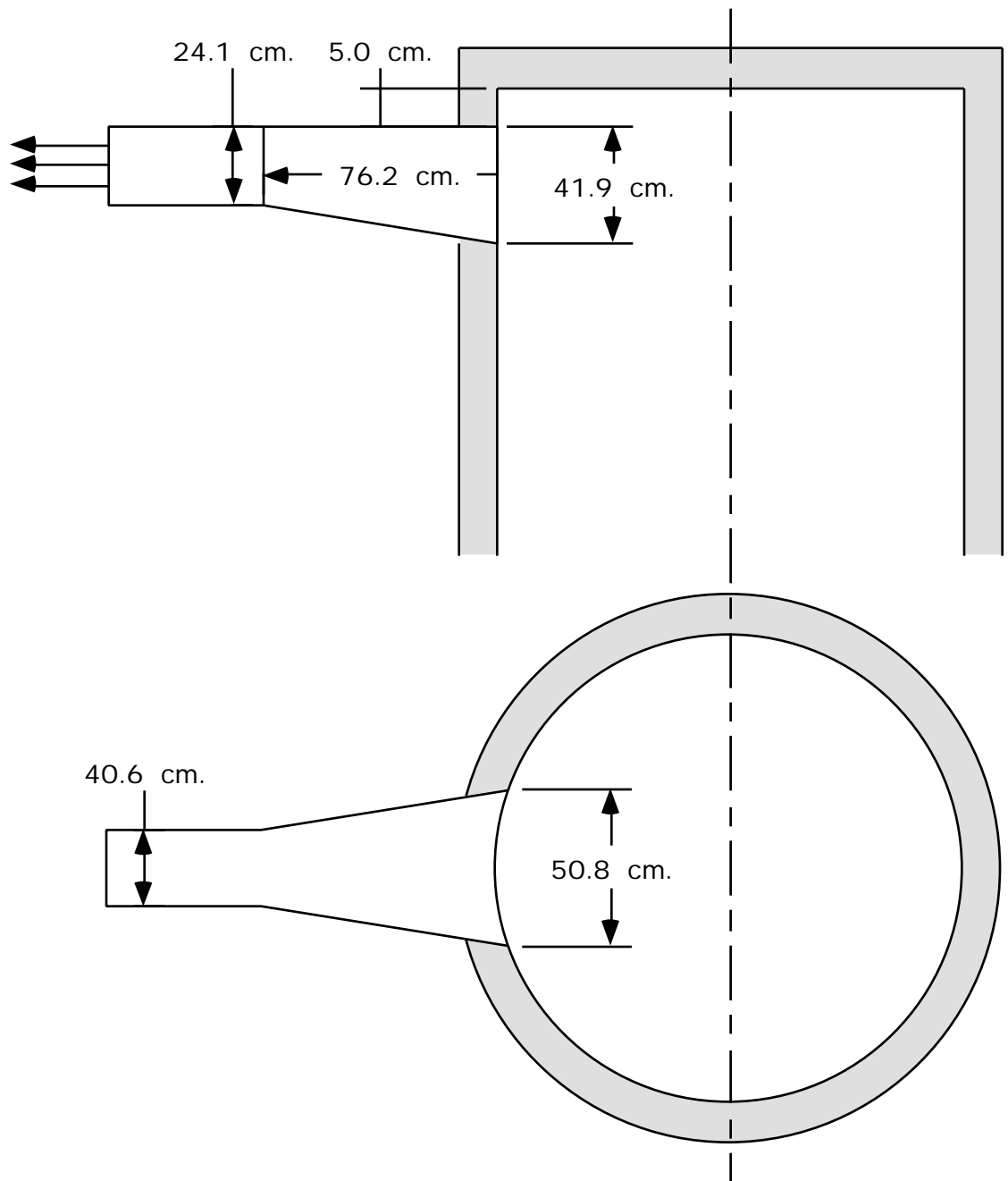


**Figure D.3 The Fireside Performance Test Facility Radiative Section.**

## A Data File Listing from the Fireside Performance Test Facility Model

```

4,                                     !NSAY..(SAY(I),I=1,NSAY) follows:
***** PCGC-3 *****
ABB-CE Fireside Performance Test Facility
      Coal Combustion Test #4
      with Over-fire air
      T      T      T      T
      F      F      T      F
      T      T      F      T      F
      T      T      F      T      T
      T      F      F      T
      T      T      F      F
      T      T      T      F      F
      F      F      T      F      F
      T      T      F      T
0.5      ,      0.6      ,      0.98
0.7      ,      0.7      ,      0.8
0.7      ,      0.7      ,      0.2
0.07     ,      1.22     ,      0.455
-9.8     ,      0.0      ,      0.0
1000     ,      100      ,      1 , 0
2        ,      2        ,      1
20       ,      100      ,      100
2.60     ,      0.0000000
0.0278   , 1.0, 0.0, 0.15, 0.05 , 0.0
0.3775   , 0.0, 0.0, 0.15, 0.08 , 2.45
0.001    , 0.0, 1.0, 0.10, 0.01 , 0.00
0.00002  ,      , 101327.0 , 1450.0
!LRSRT,LRDGD,LRDPR,LFLOW
!LPRIN,LCORD,LSMPR,LSMPT
!LCALF,LCALG,LFSOU,LCREE,LMETCEC
!LCALET,LCALGE,LCALE2,LCALH,LHPVW
!LKETM,LNLKM,LMLTM,LRLAM
!LCALN,LPRST,LTBUG,LCONS
!LRAD,LPART,LCOAL,LSFF,LREACT3
!LPRDKK,LPRDJK,LNOX,LSORB,POLLUT
!LSOOT,LCTAR,LEMPST,LCNU
!URFUVW,URFKEM,URFP
!URFFGM,URFETG,URFH
!URFTAR,URFYC,URFNU
!SOR,YSCENT,ZSCENT
!GX,GY,GZ
!MAXIT,INDOUT,IJKPRT,IOPFMT
!ISKIP,JSKIP,KSKIP
!INITPR,INDRST,INDPAR
!SORMAX,SORMIN
!FLOWPR(0.0301),FPR,TINPR,PRLS,SWNPR
!FLOWSC(0.3782),FSC,TINSC,SCLS,SWNSC
!FLOWTR,FTR,E2TR,TINTR,TRLS,SWNTR
!VISCOS,PRES,TWALL
!
      (Blank line)
ELEMENTS
THERMO
REACTANTS 1
294.400
O 2.      0.      0.      0.      O2      0.1911 M      G
N 2.      0.      0.      0.      N2      0.7214 M      G
H 2.      O 1.      0.      0.      H2O     0.0875 M      G
!
      (blank line)
REACTANTS 2
566.400
O 2.      0.      0.      0.      O2      0.21 M      G
N 2.      0.      0.      0.      N2      0.79 M      G
!
      (Blank line)
      T      F      T      T      F
100, .002, 1, 1, 0.5,
0., 20000.
0.9
64, 5, 12, 50, 15000,
1.176, 0.0, 0.0, 0.5, 0.0,
ParticleDiameter
10.0E-06, 14.00E-06, 20.00E-06, 30.00E-06,
60.0E-06,
ParticleDensity
1340.0, 1340.0, 1340.0, 1340.0,
1340.0,
ParticleVelocityLag
1.0, 1.0, 1.0, 1.0,
1.0,
ParticleTemperatureLag
1.0, 1.0, 1.0, 1.0,
1.0,
ParticleSizeMassFraction
0.266, 0.30, 0.164, 0.194,
0.076,
ParticleSchmidtNumber
0.35, 0.35, 0.35, 0.35,
0.35,
ParticleAbsorbCoefs
0.9300,0.8600,0.8200,0.8200,0.8200,
!(QAB(IPS),IPS = 1,NPS)
ParticleScatterCoefs
1.378E+00, 1.370E+00, 1.359E+00, 1.345E+00, 1.322E+00,
2.404E+00, 2.450E+00, 2.479E+00, 2.500E+00, 2.526E+00,
3.613E+00, 3.798E+00, 3.923E+00, 4.013E+00, 4.110E+00,
4.475E+00, 4.895E+00, 5.189E+00, 5.403E+00, 5.624E+00,
Last
1,
COAL0.F INPUT All Particles have the same Properties
1, 1, 5, 1, 0, 0,
2000.0,800.0,0.7,1.0,0,0.1
!NCARD
!NCRXN,NHRXN,NPROP,IEUCK,KEQ,NSHRNK
!RHOHEL,RHOMIN,THETAC,SWELL,NFRAG,GAMMA

```

```

.01, 0.000001, 0.40, 0.4 , 0.4,      !DELTPJ,DELRRJ,URFPM,URFPH,URFPV
0.55,FALSE                             !fracv,lfracv
      T      F      F                 !lcpd,LSNDCH,LNMRE
0.98, 0.93                             !(fvolk(K) K=2,3) i.e. H, O
0.50 , 0.75                             !(fvolk(K) K=4,5) i.e. N, S
      1.0000                             !XI(J)
-1.0, 373.15,                           !QHC(J),TNBP
0.91590 , 0.00000E+00, 1.44100E-01,    !OMEGAC(J),OMEGAH(J),OMEGAA(J)
0.00000E+00,                             !OMEGAW(J)
4.30000E+14, 2.29000E+08, 0.40000      , !AMJ(J,M),EMJ(J,M),YY(J,M)
0.00000E+00, 0.00000E+00,              !HGV(J,M),SIGDEV(J,M)
      0.85 , 9.99E+07 , 0.0000        , !ALJ(J,L),EL(J,L),EMM(J,L)
      0.5 , 3.E8 , 2.512E8              !XORD(J,L),ACOCO2(J,L),ECOCO2(J,L)
-9.218E+06,-3.28E7                       !HGH(J,L,1),HGH(J,L,2)
      0.8400 , 0.0600 , 0.0760        , !(WIC(J,K) K = 1,3)
      0.0180 , 0.0060 ,                !(WIC(J,K) K = 4,NLM)
H2O                                       !SLRCMP
O2                                       !OXYD(L),L = 1,NHRXN
      1.74,                             !PHIL(L) L = 1,NHRXN
0.44                                     !p0
0.0                                     !c0
5.3                                     !sigp1
420 .0                                  !mw1
44.3                                    !mdel
0.00                                    !ASTMVM
2.602e15                                !ab
2.31794e8                                !eb0
7.5312e6                                  !ebsig
0.9                                       !ac
0                                         !ec0
3.e15                                    !ag
2.88696e8                                !eg0
3.389e7                                  !egsig
3.e15                                    !acr
2.7196e8                                  !ecr
      12, 6, 5, 12, 9,                 !NTZ,NC,NTX,NTW,NE2
      0.0, 1.0, 0.0, 1.0, 0.0,        1.0, -1.0, 1.0, 0.0, 1.0,
!FMIN,FMAX,EMIN,EMAX,E2MIN,E2MAX,HLMIN,HLMAX,PIMIN,PIMAX
4,                                       !NSAYNX..(SAYNX(I),I=1,NSAYNX) follows:
      ***** PCNOX *****
      **** NOX POLLUTANT CALCULATION USING OUTPUT FROM PCGC-3 FOR THE ****
      **** PHASE AND PARTICLE PROPERTIES THROUGHOUT THE FLOW FIELD ****
      ***** BASECASE *****
2                                         !FUELNO FLG =1 S; =2 W; =3 MT; =0 no fuelno
0                                         !THRMNO FLG =1 f&r; =2 f only; =0 no calc
      1, 0.5, 0, 0,                    !RADOXY,EQTEST,RADOH,OHADJ
0.90, 0.90, 0.90, 0.05, 0.80, 0.000,  !PRNOX,PRHCN,PRNH3,FCTNO,FCTHCN,FCTNH3
      90, 2, 100, 1,                   !MXITNX,ITYNX,INDPNX,ICALCN
      1.0000, 1.0000, 0.5, 2.5,       !XIANOX,ZEDA,FN2PRT,MAXRES
      0.15,                              !chrno
      0.90, 0.30, 0.75,                !URFNOX,URFHCN,URFNH3
F      T      T                         !LRSTNO,LPLTNX,LNHTNX

```

### Appendix E. CPR Results for Additional Heights.

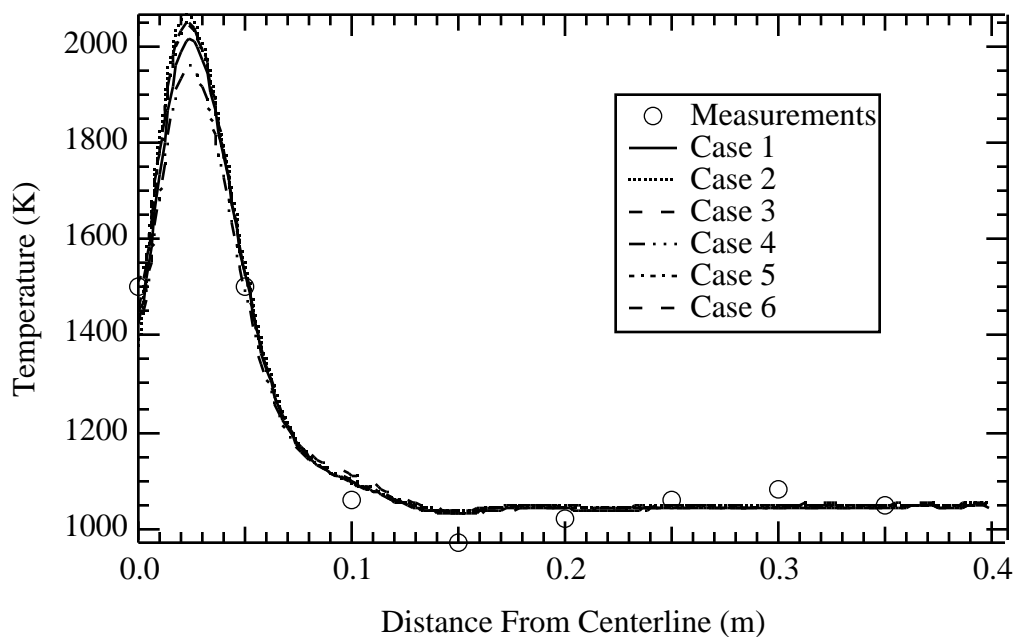


Figure E.1 Predicted and measured gas temperatures in the CPR at 15 cm below the inlet.

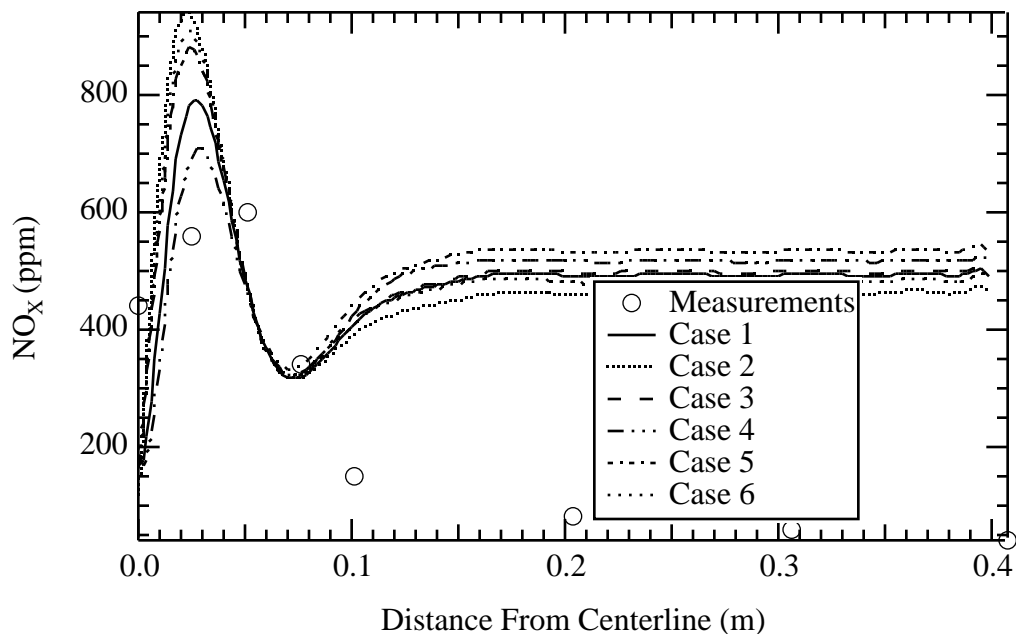
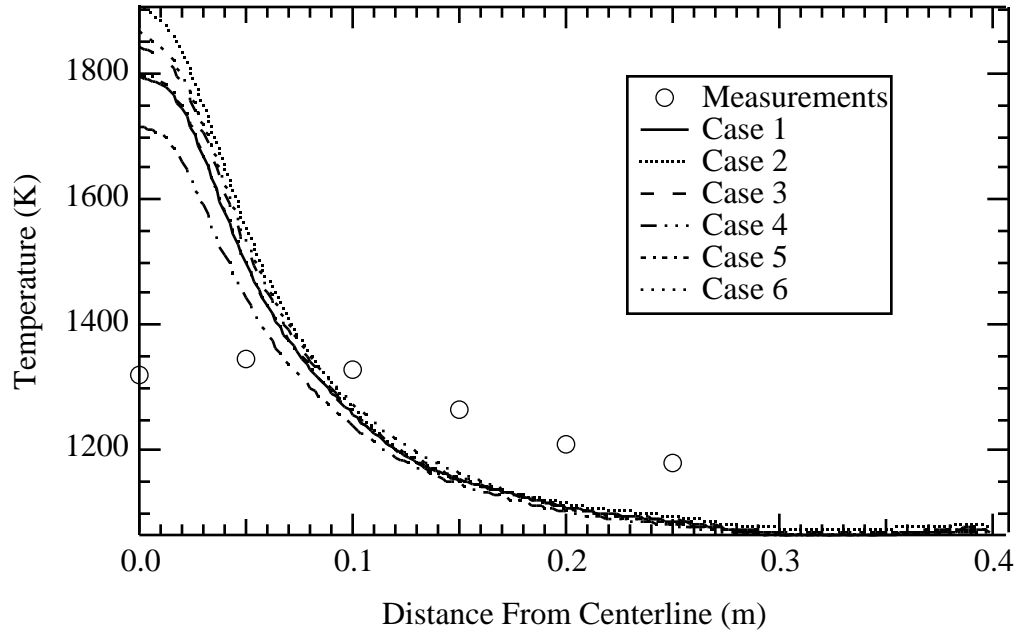
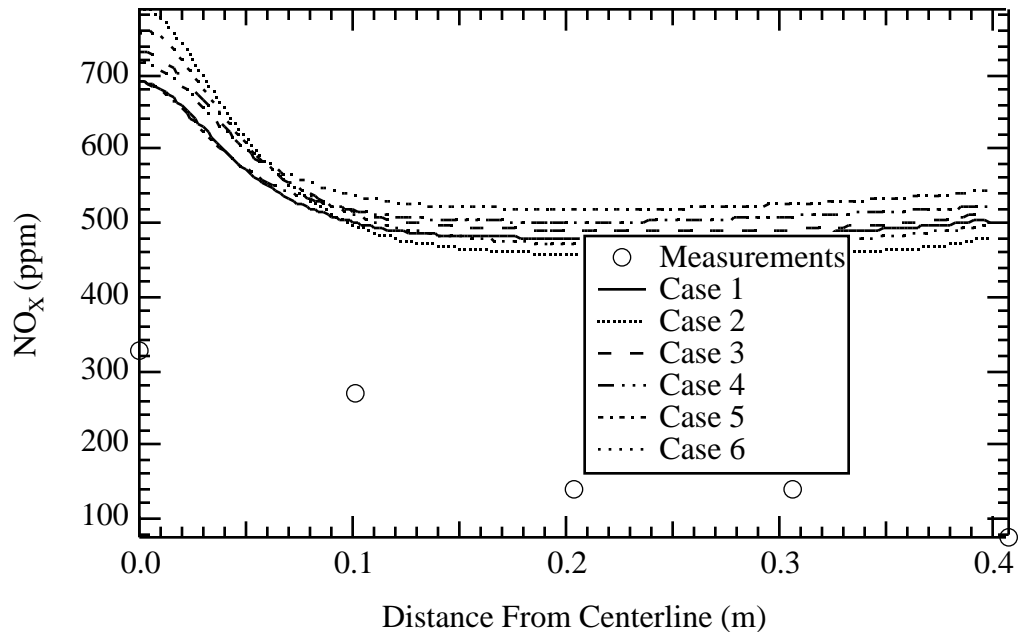


Figure E.2 Predicted and measured NO<sub>x</sub> concentrations in the CPR at 15 cm below the inlet.



**Figure E.3** Predicted and measured gas temperatures in the CPR at 55 cm below the inlet.



**Figure E.4** Predicted and measured NO<sub>x</sub> concentrations in the CPR at 55 cm below the inlet.

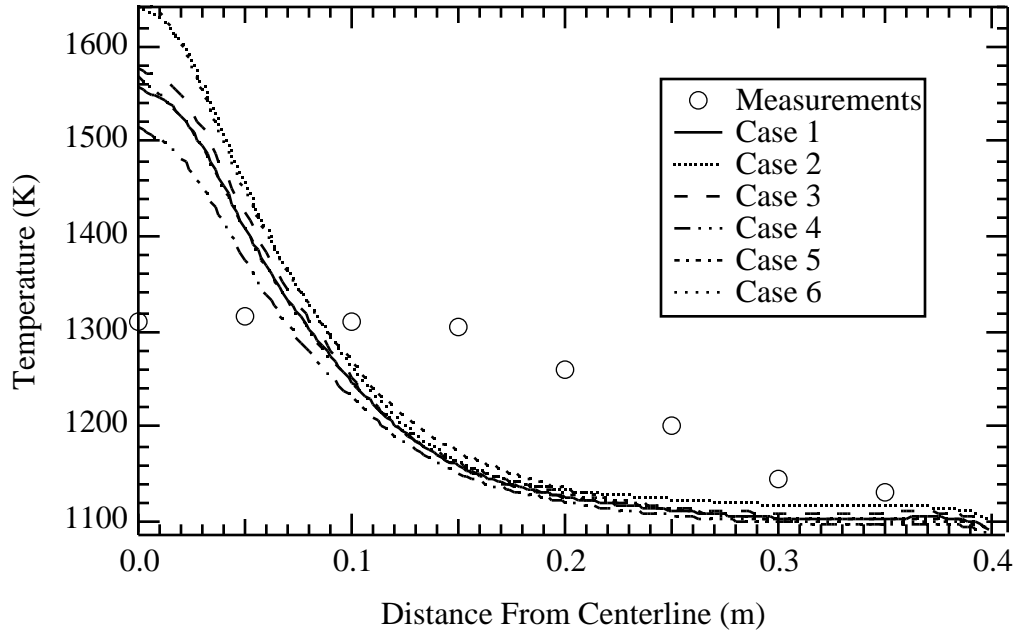


**Figure E.5 Predicted and measured gas temperatures in the CPR at 70 cm below the inlet.**

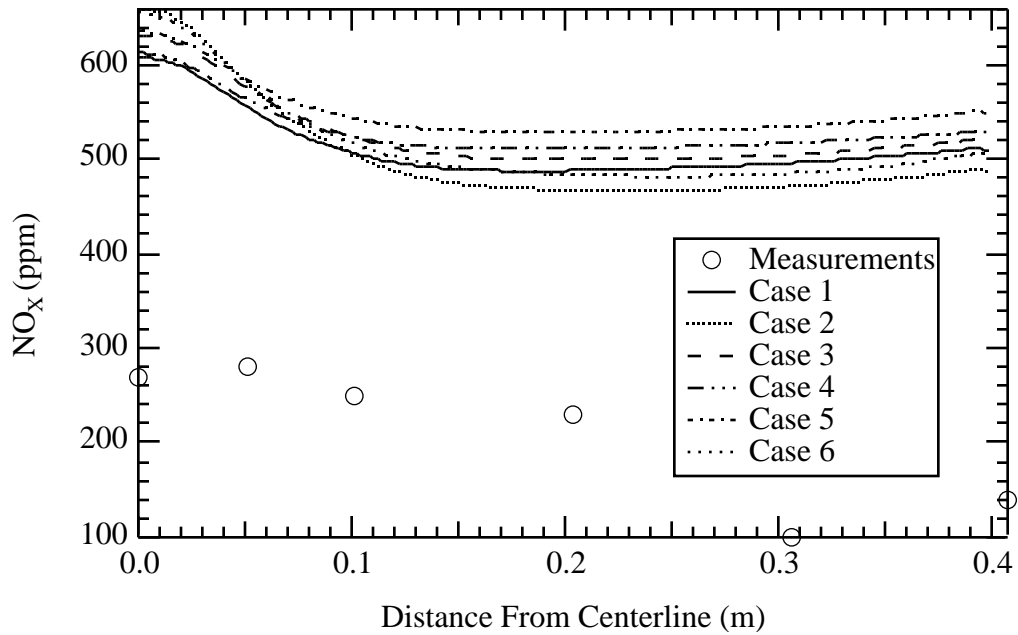


**Figure E.6 Predicted and measured NO<sub>x</sub> concentrations in the CPR at 70 cm below the inlet.**

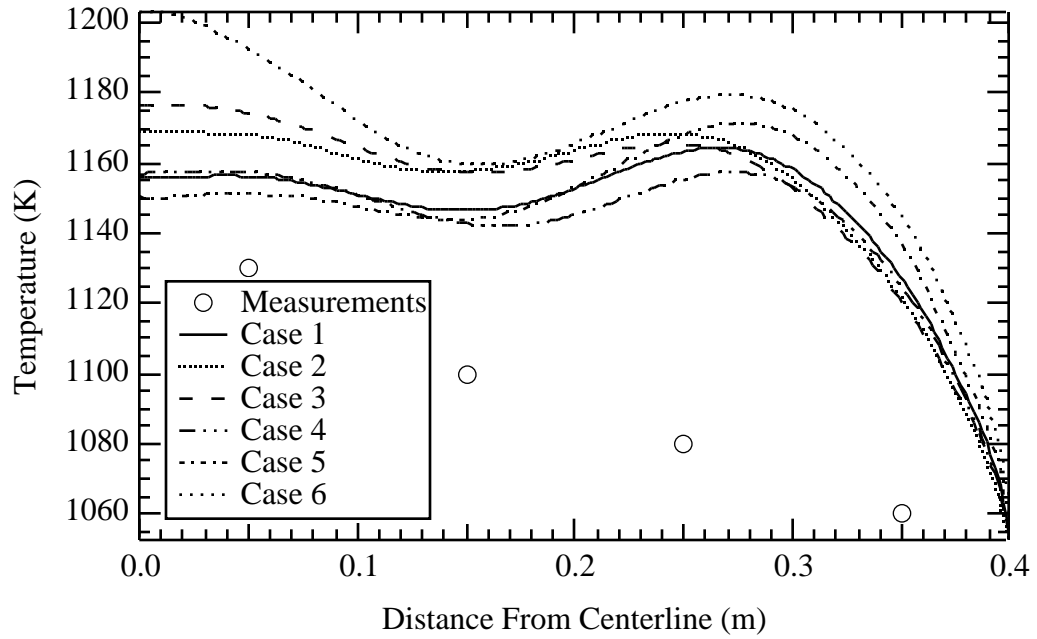


**Figure E.7 Predicted and measured gas temperatures in the CPR at 110 cm below the inlet.**

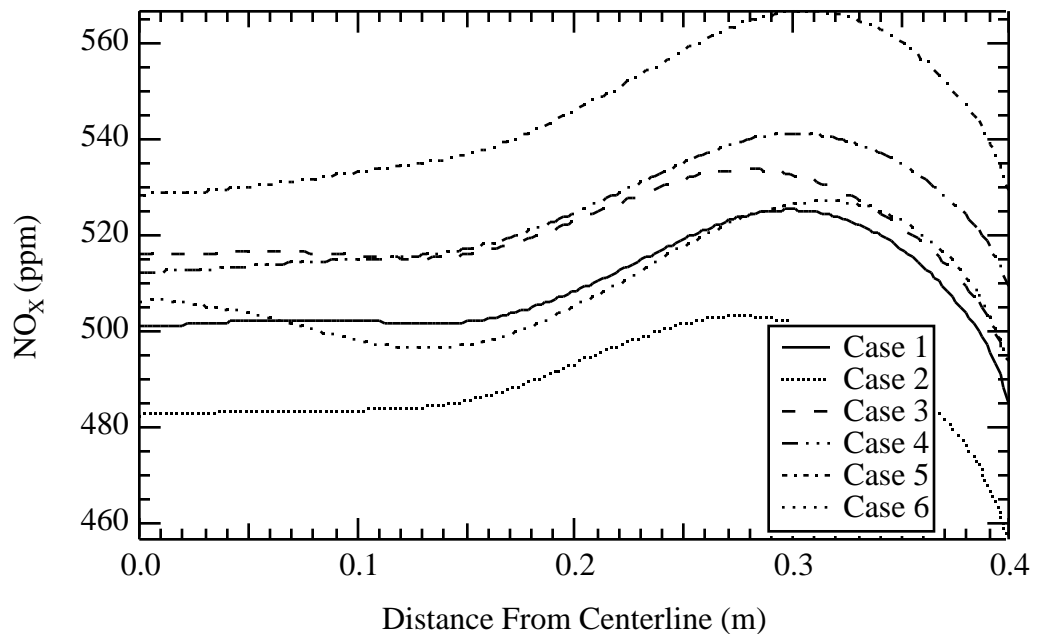


**Figure E.8 Predicted NO<sub>x</sub> concentrations in the CPR at 110 cm below the inlet.**

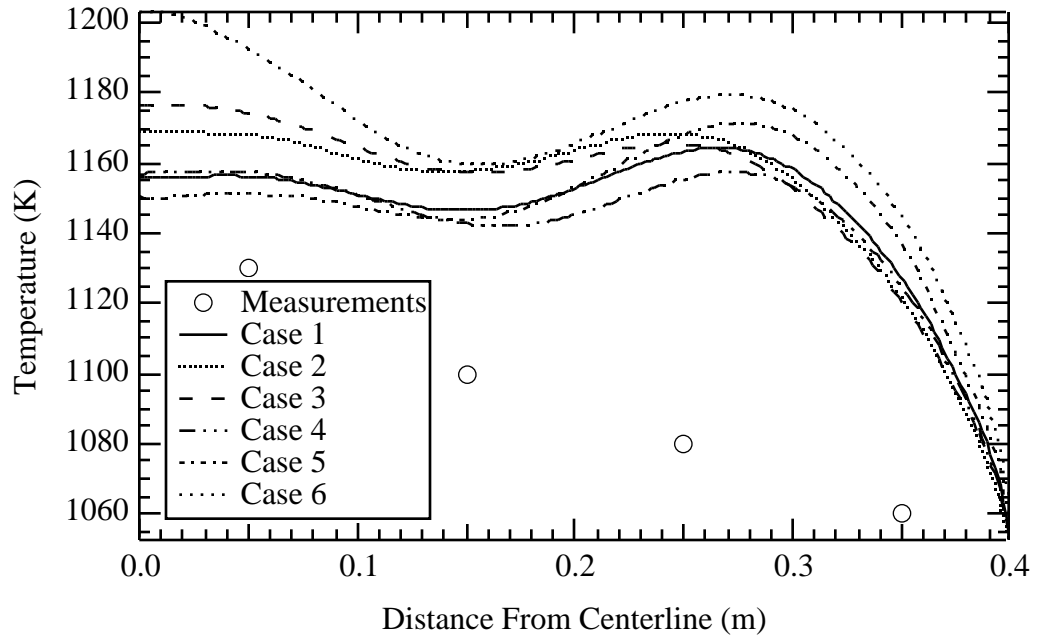


**Figure E.9** Predicted and measured gas temperatures in the CPR at 150 cm below the inlet.

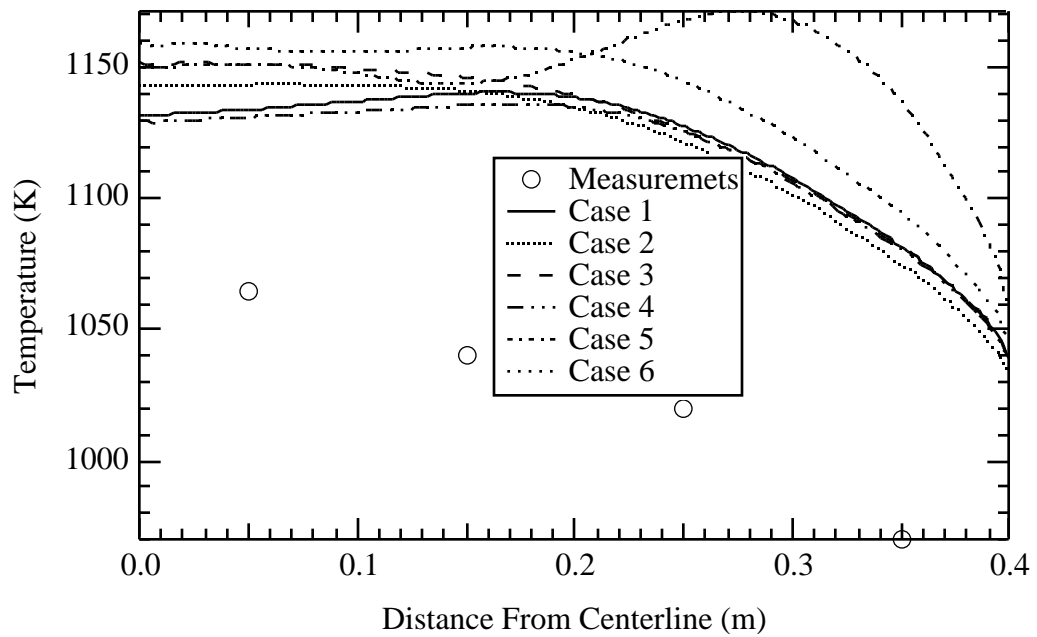


**Figure D.10** Predicted gas temperatures in the CPR at 190 cm below the inlet.

### Appendix F. FPTF Results for Additional Heights

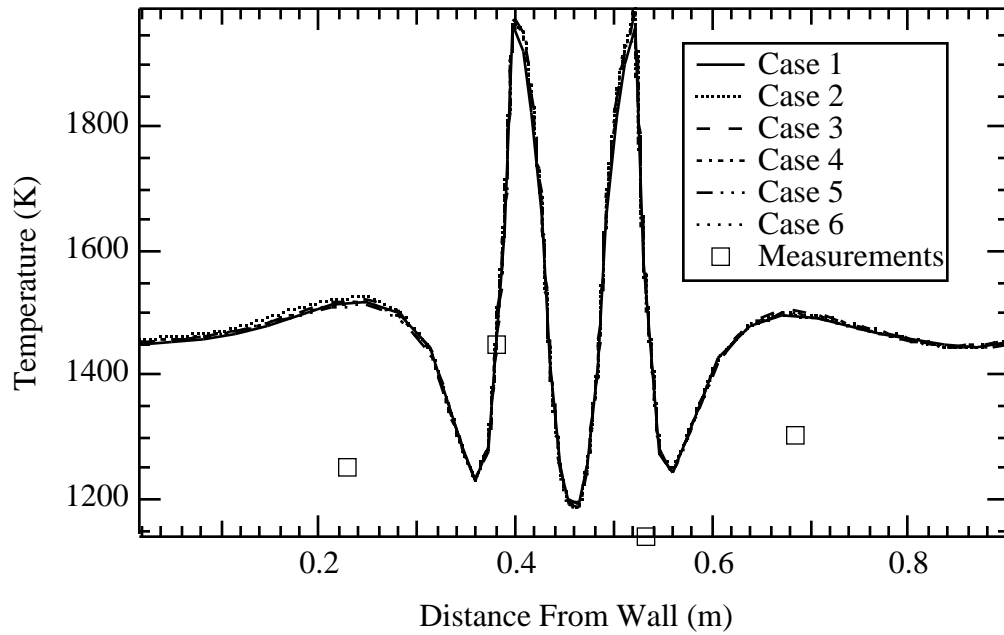


**Figure F.1** Predicted and measured gas temperatures in the FPTF at 30.5 cm above the burner.

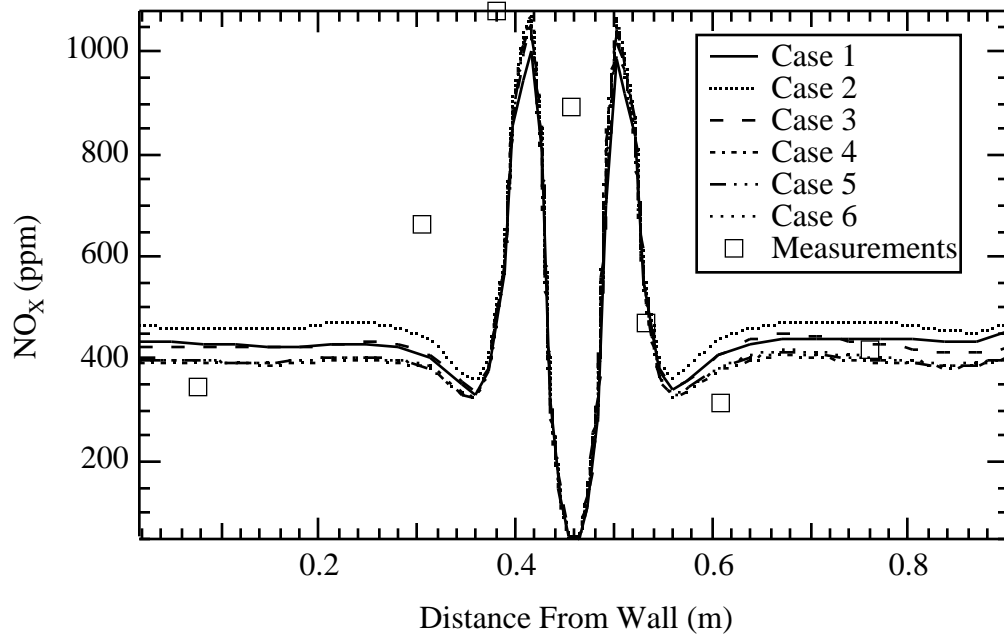


**Figure F.2** Predicted and measured NO<sub>x</sub> concentrations in the FPTF at 30.5 cm above the burner.

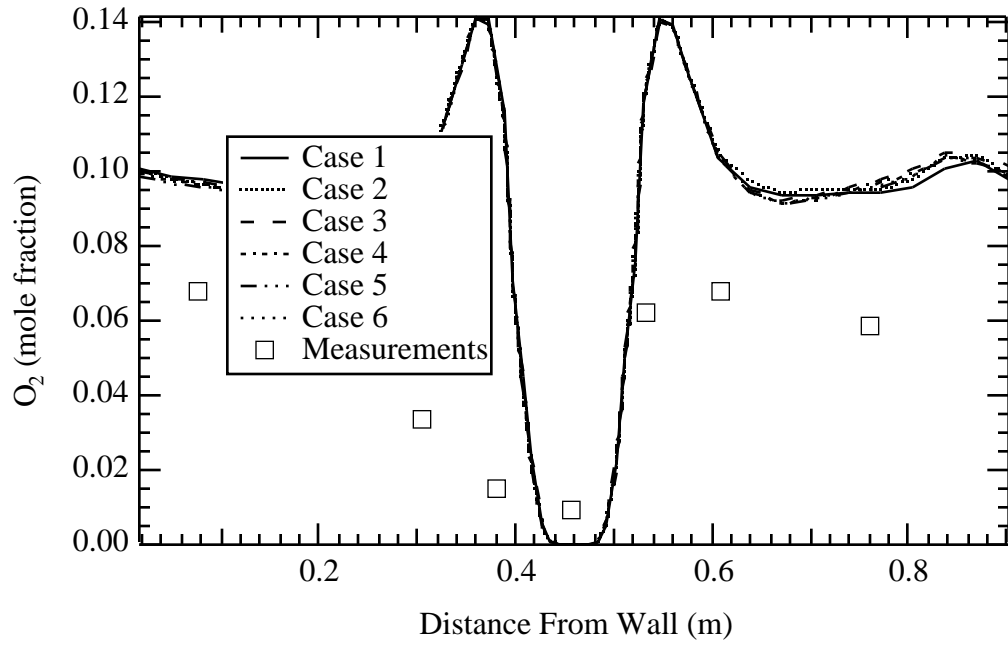


**Figure F.3** Predicted and measured  $O_2$  concentrations in the FPTF at 30.5 cm above the burner.

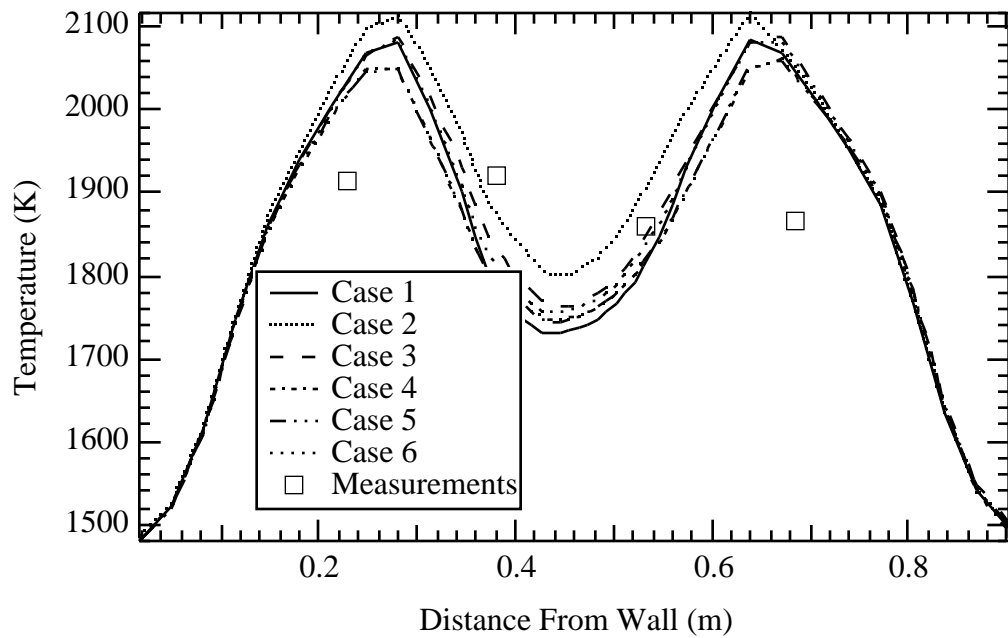


**Figure F.4** Predicted and measured gas temperatures in the FPTF at 106.7 cm above the burner.

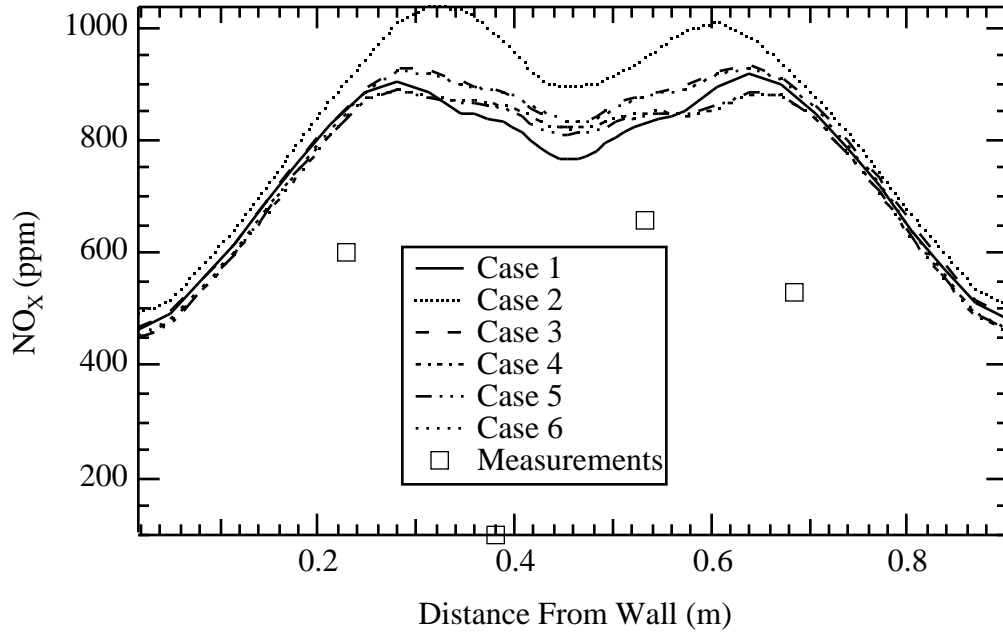


**Figure F.5** Predicted and measured  $\text{NO}_x$  concentrations in the FPTF at 106.7 cm above the burner.

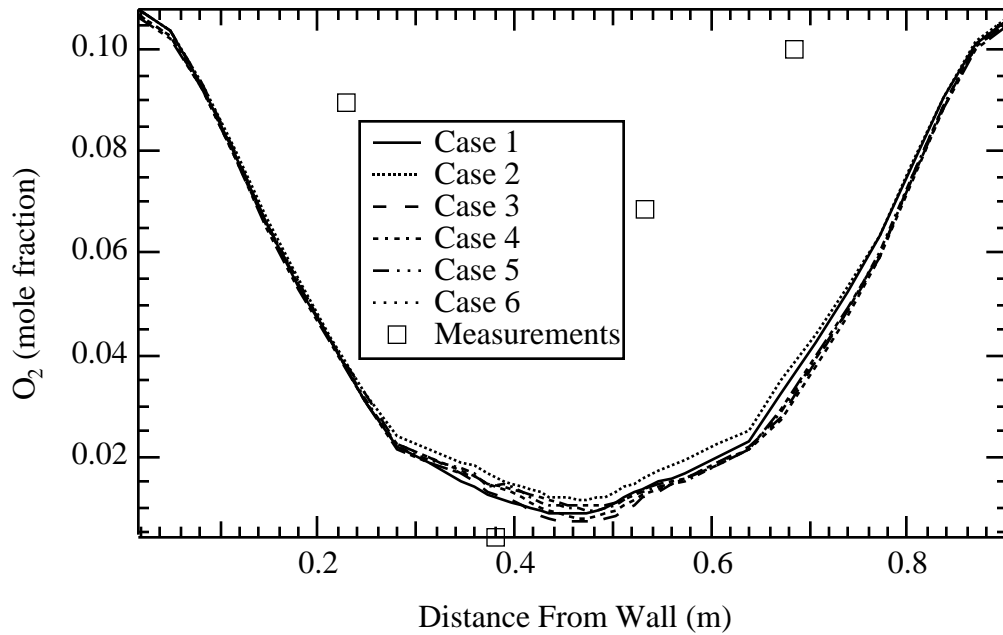


**Figure F.6** Predicted and measured  $\text{O}_2$  concentrations in the FPTF at 106.7 cm above the burner.

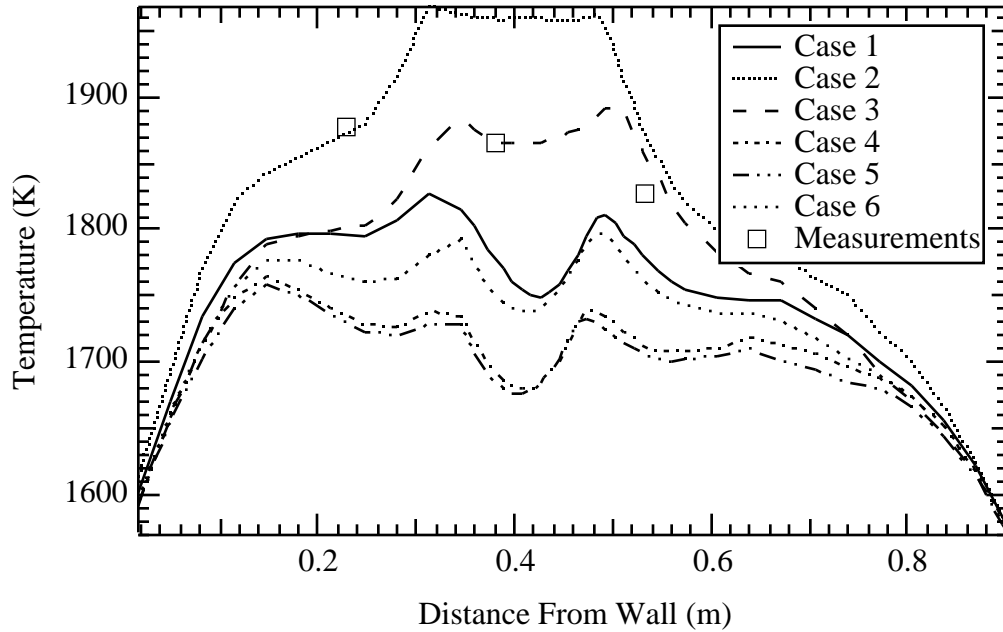


**Figure F.7** Predicted and measured gas temperatures in the FPTF at 182.9 cm above the burner.

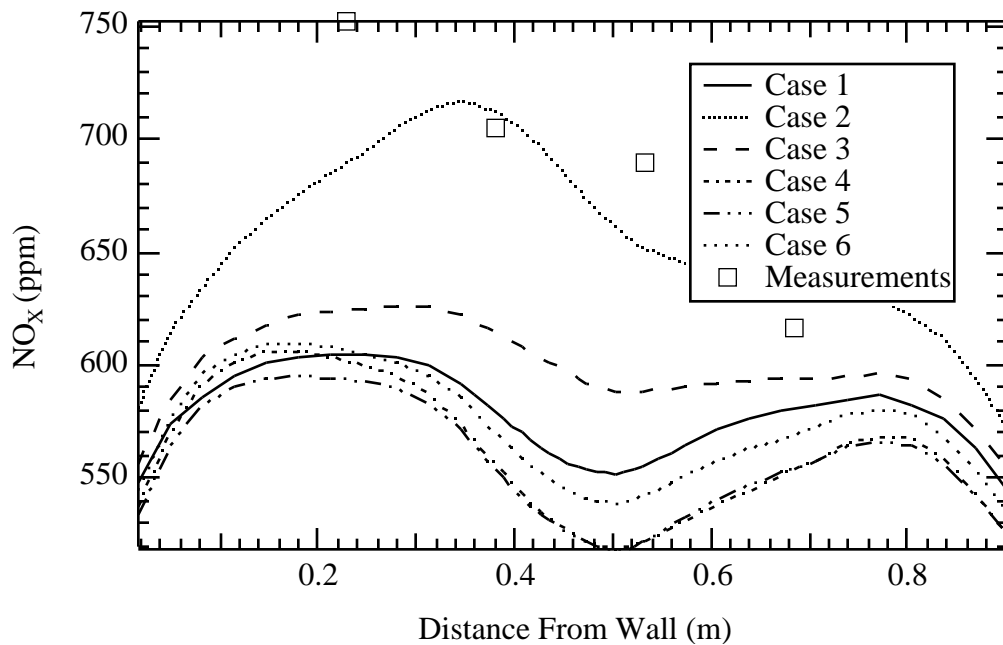


**Figure F.8** Predicted and measured  $\text{NO}_x$  concentrations in the FPTF at 182.9 cm above the burner.

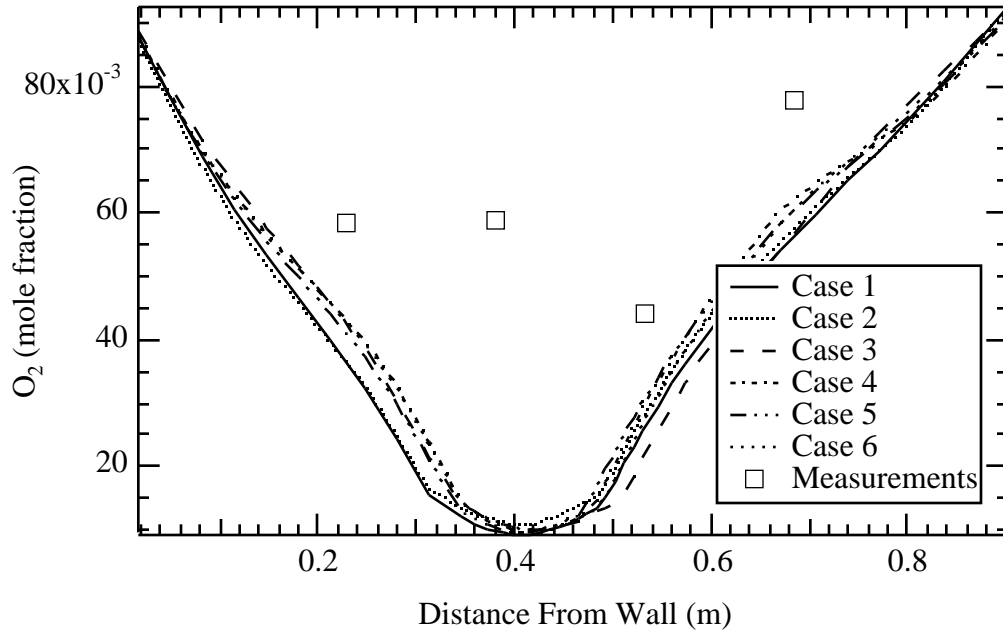


**Figure F.9** Predicted and measured  $O_2$  concentrations in the FPTF at 182.9 cm above the burner.

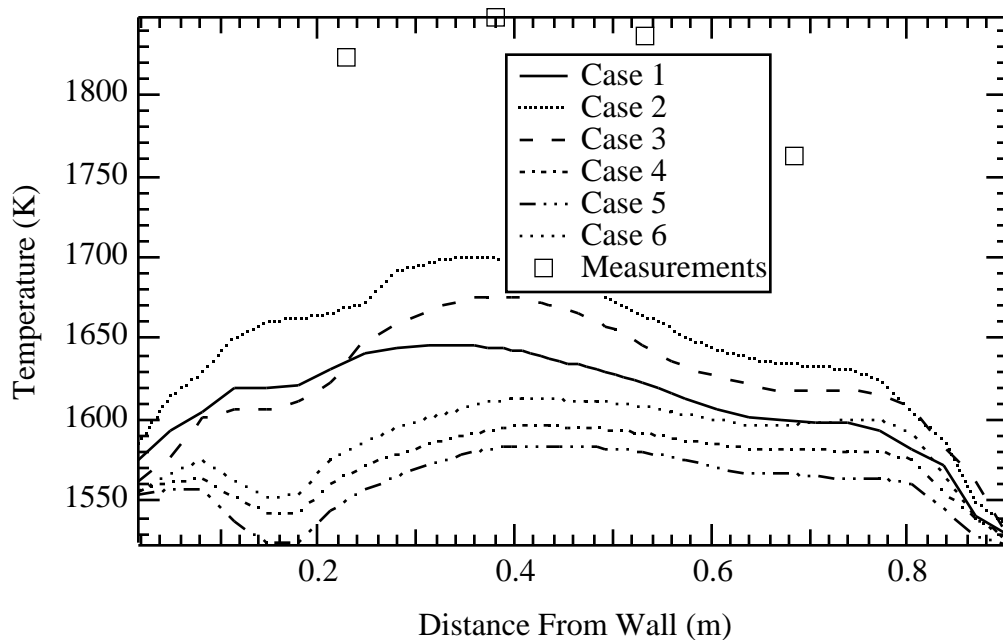


**Figure F.10** Predicted and measured gas temperatures in the FPTF at 259.1 cm above the burner.

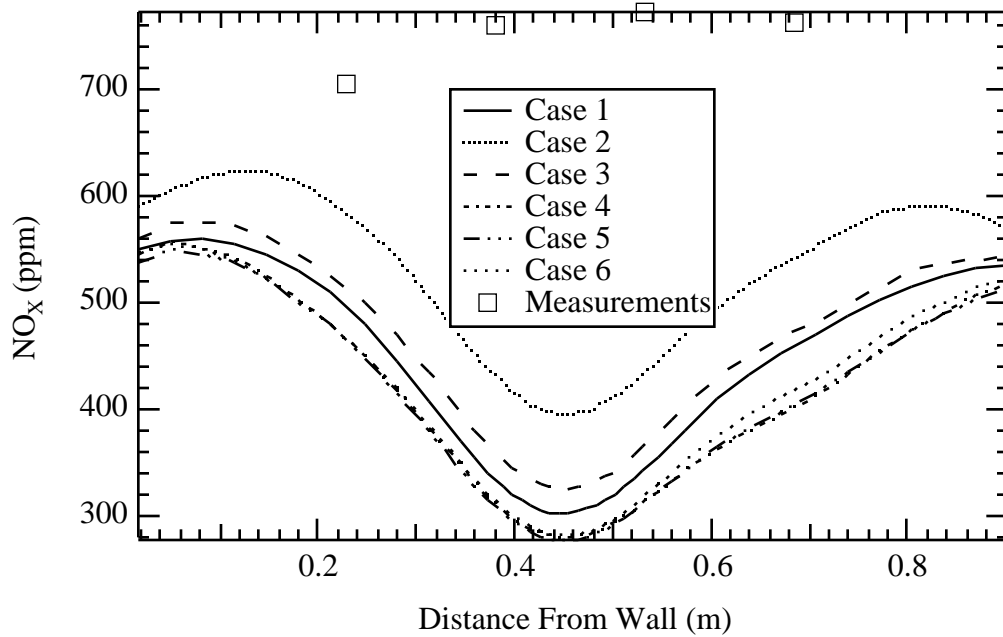


**Figure F.11** Predicted and measured  $\text{NO}_x$  concentrations in the FPTF at 259.1 cm above the burner.

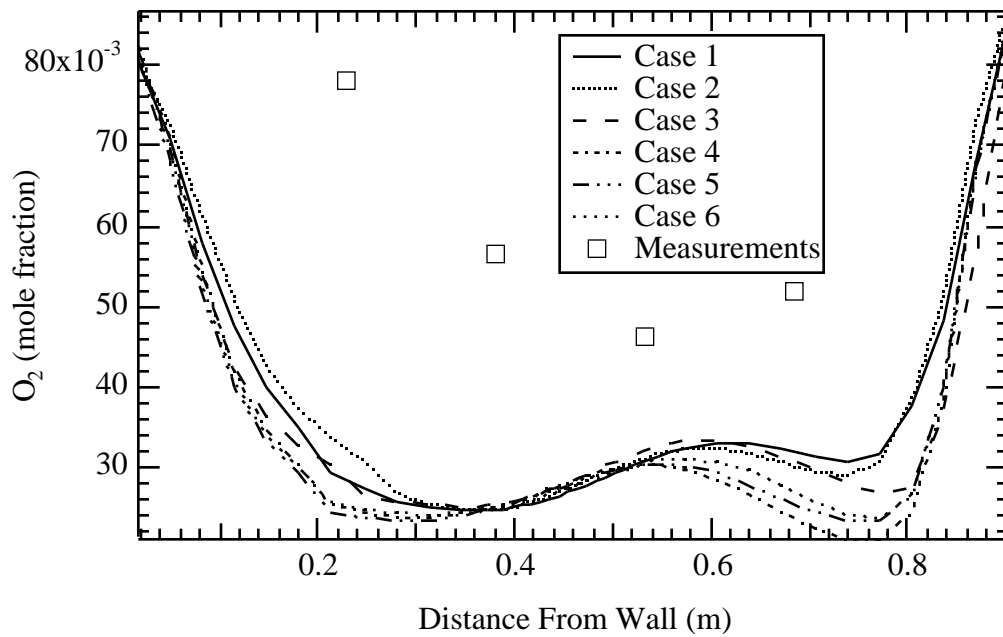


**Figure F.12** Predicted and measured  $\text{O}_2$  concentrations in the FPTF at 259.1 cm above the burner.

# Modeling Soot in Pulverized Coal Flames

Alexander L Brown

Department of Mechanical Engineering

M. S. Degree, August 1997

## ABSTRACT

Several models have been developed for predicting coal derived soot and accounting for the resulting radiative effects. Features of the models include transport equations for soot mass fraction. Required options are either an empirical or a transport equation based tar prediction, which serves as the source term for soot formation. Also, the number of soot particles per unit mass of gas may be either calculated using a transport equation or assumed average. Kinetics are based on measurements from various research. Radiative properties are calculated as a function of averaged optical constants, predicted gas temperatures, predicted gas densities and the soot mass fraction.

These models have been incorporated into comprehensive coal modeling code and evaluated based on comparisons between soot, O<sub>2</sub>, temperature and NO<sub>x</sub> measurements and predictions for three burners. Accurate prediction of soot yields have been achieved for a laminar flame. Soot is found to impact gas temperatures by as much as 300 K and NO<sub>x</sub> concentrations by as much as 250 ppm. Accuracy is found to be strongly dependent on the proper characterization of the fuel coal as well as the resolution of the model grid and turbulent flow predictions.

COMMITTEE APPROVAL:

---

Thomas H. Fletcher, Advisor

---

Dale R. Tree, Advisory Committee

---

Brent W. Webb, Advisory Committee

---

Craig C. Smith, Graduate Coordinator